

**Beate Boulgaropoulos**

# **Structure and Dynamics of an Apoptotic Model Membrane**

DISSERTATION

zur Erlangung des akademischen Grades einer Doktorin  
der technischen Wissenschaften

eingereicht an der

**Technischen Universität Graz**

durchgeführt am

Institut für Biophysik und Nanosystemforschung  
**Österreichische Akademie der Wissenschaften**

Bei: tit. Ao.Univ.-Prof. Dr.phil. Peter Laggner,  
Institut für Biochemie,  
Technische Universität Graz

2010

<b>Abstract/Kurzfassung</b>	<b>1</b>
<b>Abbreviations</b>	<b>4</b>
<b>1 Introduction</b>	<b>6</b>
<b>1.1 Apoptosis and Ceramide</b> .....	6
1.1.1 Apoptosis .....	6
1.1.2 Ceramide .....	9
1.1.2.1 Ceramide – biochemical role .....	10
1.1.2.2 Ceramide – biophysical role .....	13
<b>1.2 Interfacial catalysis</b> .....	15
<b>2 Motivation of the study</b>	<b>18</b>
<b>3 Materials and Methods</b>	<b>19</b>
<b>3.1. Lipid Model Membranes.</b> .....	19
3.1.1 General aspects. ....	19
3.1.2 Phase transitions. ....	24
3.1.3 Bilayer interactions .....	25
3.1.4 Liposome preparation .....	26
<b>3.2 Neutral Sphingomyelinase</b> .....	28
<b>3.3 Differential Scanning Calorimetry (DSC).</b> .....	32
<b>3.4 Small- and Wide-Angle X-ray Scattering (SWAXS).</b> .....	32
<b>3.5 Osmotic stress experiments</b> .....	35
<b>3.6 Fluorescence microscopy.</b> .....	37
<b>3.7 Attenuated Total Reflection Fourier Transform</b>	
<b>Infrared Spectroscopy (ATR-FTIR).</b> .....	37
<b>3.8 Photon Correlation Spectroscopy (PCS)</b> .....	38
<b>3.9 High Performance Thin-Layer Chromatography (HPTLC)</b> .....	39

<b>4 Results</b>	<b>40</b>
<b>4.1 Equilibrium study</b> . . . . .	41
4.1.1 Characterization of the Fluid-Gel Phase Coexistence Regime in an Apoptotic Model Membrane. . . . .	41
4.1.2 Effect of Ceramide on Non-Raft Proteins. . . . .	50
<b>4.2 Non-equilibrium study</b> . . . . .	55
<b>5 Discussion</b>	<b>63</b>
5.1 Equilibrium study . . . . .	63
5.2 Non-equilibrium study . . . . .	69
<b>6 Conclusions and Outlook</b>	<b>73</b>
<b>7 Bibliography</b>	<b>75</b>
<b>8 Publications</b>	<b>90</b>
<b>8.1 Characterization of the Fluid-Gel Phase Coexistence Regime in an         Apoptotic Model Membrane.</b> . . . . .	90
<b>8.2 Effect of Ceramide on Non-Raft Proteins</b> . . . . .	116
<b>8.3 Implication of Sphingomyelin/Ceramide Molar Ratio         on the Biological Activity of Sphingomyelinase</b> . . . . .	125

**Abstract**

Apoptosis is the programmed death of a cell, also known as cell suicide, which is a crucial process for all living organisms. During this controlled destruction of the cell, the interfacial enzyme sphingomyelinase hydrolyses membrane sphingomyelin and the generated ceramide plays a significant role as a lipid signalling molecule. Due to ceramide's outstanding biophysical properties, its formation strongly modulates the lateral membrane structure of domains. It has been shown that ceramide formation in model membranes leads to blebbing, which can be also observed in plasma membranes during apoptosis. However, the structural and dynamic processes within these membranes are mainly unknown.

The present study therefore focused on the dynamic structural changes within a model membrane during the sphingomyelin hydrolysis to ceramide. In the first part of the thesis the phase behaviour of the model system phosphatidylcholine/sphingomyelin in the presence of ceramide was characterized using several biophysical techniques, namely small- and wide-angle X-ray scattering, differential scanning calorimetry, infrared spectroscopy and fluorescence microscopy. In agreement with previous studies we found a gel-fluid phase coexistence region induced by ceramide, which also exists at 37°C. A detailed study of the different phases showed that the gel phase is enriched in ceramide and sphingomyelin, and that increasing ceramide stabilizes this phase. The fluid phase is enriched in palmitoyl-oleoyl-phosphatidylcholine and depleted from sphingomyelin. Sphingomyelin removal softens the fluid domains by a factor of 4, which could strongly influence the function of membrane proteins.

In the second part of this thesis the dynamic membrane processes during the enzymatic action of sphingomyelinase on membrane sphingomyelin were studied by time-resolved X-ray scattering, high-performance thin layer chromatography and photon correlation spectroscopy. In this way we were able to correlate the compositional changes of the bilayers to membrane structural adaptations and modifications on the macroscopic level. We found that the sphingomyelin/ceramide molar ratio strongly affects the structural membrane rearrangements during the enzymatic action. Down to sphingomyelin/ceramide molar ratios of 1 we found that the gel phase formation proceeds 4 times faster than sphingomyelin hydrolysis. At higher ceramide levels the membrane structural parameters slowly approached an equilibrium state. Hydrolysis of sphingomyelin stopped just before exceeding the solubility limit of ceramide. Qualitative and quantitative agreement of our findings with cell biological experiments suggests that the biological activity of sphingomyelinase depends strictly on the evolving sphingomyelin/ceramide molar ratio.

### Kurzfassung

Apoptose stellt eine Form des programmierten Zelltodes dar und dient der gezielten Entfernung von Zellen, die für die Entwicklung oder den Fortbestand eines Organismus hinderlich sind. Eine Schlüsselrolle in diesem Prozess spielt das Lipidsignalmolekül Ceramid, das durch enzymatische Hydrolyse des Membranbausteines Sphingomyelin gebildet wird und aufgrund seiner einzigartigen biophysikalischen Eigenschaften zu Modulationen der Membranstruktur führt. Es ist bekannt, dass die Ceramidproduktion in Modellmembranen zu Bläschenbildung führt, was auch in Plasmamembranen von Zellen während der Apoptose beobachtet werden kann. Die strukturellen und dynamischen Prozesse in der Membran selbst sind jedoch weitgehend unbekannt.

In dieser Arbeit wurden daher die dynamischen strukturellen Veränderungen in einer Modellmembran während der Umsetzung von Sphingomyelin zu Ceramid untersucht. Im ersten Teil wurde das Phasenverhalten des Modellsystems Phosphatidylcholine/Sphingomyelin in Gegenwart von Ceramid mit Hilfe verschiedener biophysikalischer Methoden, nämlich Röntgenklein- und -weitwinkelstreuung, Kalorimetrie, Infrarot-Spektroskopie und Fluoreszenzmikroskopie, charakterisiert. Übereinstimmend mit früheren Studien wurde ein von Ceramid induzierter Phasenkoexistenzbereich gefunden, der bei physiologischer Temperatur existiert. Eine detaillierte Untersuchung der verschiedenen Phasen zeigte eine Anreicherung der Gelphase mit Sphingomyelin und Ceramid und eine Stabilisierung der Gelphase mit zunehmendem Ceramidgehalt. Die fluide Phase ist mit Phosphatidylcholine angereichert und der Sphingomyelingehalt ist herabgesetzt. Dies führt zu einer 4-fachen Herabsetzung der Membranbiegefestigkeit, was einen großen Einfluss auf die Funktion von Membranproteinen haben kann.

Im zweiten Teil wurden die dynamischen Membranprozesse während der enzymatischen Hydrolyse von Sphingomyelin in Anwesenheit von Sphingomyelinase mittels zeitaufgelöster Röntgenstreuung, Dünnschichtchromatographie und dynamischer Lichtstreuung untersucht. Dadurch war es möglich, die Veränderung der Membranzusammensetzung mit den Adaptionen der Membranstruktur und morphologischen Veränderungen in Beziehung zu setzen. Unsere Daten zeigen, dass die Neuordnung der Membranstruktur stark vom molaren Verhältnis Sphingomyelin zu Ceramid abhängt. Bis zu einem etwa equimolaren Verhältnis bildet sich die Gelphase viermal schneller aus als der Sphingomyelinabbau selbst vonstatten geht. Bei höheren Ceramidgehalten nähern sich die strukturellen Parameter allmählich dem Gleichgewichtszustand an. Die Hydrolyse von Sphingomyelin hört auf, bevor das

Löslichkeitslimit für Ceramid in der Membran erreicht wird. Die sowohl qualitative als auch quantitative Übereinstimmung unserer Ergebnisse mit solchen von zellbiologischen Experimenten lassen auf die Korrelation der biologischen Aktivität des Enzyms mit dem Verhältnis von Sphingomyelin zu Ceramid in der Membran schließen.

## Abbreviations

<b>A<sub>c</sub></b>	Area per lipid chain
<b>aSMase</b>	Acid Sphingomyelinase
<b>ATR-FTIR</b>	Attenuated total reflexion fourier transform infrared spectroscopy
<b>Bc SMase</b>	<i>Bacillus cereus</i> Sphingomyelinase
<b>CAPK</b>	Ceramide activated protein kinase
<b>Cer</b>	Ceramide
<b>Chol</b>	Cholesterol
<b>cmc</b>	Critical micelle concentration
<b>C<sub>p</sub></b>	Heat capacity
<b>d</b>	Lamellar repeat distance
<b>DAG</b>	Diacylglycerol
<b>d<sub>B</sub></b>	Bilayer thickness
<b>DMPC</b>	Dimyristinoyl-phosphatidylcholine
<b>DNA</b>	Deoxyribonucleic acid
<b>DOPC</b>	Dioleoyl-phosphatidylcholine
<b>DPH</b>	Diphenylhexatriene
<b>DSC</b>	Differential scanning calorimetry
<b>d<sub>w</sub></b>	Bilayer separation
<b>E. coli</b>	Escherichia coli
<b>ERK</b>	Extracellular signal regulated kinases
<b>ESR</b>	Electron spin resonance spectroscopy
<b>FAN</b>	Factor activating nSMase
<b>Fas</b>	Cell surface receptor protein of the TNF receptor family, that induces apoptosis on binding Fas-ligand
<b>FWHM</b>	Full-width at half maximum
<b>GUV</b>	Giant unilamellar vesicle
<b>HPTLC</b>	High performance thin layer chromatography
<b>IR</b>	Infrared spectroscopy
<b>IRE</b>	Internal reflection element
<b>L</b>	Domain size
<b>L<sub>α</sub></b>	Lamellar fluid phase
<b>L<sub>β</sub></b>	Lamellar gel phase

<b>LUV</b>	Large uni lamellar vesicle
<b>MLV</b>	Multi lamellar vesicle
<b>MM</b>	Michaelis-Menten
<b>NFA</b>	Non hydroxy fatty acid
<b>NF-<math>\kappa</math>B</b>	Nuclear factor ' $\kappa$ -light-chain-enhancer' of activated B-cells
<b>NMR</b>	Nuclear magnetic resonance
<b>NMWL</b>	Nominal Molecular Weight Limit
<b>nSMase</b>	Neutral Sphingomyelinase
<b>OLV</b>	Oligo lamellar vesicle
<b>Ox-LDL</b>	Oxidized human low density lipoproteins
<b>PC</b>	Phosphatidylcholine
<b>PCS</b>	Photon correlation spectroscopy
<b>PDI</b>	Poly dispersity index
<b>PEG</b>	Poly ethylen glycol
<b>PKC</b>	Protein kinase C
<b>POPC</b>	Palmitoyl-oleoylphosphatidylcholine
<b>PP</b>	Protein phosphatase
<b>Raf</b>	Raf-Proteinen (rapidly growing fibrosarcoma or rat fibrosarcoma) Raf proteins belong to the proteinkinases. Isoformes: A-Raf, B-Raf und C-Raf ( Raf-1)
<b>SAXS</b>	Small angle X-ray scattering
<b>SL</b>	Sphingolipid
<b>SM</b>	Sphingomyelin
<b>SMase</b>	Sphingomyelinase
<b>SUV</b>	Small unilamellar vesicle
<b>SWAXS</b>	Small- and wide- angle X-ray scattering
<b>T<sub>m</sub></b>	Main transition temperature
<b>TNF<math>\alpha</math></b>	Tumor necrosis factor $\alpha$
<b>ULV</b>	Unilamellar vesicle
<b>WAXS</b>	Wide angle X-ray scattering
<b>Z<sub>Av</sub></b>	Average particle size



# **1 Introduction**

## **1.1 Apoptosis and Ceramide**

Apoptosis is the programmed death of a cell; it is characterized by a fixed pathway and follows a characteristic morphology. Ceramide (Cer) plays an important, although not fully understood role in apoptosis and other vital cell processes.

### **1.1.1 Apoptosis**

During the apoptotic process the cell plays an active role in its own death and dies in a controlled and regulated manner. Therefore apoptosis is often referred to as cell suicide. The cell disposal due to apoptosis occurs without inflammatory responses. The balance between apoptosis and proliferation of the single cells is vitally important for any multicellular organism. Out of balance situations result in various diseases, like cancer or Alzheimer. Cancer cells rarely undergo apoptosis, which result in uncontrolled cell proliferation, whereas in Alzheimer disease, apoptosis could be responsible for the loss of neurons.

Apoptosis is characterized by several key phases (1). In the initiator phase, it can be triggered by a variety of stimuli, which can have extra cellular origin (extrinsic inducers), like binding of death receptors, or intra cellular origin (intrinsic signals) like cellular stress responses (2, 3). Cellular stress can occur from the exposure of the cell to radiation, chemicals, from viral infection or oxidative stress caused by free radicals (4). The apoptotic signal must either cross the plasma membrane or a second messenger must transmit the effect to a response. This leads to the initiation of the apoptotic pathway via regulatory proteins, which allow the apoptotic process to be stopped if there is no longer need for the cell to die. Cer is known to be involved in this process, but its second messenger role still remains disputed. Van Blitterswijk et al. (5) review the roles of Cer as a second messenger and/or biophysical modulator of the membrane structure (Fig.1.1). In plasma membranes Sphingomyelin (SM) is a major component, where it can cover up to 20% of the total phospholipid content (6, 7) and it is located extensively in the outer leaflet of the bilayer (8-11). The plasma membrane harbours a fraction of acid Sphingomyelinase (aSMase) and neutral Sphingomyelinase (nSMase) (4), which catalyse the

hydrolysis of SM to Cer and water soluble phosphocholi. Cer formation occurs rapid and transient in the initiator phase of apoptosis. The aSMase performs its action on the major SM pool at the outer leaflet of the membrane. The generated Cer facilitates death receptor clustering at the membrane surface, possibly by Cer's property to stabilize membrane rafts (12, 13) and plays a membrane structural role. The nSMase acts on the minor SM pool in the inner leaflet of the plasma membrane and the generated Cer may have second messenger function and possibly play a membrane structural role. In the initiator phase the cells maintain their morphology to a large extent.

An alternative apoptotic regulation can happen by targeting mitochondria functionality. This can occur via pore formation of the mitochondrial membrane with subsequent efflux of apoptotic effectors, like mitochondrial *cytochrom C*. Cer is known to be involved in this process (14-16).

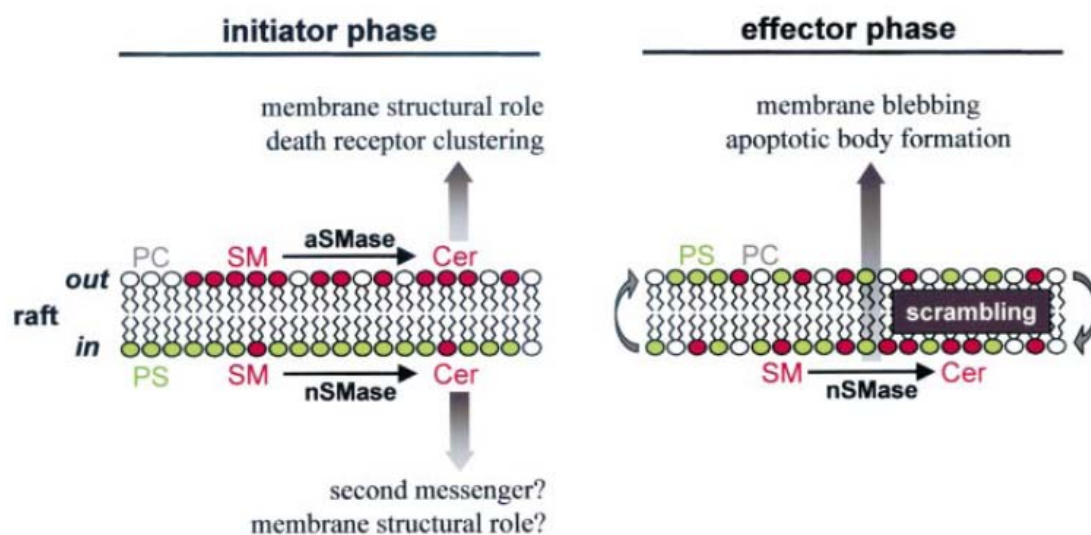


Figure1.1 Function of SM hydrolysis during the initiation and effector phases of apoptosis, taken from (5)

In the effector phase of apoptosis the bilayer asymmetry gets lost due to lipid scrambling and nSMase hydrolyses SM in the inner leaflet at the plasma membrane, which leads to Cer generation (Fig.1.1). The Cer formation in this apoptotic phase occurs slow and sustained (5), the Cer level increases up to several times and the resulting changes in the membrane are blebbing and apoptotic body formation.

During the execution phase of apoptosis a cholesterol efflux from the membrane caused by the SM breakdown occurs (17), which again leads to changes in the biophysical properties of the plasma membrane, such as blebbing and vesiculation at the cell surface (2). The cell shows distinct characteristic morphological features (18). It shrinks, the cytoplasm appears dense and the organelles tightly packed. The chromatin condenses, the nuclear envelope becomes discontinuous and the DNA is fragmented. Finally the nucleus breaks and it comes to the formation of apoptotic bodies, which are then phagocytosed (3, 5) (Fig.1.2).

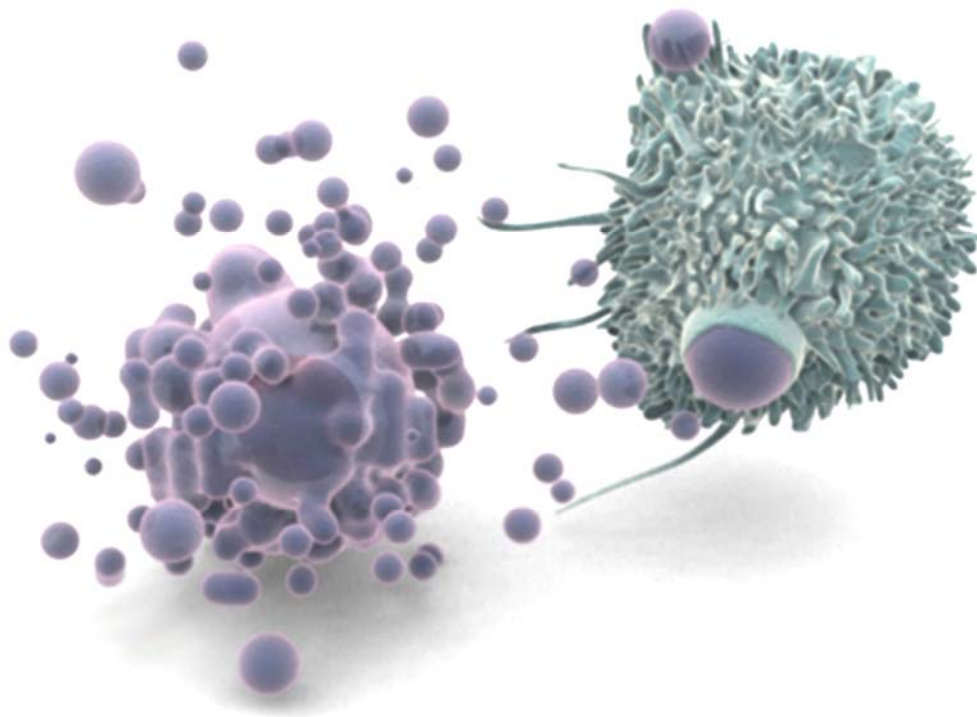


Figure 1.2 Picture of an apoptotic cell and a white blood cell, taken from the U.S. National Library of Medicine

This apoptotic body formation is the most eye-catching structural change at the surface of an apoptotic cell (19, 20) (Fig.1.2). However, little is known about the dynamics and the dynamic lipid organization on the molecular level in the plasma membrane during these enormous structural changes (21). A large number of studies exist, where the morphologic changes as well as the changes in lipid composition during apoptosis in different cell lines and initiated by different stimuli were observed, for a review, see (4). The resulting generation of the apoptotic characteristics in these biological systems differs not only among the different cell lines, but different results were also observed for individual cells within a cell line. Further it is also

strongly dependent on the apoptotic stimulus (22). Rudolf et al. (23) studied the morphological changes of four different human cancer cell lines, with two different apoptotic inducers and found a series of diverse responses. Interestingly, the common feature of all cell lines was that individual cells entered asynchronously into the blebbing stage. There were remarkable differences in the course of blebbing, i.e. numbers of different blebbing stages. The whole process of apoptosis induced in human cancer cells took between 6 and about 14 hours. The time for the Cer production, induced by various different effectors and in different cell lines, lies in a range between 1 minute (primate epithelial cells /oxidative stress) (24) and 16 hours (human fibroblasts/OxLDL) (25).

### 1.1.2 Ceramide

Cer is one of the simplest sphingolipids with a number of outstanding biophysical properties and the potential to mediate biochemical processes (26-33). It is an extremely hydrophobic lipid. This property explains the important biological role of Cer as a component of the *stratum corneum* ensuring the water impermeability of the skin (34). The most abundant Cer molecules are those with a fatty acyl chain of 16 carbon atoms or longer.

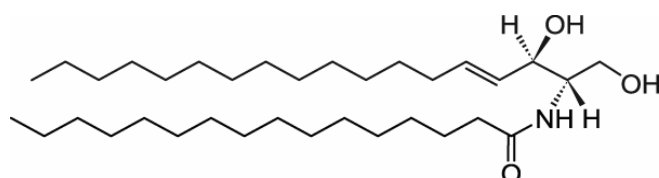


Figure 1.3 Molecular structure of C16:0-Cer (N-Palmitoyl-D-erythro-Sphingosine)

Cer is composed of a sphingosine moiety with a fatty acid attached by an amide linkage (Fig.1.3). It is an amphipatic, non swelling lipid with a small polar hydroxyl-headgroup and two hydrophobic fatty acid chains. In mixtures with other phospholipids Cer has the ability to strongly modulate the membrane structure, which might play a role in Cer-mediated cell functions (5, 17, 35-38). Pure C16:0-Cer was characterized by Shah et al. (39) with DSC and X-ray diffraction techniques. Fully hydrated Cer shows a well-ordered meta stable bilayer phase at room temperature. Upon increasing the temperature, an exothermic transition occurs at 64.2°C to form a stable bilayer phase with crystalline chain packing. Further heating

converts the crystalline phase into a disordered fluid phase of undefined structure, through to an endothermic transition at 90°C.

### 1.1.2.1 Ceramide - biochemical role

#### Biosynthesis and degradation of Cer

Cer can be generated in cells either by de novo synthesis or through the breakdown of other sphingolipids (11, 40, 41), (Fig.1.4). The biosynthesis of Cer starts with the condensation of serine and palmitoyl-CoA by the enzyme *serine-palmitoyl-transferase*, which is located on the surface of the cytosolic leaflet of the endoplasmic reticulum (42, 43). This leads to the formation of 3-ketosphingosine. The keto-group is then reduced to yield dihydrosphingosine, which gets in turn N-acylated by the enzyme *dihydroceramide-synthase*. Introduction of a trans-double-bond at C<sub>4</sub> to form Cer is done by *dihydroceramide-desaturase*. The major regulatory steps in the Cer biosynthesis are the ones catalysed by *serine-palmitoyl-transferase* and *ceramide-synthase*. Cer is the basic building block for the generation of several complex sphingolipids, which takes place in the Golgi apparatus (44).

Cer production from SM hydrolyses is catalysed by a SM specific phospholipase C, called *sphingomyelinase* (SMase) and can be activated by a variety of stimuli (45, 46).

Degradation of Cer and other simple sphingolipids takes place in the acidic late endosomes and lysosomes as well as in the non-lysosomal compartments such as the caveolae in the plasma membrane (5, 17). The breakdown of complex sphingolipids leads to the formation of firstly Cer and then sphingosine, which Sphingosine can be phosphorylated to sphingosine-1-phosphate or reincorporated into Cer (Fig.1.4).

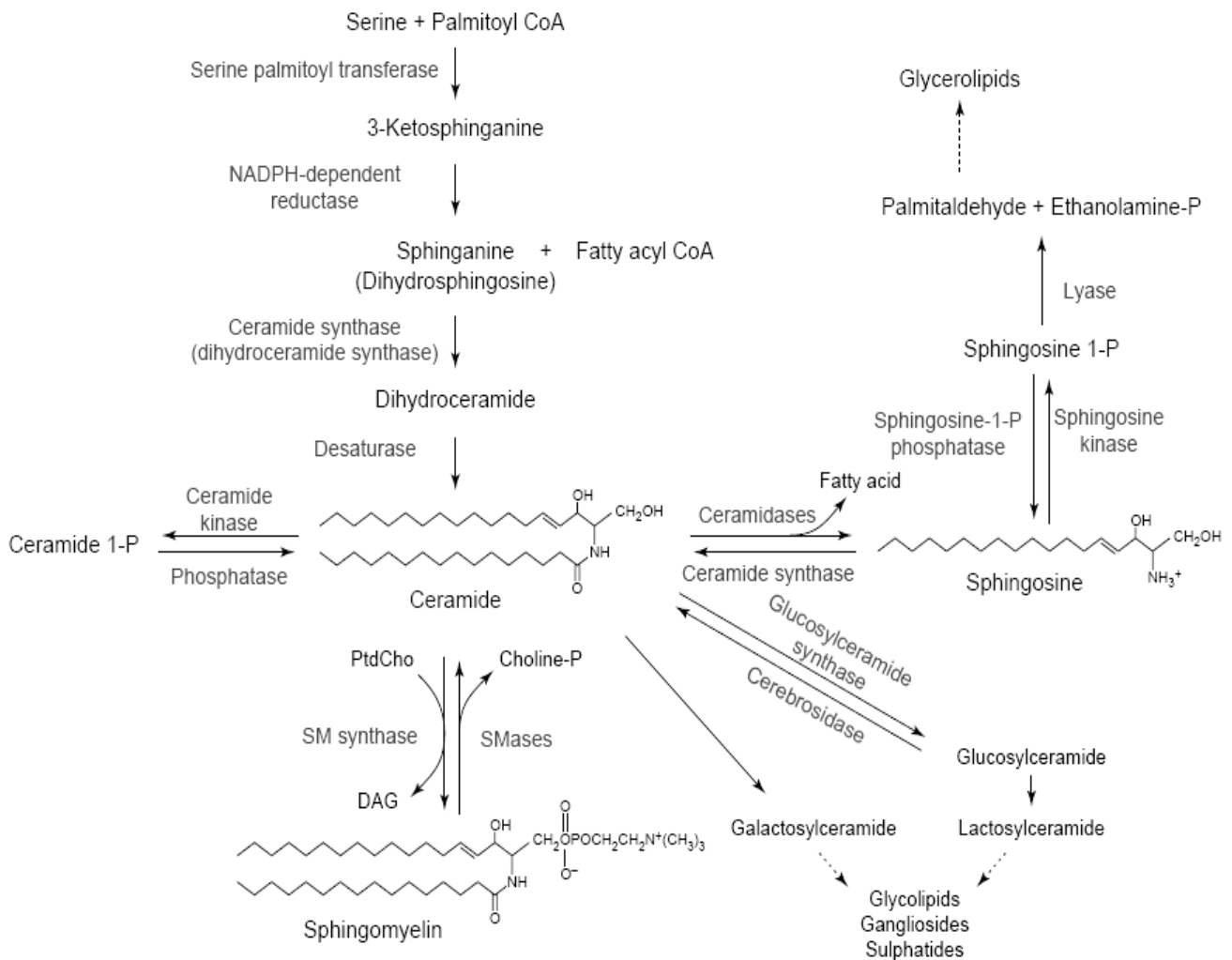


Figure 1.4 Cer biosynthesis and degradation, taken from (40)

Cer and sphingosine on the one hand, and sphingosine-1-phosphate (sphingosine-1-P) on the other hand play antagonist roles. Cer and sphingosine mediate apoptosis, cell cycle arrest, and differentiation, whereas sphingosine-1-P promotes proliferation, survival, and inhibition of apoptosis (47). The balance between these pro- and anti-apoptotic sphingolipids is called the “sphingolipids-rheostat” and determines the survival fate of various cells (48).

Ceramide as second messenger

Secondary messengers are a component of signal transduction cascades. Changes of their concentration level within a cell result in activation of effector proteins to exert a cellular response. Comprehensive reviews about Cer’s second messenger function can be found in (11,

35, 40, 41, 49). Cer seems to have second messenger function in several vital cellular processes, including apoptosis, growth suppression, differentiation and cell senescence (27, 33, 40, 41, 50-55). This is supported by the repeated findings that many inducers of stress response- like heat, UV radiation and chemotherapeutic agents- result in Cer accumulation (49, 56). However, the second messenger function of Cer still remains controversial (5, 57). The outcome of the effect induced by Cer is largely dependent on a number of factors, like the cell line or the experimental setup used.

Cers can modulate enzyme action by binding to specific sites in the target protein. This mechanism may operate not only on proteins that are permanently bound to membranes, but also on protein molecules, which are transiently recruited to the bilayer where Cer is located. Two groups of Cer target proteins with Cer-binding sites can be distinguished (35):

- (i) Cer-binding membrane-related proteins: A proposed direct target of Cer is *Cer-activated protein kinase* (CAPK), an at least transiently membrane-bound enzyme, which was recently shown to be the previously defined kinase suppressor of *Ras* (58). Other at least transiently membrane-bound proteins as Cer targets are *kinases C* (PKC) (59) and c-Raf-1 (60). It has been proposed that Cer binds proteins in this group through their cysteine-rich domains (61).
- (ii) Cer-binding proteins with no known membrane-binding capacity: The *protein-phosphatases* PP1 and PP2A have been identified as key targets for Cer action. Cer activates serine–threonine protein phosphatases of both the PP1 and PP2A families at least in vitro. The aspartic protease *Cathepsin D* was discovered as a Cer-binding protein, and evidence has been provided that Cer induces the proteolytic activity of this lysosomal enzyme in cells (62).

The mechanisms of action of Cer, which targets are directly activated in cells and what specific functions they mediate are still not clear.

### 1.2.2.2 Ceramide - biophysical role

Cer modulates phospholipid bilayers in several ways. Comprehensive reviews are given in (26, 35, 63, 64). The impact of Cer on lipid model membranes was studied by several groups with a variety of techniques and can be summarised as follows:

- (i) Cer gives rise to in-plane phase separation of Cer-rich and Cer-poor domains;
- (ii) Cer increases the order of the acyl chains in the bilayer;
- (iii) Cer facilitates the transition from bilayer to non bilayer structures, membrane fusion and leakage;
- (iv) Cer induces transbilayer lipid movement.

Ad (i) Cer and other sphingolipids segregate into lateral domains within the plane of the lipid bilayer (52, 65, 66). This is due to the fact that sphingolipids act as both acceptors and donors of hydrogen bonds, which results in strong intermolecular interactions between sphingolipid head groups perpendicular to the lipid bilayer (67). Cer rich domain formation was first reported with bovine brain Cer (68), but also synthetic C16:0-Cer in mixtures with various phospholipids tend to form Cer enriched domains (69, 70). Domain formation also occurs with natural Cers (brain, egg) with various synthetic phospholipids, which was shown by DSC and IR measurements (71).

Ad (ii) Natural as well as synthetic C16:0-Cer was found to increase the order in PC bilayers, which was shown by several techniques, like DPH fluorescence (72) and DNMR (65, 68, 73). Also in situ generated Cer increases the order of the acyl chains in mixture with POPC (69). Massey et al. (74) found an ordering effect of Cer in PCs as well as in bilayers composed of natural SM with fluorescence probe techniques.

Ad (iii) Cer induces non lamellar phases (75, 76) like inverted hexagonal phases, which might be involved in membrane fusion and fission processes (77, 78). Several studies exist, which observe non lamellar phase formations triggered by Cer (71, 79). Another effect of Cer is the induction of leakage in lipid vesicles with vesicle-vesicle aggregation and fusion as possible consequence. Interestingly leakage has only been observed, when



Cer is added to or generated in a pre existing lipid bilayer. Cer incorporated into lipid composition during vesicle preparation would not induce leakage (26).

Formation of membrane defects and leakage induced by Cer in a phospholipid membrane were reported by Huang et al. (65), Montes et al. (80) and Ruiz-Arguello et al. (79). The latter observed vesicle aggregation as well. Montes (80) loaded SM containing large unilamellar vesicles with dextran molecules. Cer generated through *Bc* SMase action led to leakage of the vesicles and the release of these molecules with a molecular weight as high as about 20 kDa. This result was important, because it suggested the involvement of Cer in the *cytochrome C* release from mitochondria in the activation of apoptosis.

Ad (iv)            Enzymatic generation of Cer at one side of the bilayer leads to transbilayer (flip-flop) movement of the Cer molecules (75, 81-83).

The property of Cer to modulate the membrane structure exerts influence on other membrane components and/or molecules that interact with the membrane. These can be proteins, which are permanently or transiently related to membranes and Cer would as a consequence influence protein function by modifying the bilayer properties (35). Especially intrinsic membrane proteins are very sensitive to changes in the physical state of the bilayer such as fluid to gel phase transition or the induction of non lamellar phases (84-86). Other Cer-induced changes in bilayer properties that could influence the activity of proteins are the lateral segregation of Cer into certain membrane domains and Cer's property to stabilize membrane rafts (12, 13), which serve as meeting-platform for proteins.

## 1.2 Interfacial catalysis

The concentration of free SM molecules in the aqueous environment in equilibrium with the membrane enclosed ones is estimated to be smaller than 1 pmol (87) - this is far too low to ensure the efficient catalytic turnover via classical water soluble Michaelis - Menten (MM) - complexes. Hence, the catalytic turnover must happen at the lipid–water interface. Therefore additional constraints and rate constants which describe the residence time at the interface must be introduced for interfacial catalytic turnover. ( $k_d$  and  $k_b$ , respectively in Fig.1.5)

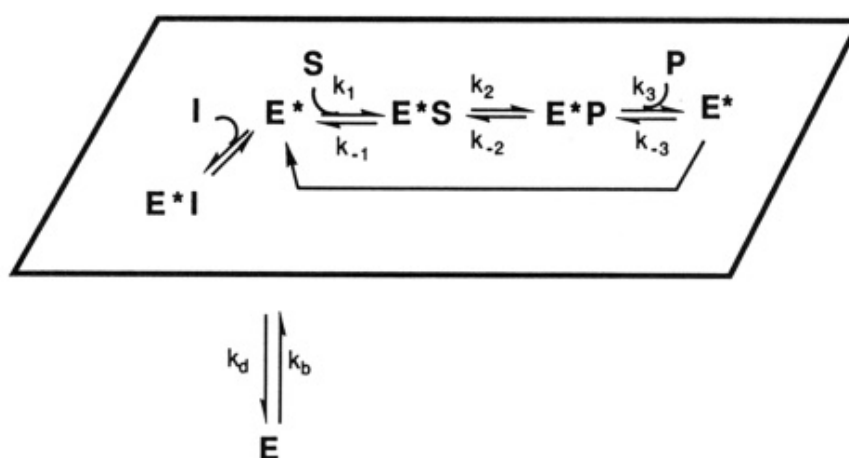


Figure 1.5 Scheme of interfacial catalysis.  $E$  to  $E^*$ : Binding of the enzyme to the surface. The reactions in the box are the interfacial steps where the substrate enters the catalytic site, followed by the catalytic step and the product release.  $E$ : Enzyme in aqueous phase,  $E^*$ : Enzyme, bound to the bilayer,  $S$ : Substrate,  $P$ : Product.  $k_d$ ,  $k_b$ ,  $k_1$ ,  $k_{-1}$ ,  $k_2$ ,  $k_{-2}$ ,  $k_3$ ,  $k_{-3}$  are rate constants. This scheme was taken from (88).

During the steady state,  $E$  is in equilibrium with the enzyme in the interface ( $E^*$ ) and the total amount of enzyme stays constant. In this case, the features of interfacial catalysis are comparable to the standard treatment of enzyme kinetics as it is applied to numerous cases of water-soluble substrates, and one can use the integrated MM-equation to fit the data set and extract kinetic parameters. MM assumes steady state conditions, which means that the binding steps at the catalytic site are faster than the rate of change of the surface composition.

Two limit cases of the interfacial enzyme working on vesicles can be assumed: First, the enzyme is working in the scooting mode with high processivity (Fig.1.6). The residence time of the enzyme at the vesicle interface is very long compared with the time for a single turnover

and the enzyme stays at the surface, even if all the substrate is converted. In the scooting mode the overall rate of the enzymatic process is not influenced by the absorption/desorption of the enzyme from the interface in between the catalytic turnover.

The other extreme mode of action would occur, when the enzyme leaves the interface after each turnover cycle with no interfacial processivity in the hopping mode (Fig.1.6). The rate constants  $k_d$  and  $k_b$ , describing the binding and the dissociation of the enzyme from the interface will be part of the overall rate of the catalytic turnover.

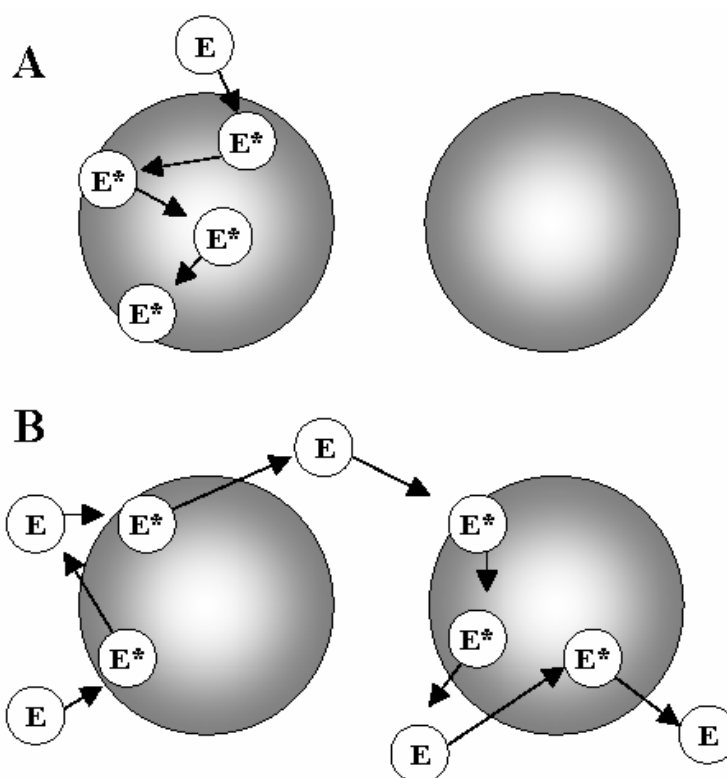


Figure 1.6 Two extreme cases of the mode of action for an interfacial catalysis on vesicles are sketched. A: 'Scooting mode': The enzyme working in the scooting mode does not leave the surface, even if all substrate is converted. B: 'Hopping mode': The enzyme is working with zero processivity and would leave the interface after each catalytic cycle. The Sketch was adapted from (87)

However, kinetics cannot be described when the residence time of the enzyme at the interface is unknown, when it is not constant over the time course of the reaction progress, or when the zero processivity condition cannot be unequivocally established (89). The process of desorption and adsorption of the enzyme to the bilayer is described by  $k_d$  and  $k_b$ , respectively.

This process modifies the amount of  $E_{\text{total}}$  for the MM-formalism. These parallel kinetic processes, which influence the overall rate of the catalytic turnover need to be eliminated or at least explicitly considered to allow to study the kinetic rate constants of the interfacial catalysis.

Thus, to be able to calculate kinetic parameters of the interfacial enzyme kinetics, the following constraints need to be fulfilled (87, 88):

- (i) All enzyme molecules are bound to vesicles.
- (ii) The integrity of vesicles is maintained during the course of the reaction.
- (iii) The substrate, enzyme and products do not exchange neither between vesicles nor across the bilayer.
- (iv) The uniformity of the environment that the enzyme molecules “see” during the course of hydrolysis must be ensured.

If these conditions are met, it is possible to compare the features of interfacial catalysis to the standard treatment of enzyme kinetics, as it is applied to numerous cases of water-soluble substrates. Then, the integrated MM equation can be used to fit the data set, and kinetic parameters can be extracted (88).

### 2 Motivation of the study

As detailed in the previous chapter, plasma membrane SM is hydrolysed by SMase to yield Cer and phosphocholine during specific stress conditions. Cer is involved in several vital cell processes, most likely due to the modulation of the membrane structure. Previous studies have shown that the morphological changes in model membranes resemble very much those occurring during apoptosis. However, the structural and dynamic processes within these membranes are mainly unknown.

The aim of the present study was to relate the dynamic molecular compositional changes to structural kinetics evolving on the membrane level. This was achieved by a combination of time-resolved X-ray scattering and chromatography. Further, these changes needed to be correlated to the phase behaviour of the model system under equilibrium conditions. Hence, a broad combination of biophysical techniques was applied to determine the corresponding phase diagram.

The subsequent chapter describes the applied materials and methods. The results and discussion are presented in the chapters 4 and 5, and the resulting papers of this thesis can be found in chapter 8.

### 3 Materials and Methods

This study was performed on a model system, which consists of two parts:

I Lipid part (liposomes)

II Protein part (bacterial SMase)

#### 3.1 Lipid model membranes

Lipid membranes define the entity of cells and organelles. Biological membranes are a 'meeting point for lipids and proteins' (90) and play an important role in many biological processes, like transport processes and signal transduction. In 1972, Singer, S.J. and Nicholson, G.L. presented their Fluid-Mosaic-Model (91), in which the membrane lipids were regarded as a fluid matrix for the membrane proteins. But if this would be the only function of the membrane lipids, why would nature use so many different lipid species? (92). Verkleij, A.J. et al. (93) showed in the year 1973 that lipids are asymmetrically distributed between the two leaflets of biological bilayers and that microdomain formation occurs. These microdomains can serve as spatio-temporal platforms for signalling molecules (94).

To gain a molecular-level understanding of the membrane processes, mainly during the conversion of one single membrane component into another, and of the consequences on the overall membrane structure, it is necessary to eliminate the manifold parallel influences coming from the interactions of the various kinds of membrane components among each other. This can be done by studying artificial lipid bilayers, consisting of two or three different lipid species. In this work, a lipid model system, composed of POPC, SM and Cer was used to mimic the plasma membrane.

##### 3.1.1 General aspects

Liposomes are hollow spheres made up of lipid bilayers and they include water. These lipid aggregates form in excess water and can be unilamellar vesicles (ULVs), oligolamellar vesicles (OLVs) or multilamellar vesicles (MLVs), dependent on the bilayer interactions and preparation technique. MLVs are onion like structures, which can have a size of several hundreds nm in diameter and consist of several hundred correlated bilayer stacks. ULVs in

### 3 Materials & Methods

contrary are bordered by one single lipid bilayer and OLVs are built up by a few stacked bilayers. ULVs can be prepared from MLVs by extrusion and can be classified according to their size: Small unilamellar vesicles (SUVs) have a diameter of about 25 nm, large unilamellar vesicles (LUVs) of about 100 to 250 nm and giant unilamellar vesicles (GUVs) are bigger than 250 nm.

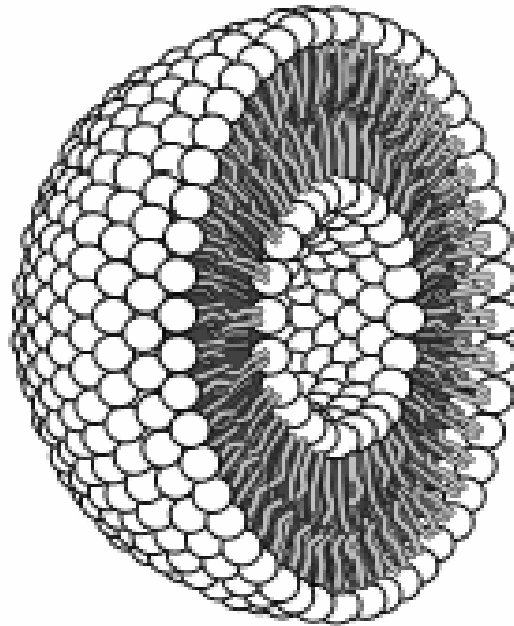


Figure 3.1 Schematic presentation of a liposome, adapted from [http://en.wikipedia.org/wiki/Lipid\\_bilayer](http://en.wikipedia.org/wiki/Lipid_bilayer)

Biological membranes are built up by a large variety of lipid species, which differ in their backbones, head groups, length and saturations of the fatty acid chains. An overview of the different lipid molecules and their classification according to the lipid backbone is presented in Fig.3.2.

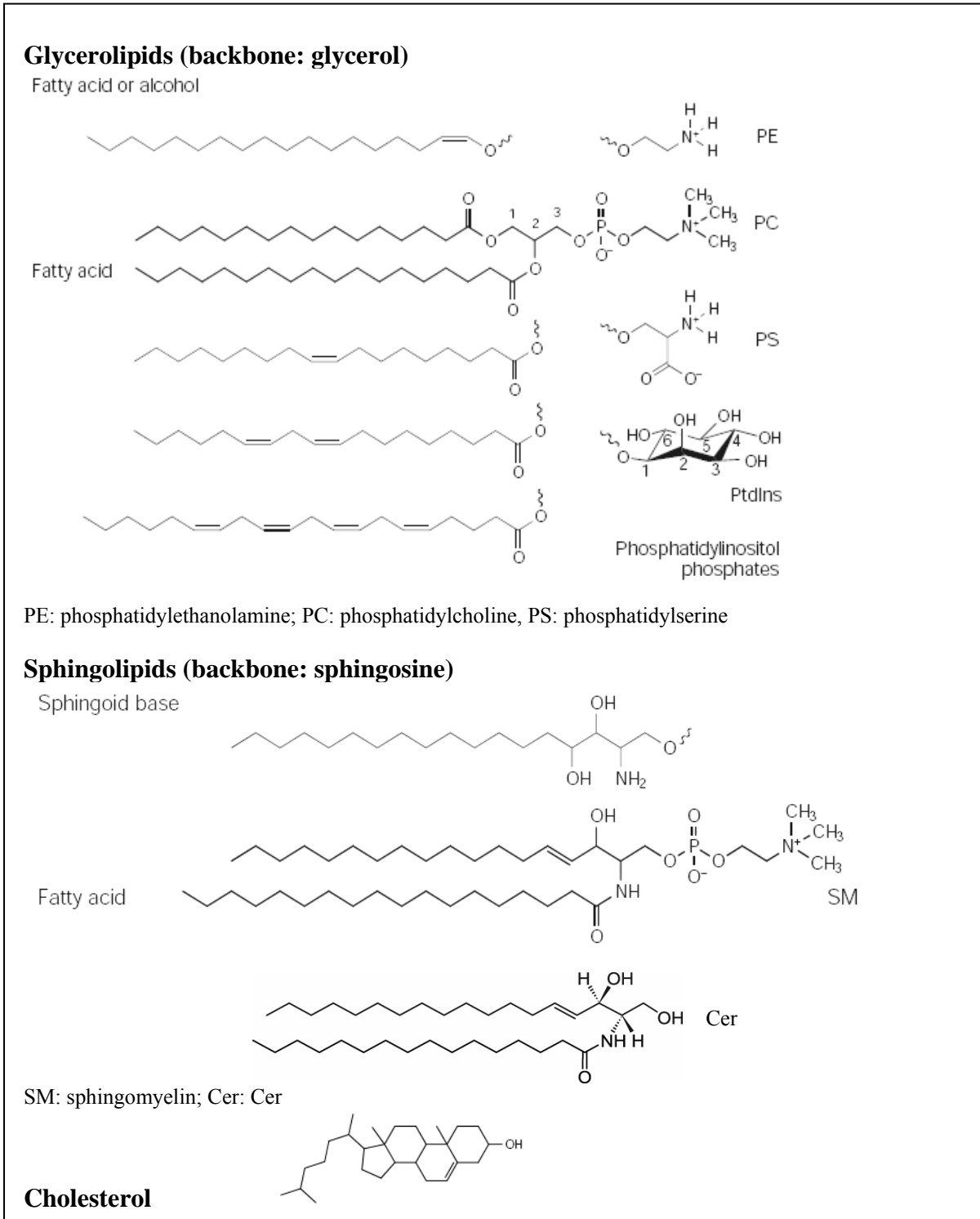


Figure 3.2 Classification of membrane lipids, adapted from (38)



Lipids are amphipathic molecules, consisting of a hydrophilic headgroup and hydrophobic tails, as sketched in Fig.3.3.

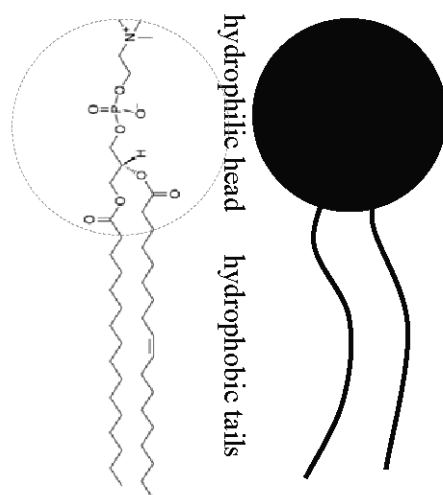


Figure 3.3 Scheme of an amphipathic lipid molecule

At concentrations above the critical micellar concentration (*cmc*) ( $10^{-8}$  to  $10^{-10}$  M) in aqueous solution these molecules self-assemble and form a variety of ordered structures.

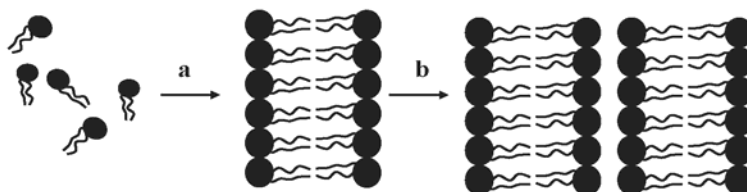


Figure 3.4 Hydrophobic effect leads to aggregation (a) of the single lipid molecules in an aqueous environment to bilayer structures, which assembly into multilayer arrays (b). The sketch was adapted from (7).

Hydrophobic effects are responsible for the aggregation of single lipid molecules in an aqueous environment. Aggregation minimizes the contact of the hydrophobic acyl chains with water, which would induce more ordered water structure and therefore would lead to a net increase of the free energy. The free energy cost is minimized, however, if the hydrophobic portions of a molecule cluster together (Fig.3.4).

These lipid aggregates form higher molecular assemblies, which are held together by non covalent forces and exhibit a great variety of different kinds of organized structures, depending on


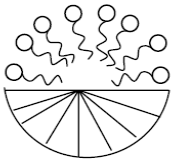

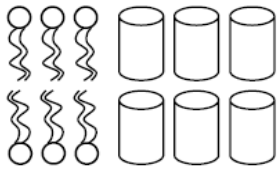

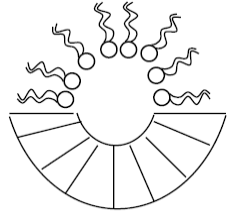
- (i) the shape of the lipid molecules
- (ii) temperature
- (iii) concentration
- (iv) degree of hydration
- (v) pressure
- (vi) ionic strength
- (vii) pH of the aqueous environment

A crucial factor for the geometrical organization of the lipid assemblies is the shape of the lipid molecules themselves. Therefore Israelacchvili (95) introduced the critical packing parameter P, defined as

$$P = \frac{v}{(A \cdot l)} \quad (1)$$

where  $v$  is the volume of the hydrocarbon chains,  $l$  the chain length and  $A$  the area per headgroup. The effect of the molecular shape on the packing properties of phospholipids is overviewed in Tab3.1.

Table 3.1 Packing properties of phospholipids depending on their molecular shape.

Species	P	Shape	Organisation
Soaps Detergents	0.3- 0.6	inverted cone 	
Phosphatidylcholine Phosphatidylserine Sphingomyelin	~1	Cylinder 	
Phosphatidylethanolamine Cholesterol Ceramide	>1	Truncated cone 	

Molecules with  $P < 0.3 - 0.6$ , like detergents or soaps, have a conical shape and tend to form micellar structures. Cylindrical molecules, like phosphatidylcholine and sphingomyelin with a packing parameter of  $\sim 1$  form lamellar structures. These lamellar structures are flat for  $P = 1$  and can be bent in any direction when the value differs from 1. Packing parameters bigger than 1 belong to lipid molecules with a small headgroup, like Cer. These lipids have a conical molecular shape and form inverted phases.

#### 3.1.2 Phase transitions

Aqueous phospholipid dispersions show temperature dependent phase transitions at a given degree of hydration. This polymorphism of phospholipid bilayers was classified by Luzzati (96) in the following way:

The lattice type is given by a capital letter (L = lamellar, H = hexagonal, Q = cubic). Normal (oil in water) or reversed phases (water in oil) are denoted with the subscripts I and II. The chain configuration is indicated by inferior letters ( $c$  = crystalline,  $\beta$  = ordered gel-like,  $\alpha$  = liquid-like,  $\delta$  = helical coiled) and the tilt of the acyl chains with respect to the bilayer normal is denoted by a superior dash (e.g.  $L_{\beta}'$  = lamellar gel phase with tilted acyl chains).

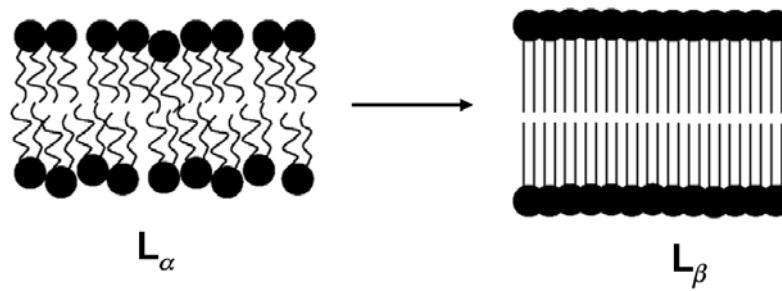


Figure 3.5 Transition from the fluid phase ( $L_\alpha$ ) to the gel phase ( $L_\beta$ )

The phase generated in the presence of Cer in a lamellar fluid POPC/SM bilayer at physiological temperature is the lamellar gel phase  $L_\beta$  (Fig.3.5).

### 3.1.3 Bilayer interactions

A multi lamellar aggregation of lipids is determined by an interplay of various forces between the adjacent correlated bilayers (97). In general, these forces can be attractive or repulsive and they will be shortly discussed in the following.

Steric repulsive forces are considered as hard sphere interactions, and they have the smallest coverage between adjacent bilayers.

Hydration forces are repulsive forces as well. They exhibit an exponential decay with bilayer separation  $d_w$  with a decay length between 1 and 3 Å. Their origin is not known yet, but they may arise due to the perturbation of the water at the lipid surface or from the protrusion mode of single lipid molecules. Hydration forces can be determined experimentally by osmotic pressure experiments in combination with X-ray scattering and their free energy is given by

$$f_h(d_w) = \lambda_h P_h e^{-\frac{d_w}{\lambda_h}} \quad (2)$$

where  $\lambda_h$  is the decay constant of the hydration forces and  $P_h$  a scaling constant.

The dominant and single attractive force between correlated lipid bilayers is the van der Waals force, which is caused by charge fluctuations. The van der Waals interaction free energy can be approximated by

$$f_{vdW}(d_w) \cong -\frac{H}{12\pi} \left( \frac{1}{d_B^2} + \frac{2}{(d_B - 2d_w)^2} - \frac{2}{(d_B + d_w)^2} \right). \quad (3)$$

$H$  is called Hamaker constant and is usually in the range from  $10^{-20}$ - $10^{-21}$  J and  $d_B$  is the bilayer thickness.

The van der Waals attraction between adjacent bilayers within a bilayer stack can be completely overcome by electrostatic repulsion forces in case of charged bilayers and leads to the spontaneous formation of ULVs.

Bilayer undulations within a bilayer stack also lead to repulsive interaction within the multilamellar lipid system, depending on temperature and bilayer rigidity (98).

#### 3.1.4 Liposome preparation:

POPC, Egg-SM, and C16:0-Cer (N-palmitoyl-D-*erythro*-sphingosine) were purchased from Avanti Polar Lipids (Alabaster, AL, USA) and used without further purification. All other chemicals (salts, solvents in pro analysis quality) and polyethylene glycol (PEG,  $M_w = 8000$  g/mol) were from Sigma-Aldrich. 18 M $\Omega$ /cm water (UHQ PS, USF Elga, Wycombe, UK) was used for all liposomal preparations. Two different types of samples were prepared. The first type was a lipid suspension of MLVs with a known amount of Cer in a POPC/SM mixture. The second sample type was a lipid suspension of LUVs composed of a binary, equimolar mixture of POPC and SM, which was used for the enzyme reaction studies.

#### Multilamellar vesicles

Lipid stock solutions were prepared by dissolving weighted amounts of dry lipid powder in chloroform/methanol (2/1, v/v). The appropriate volumes of the stock solutions were mixed and the organic solvent was evaporated at room temperature under a gentle stream of nitrogen. The samples were then placed under vacuum for at least 12 h to form a thin lipid film on the bottom of glass vials. The dry lipid films were suspended in water for the IR experiments and in Napi buffer (20mM NaPi, 130 mM NaCl, pH = 7.4) for the X-ray and DSC experiments and incubated for 4 h in the fluid phase of the system with intermittent vigorous vortex mixing. At least 8 freeze-thaw circles were performed. The final lipid concentrations of the MLV suspensions were 1 mg/ml for DSC measurements, 200 mg/mL for steal-capillary DSC experiments, 20 mg/ml for the IR and 50 mg/ml for X-ray diffraction experiments.

#### Unilamellar vesicles

MLV suspensions were prepared as described above, but hydrated in 10 mM HEPES buffer (200 mM NaCl, 2 mM MgCl<sub>2</sub>, 10 mM CaCl<sub>2</sub>, pH = 6.8). The total lipid concentration of the liposomal dispersions was 50 mg/ml. The POPC/SM MLVs were then transformed into monodisperse large unilamellar vesicles (LUVs), by extrusion through a 100 nm membrane filter (Nucleopore, Whatman International Ltd. Maidstone, UK). The LUVs were subsequently concentrated to about 70 mg/ml by centrifugation through a pre-rinsed centricon centrifugal filter device with a Ultracel YM-30 membrane (Millipore, Carrigtwohill, Co. Cork, Ireland) (30 000 NMWL, 4500g, 20 min). The average LUV size was 1200 Å with a polydispersity index < 0.1 as determined by photon correlation spectroscopy (PCS).

### 3.2 Neutral Sphingomyelinase

Sphingomyelinase (SMase) or *sphingomyelin-phosphodiesterase* is a specific divalent metal-ion dependent phospholipase C (E.C 3.1.4.12). It catalyses the hydrolysis of membrane bound sphingomyelin to Cer and water soluble phosphocholine (99). The activation of SMase is part of a major lipid signalling pathway (46) and can be induced by several ways, like tumor necrosis factor- $\alpha$  (TNF- $\alpha$ ), Fas-ligand and various chemotherapeutic agents (56, 99). SMase is an interfacial enzyme and therefore, the catalytic turnover takes place at the lipid-water interface (88, 89), where it is fully active as a 34 kDa monomer (87). According to (100, 101), Sphingomyelinases can be classified into the following categories:

- (i) Acidic SMase (aSMase)
- (ii) Secretory SMase (sSMase)
- (iii) Neutral  $Mg^{2+}$ -dependent SMase (nSMase)
- (iv) Neutral  $Mg^{2+}$ -independent SMase
- (v) Alkaline SMase
- (vi) bacterial SMase

Acidic SMase has a pH optimum of about 5 and is found mainly in the acidic environment of lysosomes. Lack of aSMase causes a neurological disorder, known as Niemann-Pick disease (102).

The sSMase is another form of an acidic enzyme. It derives from the same precursor as aSMase, but is targeted rather to the Golgi secretory pathway than to lysosomes (103). It might play a role in signal transduction via the SM pathway (104).

$Mg^{2+}$ -dependent nSMases are integral membrane proteins in mammals and soluble proteins in bacteria.  $Mg^{2+}$ -independent nSMase is of unknown function and located in the cytoplasm (105). As integral membrane protein, nSMases are performing the Cer production within the membranes and have pH optima near 7. Neutral SMases appear to be ubiquitous in mammalian tissues. A number of nSMase-isoforms with different biochemical and chromatographical properties exists (106). A review on the physiological aspects of neutral SMases is given in (99).

### 3 Materials & Methods

Alkaline SMase resides in bile and the digestive tract (46). and intestinal alkaline SMase may have antiproliferative effects on colon cancer cells (107)

A whole group of SMases exists in bacteria and have been isolated from a variety of organisms, like *Bacillus cereus*, *Staphylococcus aureus* and others (108-110). Neutral SMase from *Bacillus cereus* is the best characterized amongst them (108, 111-113) and was therefore taken as a model enzyme for the poorly characterized mammalian nSMase in this study. The expression of the gene encoding for the *Bacillus cereus* nSMase was first performed in the year 1988 in *E. coli* (108). Once the sequences of this bacterial enzyme were known, a number of other SMases were identified. Only about 20% of the sequence of mammalian, yeast and bacterial SMases are identical, but the similarity of certain residues in the catalytic region of the enzymes (109, 112) suggests a common catalytic mechanism for the nSMase family (111). The crystal structure of the neutral sphingomyelinase from *Bacillus cereus* was solved in 2006 (111) and is shown in Fig 3.6.

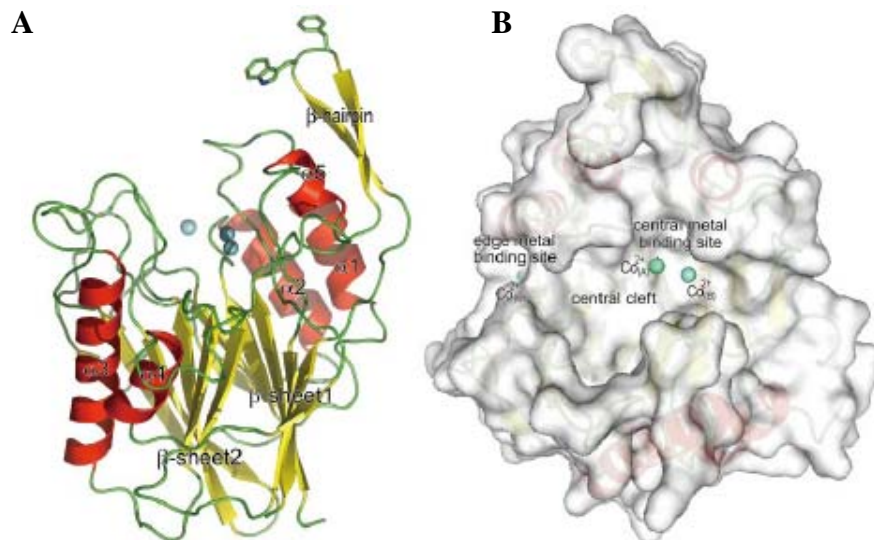


Figure 3.6 A: Ribbon presentation of the overall structure of SMase from *Bacillus cereus*, taken from (111).  $\alpha$ -Helices,  $\beta$ -sheets, and loops are colored in red, yellow, and green, respectively. The bound  $\text{Co}^{2+}$  ions are shown as blue spheres. B: Water-accessible surface of the  $\text{Co}^{2+}$ -bound *Bc*-SMase, superimposed on the ribbon representation.

The relative catalytic activities depend on the type of metal ion bound to the active site. A high activity is found in the presence of  $\text{Co}^{2+}$ ,  $\text{Mn}^{2+}$ , and  $\text{Mg}^{2+}$ , whereas the activity decreased when  $\text{Ca}^{2+}$  and  $\text{Sr}^{2+}$  are bound.



### 3 Materials & Methods

The overall structure of *Bc*-SMase consists of  $\alpha/\beta$  motifs and is independent of the type of metal ion bound. One characteristic feature is the hydrophobic  $\beta$ -hairpin-structure, which has hydrolytic activity and is needed for the binding of *Bc*-SMase to the cell membrane (111, 114). On the basis of the crystal structure it was proposed that SM hydrolysis proceeds by acid–base catalysis through a pentavalent phosphorus transition state (111).

As *Bc*-SMases carry out processive catalytic turnover at the lipid–aqueous environment interface (87), they need to bind to the membrane to perform their catalytic action. Bacteria may use SMases to invade eukaryotic cells (114, 115) and their SMases are able to bind on the cell surface. A binding model of the fully active SMase monomer at the interface between the SM membrane and the aqueous environment was presented by (111), (Fig 3.7).

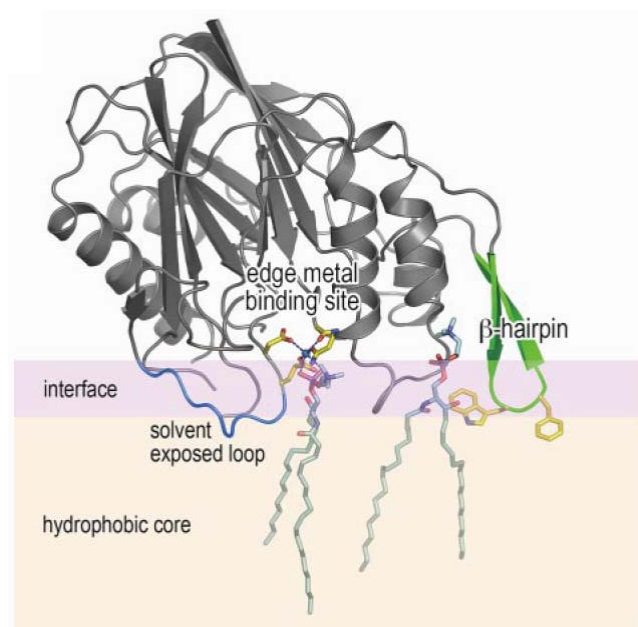


Figure 3.7 Binding model of *Bc*-SMase to the SM membrane. The enzyme is shown as a ribbon model. Solvent exposed loop: Blue,  $\beta$ -hairpin: Green. The amino acid residues participating in the edge metal-binding site and the exposed aromatic amino acid residues of Trp-284 and Phe-285 are shown by the stick models with yellow carbons. The bound metal ion at the edge metal-binding site is coloured in blue. The bound SMs are shown as stick models with cyan carbons. The binding model was taken from (111).

The enzyme activity of bacterial SMase is highly dependent on the physical membrane state (84). It increases by several orders of magnitude when the lipid matrix goes from the gel to the liquid crystalline state (85, 116). Thus the activity is dependent on the membrane

### **3 Materials & Methods**

composition, because the lipid components of a membrane determine the physical membrane state (45) at a given temperature (working temperature of the enzyme). In mixed PC/SM vesicles, the lag time of the SMase catalyzed reaction strongly depends on the SM to PC ratio of the vesicle (85). The influence of the physical membrane state on the enzyme activity suggests a connection with the lateral pressure acting on the enzyme (117). A review on enzymology and membrane activity is given in (45).

### 3.3 Differential Scanning Calorimetry (DSC)

DSC experiments give the change of the heat capacity of the sample as a function of the temperature. Therefore, the obtained thermograms reveal informations about the thermotropic behaviour of the sample.

DSC measurements were performed on a MicroCal VP-DSC high-sensitivity differential scanning calorimeter (MicroCal, Northhampton, MA, USA). The samples with Cer were performed with steel capillary inserts. 10  $\mu\text{l}$  of the lipid dispersion were poured into stainless steel capillaries, which were sealed with nylon plugs and subsequently inserted into the calorimeter cell containers. The cell containers were filled with a glycerol solution to prevent freezing of the cell content. Each DSC experiment consisted of three heating and three cooling scans. Samples were tempered for 30 min before each heating and cooling scan, respectively. The scan rate for all experiments was 0.5°C/min. MicroCal's Origin software (MicroCal) was used for data acquisition and analysis throughout. The phase-transition temperatures were derived from the temperatures at the peak maximum of the heat capacity ( $c_p$ ) versus temperature curve (118). The total lipid concentrations of the samples were 1 mg/ml for the DSC measurements without steel capillary and 200 mg/mL for steel capillary DSC experiments.

### 3.4 Small- and Wide-Angle X-ray Scattering (SWAXS)

X-ray scattering provides an insight into membrane structures via the electron density distribution. The measurement principle is based on the elastic interaction of X-ray radiation (CuK $_{\alpha}$  radiation,  $\lambda = 1.54 \text{ \AA}$ ,  $E = 8 \text{ keV}$ ) with the electrons of the sample. The thus accelerated electrons emit radiation as spherical waves, which can interfere constructively with each other and therefore cause diffraction peaks. The resulting scattering pattern represents the electron density distribution in the sample.

If the sample contains no ordered structure (i.e. a lipid suspension of ULVs) no interference effects occur and a diffuse scattering pattern is obtained. According to Bragg's law  $n\lambda = 2d \sin\theta$ , the dimensions of an object are reciprocal to the angles to which the X - rays are scattered. Thus a scattering pattern reveals details about the long range positional correlations

within the sample with spacings from 10 Å to 1500 Å in the small-angle range and information about short range organization (between 3 Å and 5 Å) in the wide-angle range.

#### 3.4.1 X-ray scattering measurements with samples of well defined composition measured in equilibrium (laboratory X-ray source)

SWAXS experiments were performed on a SWAXS camera (System 3, Hecus X-ray Systems, Graz, Austria). The X-ray camera was mounted on a sealed-tube generator (GE-Seifert, Ahrensburg, Germany) operating at 2 kW.  $\text{CuK}\alpha$  radiation ( $\lambda = 1.542 \text{ \AA}$ ) was selected using a Ni filter in combination with a pulse height discriminator. The X-ray beam size was set to 0.5 mm x 3.5 mm (V x H). The SWAXS patterns were recorded using two linear, one-dimensional, position-sensitive detectors (PSD 50, Hecus X-ray Systems, Graz, Austria) for the wave vector ( $q = 4\pi \sin\theta/\lambda$ ) of  $10^{-3} \text{ \AA}^{-1} < q < 1 \text{ \AA}^{-1}$  (SAXS) and  $1.2 \text{ \AA}^{-1} < q < 2.7 \text{ \AA}^{-1}$  (WAXS). Samples were filled in 1-mm thin-walled quartz-glass capillaries in thermal contact with a programmable Peltier unit and were equilibrated for 10 min at each temperature before measurement. Exposure times were 3600 s simultaneously for SAXS and WAXS. Calibration in the wide-angle region was performed with para bromo-benzoic acid (119) and in the small-angle region by the use of silver-stearate ( $d = 48.68 \text{ \AA}$ ).

From the background corrected small-angle X-ray data the lamellar repeat distances were derived by applying a full  $q$ -range model (120) for all Cer concentrations smaller than 35 mol%. The sample with 35 mol% Cer showed a distinct phase separation in the small angle range and thus the lamellar repeat distances were derived from  $d = 2\pi n/q_n$ , where  $n$  is the order-number of the appropriate peak and  $q_n$  the peak maximum of the SAXS Bragg peak of this particular order.

The background corrected WAXS peaks were fitted with Lorentzians, from where we took the full width at half maximum ( $\Delta q$ ) and the center of the peak ( $q_{11}$ ) to calculate the area per lipid chain, given by  $A_c = 8\pi^2 / (\sqrt{3} \cdot q_{11}^2)$  and the correlation length as value for the domain size (121)  $L = 2\pi / \sqrt{\Delta q_{corr}}$ .  $\Delta q_{corr}$  is the full width at half maximum (FWHM) of the corresponding peak corrected with the FWHM of the vertical beam profile.

#### 3.4.2 X-ray scattering experiments on osmotically stressed samples (synchrotron radiation)

Synchrotron small- and wide-angle X-ray diffraction experiments were performed at the Austrian SAXS beamline at Elettra (Trieste, Italy) (122, 123) using 8 keV photons and a sample to detector distance of 1.126 m with typical exposure times of 2 min. SAXS patterns were recorded with a mar345 image plate detector. A one-dimensional position sensitive detector was used to measure the WAXS signal. Samples were contained in 1 mm quartz-glass capillaries and equilibrated at 37°C for 10 minutes prior to exposure. Primary data reduction was performed using ([http://www.esrf.eu/computing/scientific/FIT2D/FIT2D\\_INTRO/fit2d.html](http://www.esrf.eu/computing/scientific/FIT2D/FIT2D_INTRO/fit2d.html)), (124). Electron density profiles were derived from the integrated Bragg intensities of background corrected SAXS patterns using standard techniques (120). The membrane thickness  $d_B$  was defined as  $d_{HH} + 10 \text{ \AA}$  (125), where  $d_{HH}$  is given by the distance between the two maxima of the electron density profile. The bilayer separation for a given osmotic pressure is then given by  $d - d_B$ , where the lamellar repeat distance  $d$  is calculated from the Bragg peak positions.

#### 3.4.3 Time-resolved X-ray studies (synchrotron radiation)

Time-resolved SWAXS experiments were performed at the above mentioned beamline using two linear one-dimensional gas detectors, covering the scattering vectors  $q$  from  $0.01 \text{ \AA}^{-1}$  to  $0.6 \text{ \AA}^{-1}$  and  $0.67 \text{ \AA}^{-1}$  to  $1.95 \text{ \AA}^{-1}$ , respectively. Samples containing SMase were prepared by manual mixing of LUV suspension (30  $\mu\text{L}$ ) and enzyme solution (70  $\mu\text{L}$ ). The enzyme solution was obtained by dissolving 10 U of nSMase in 70  $\mu\text{L}$  10 mM HEPES buffer (200 mM NaCl, 2 mM  $\text{MgCl}_2$ , 10 mM  $\text{CaCl}_2$ , pH = 6.8), which contained additionally 2 mM o-phenanthroline to inhibit traces of contaminant phospholipase C activity of the enzyme (82). Reaction batches were rapidly transferred into the sample holder and measurements were started about 70 seconds after mixing enzyme and lipids. Diffraction patterns with an exposure time of 10 s were taken every minute. No signs of radiation damage were observed during and after all experiments. Changes of the acyl chain-correlation peak-intensities during the enzyme reaction were obtained by first removing high frequency noise from the WAXS data as described in (126). A constant background was defined by a linear fit in a

narrow range of the WAXS gel peak and subsequently subtracted from the WAXS data. The resulting peak parameters were derived from Lorentz fits. Similarly, first order Bragg peaks of the SAXS patterns were analyzed using Lorentz functions. The full width at half maximum of the peaks  $\Delta q$  was corrected for the instrumental resolution  $\delta q = 2.2 \times 10^{-3} \text{ \AA}^{-1}$  and used to calculate the average domain size  $L$  (see above). Finally, the average number of layers was derived from the SAXS data, applying  $N_{layer} = L_{SAXS} / d$ , where  $d$  is the lamellar repeat distance. The average number of lipids per gel phase domain was estimated from  $N_{lip} = L_{WAXS} / \sqrt{A}$ , where the lateral area per lipid was given from the WAXS peak position as  $A = 16\pi^2 / (\sqrt{3}q_{11}^2)$ , (127).

### 3.5 Osmotic stress experiments

Osmotically stressed samples were prepared by centrifuging the fully hydrated MLVs and subsequent removal of the supernatant. The supernatant was replaced by a polyethylene glycol solution ( $M_w = 8000 \text{ g/mol}$ ) of a given concentration and the sample was left to equilibrate for at least two days. Osmotic pressures of a given PEG solutions as a function of temperature were determined using a Knauer (Berlin, Germany) vapor pressure osmometer.

Analysis of Equation of State: In the present system, the applied osmotic pressure was calculated as follows:

$$\Pi = -\frac{H}{6\pi} \left( \frac{1}{d_w^3} - \frac{2}{(d_w + d_B)^3} + \frac{1}{(d_w + 2d_B)^3} \right) + P_h e^{-\frac{d_w}{\lambda_h}} + \frac{k_B T}{32\lambda_h} \sqrt{\frac{P_h}{K_C \lambda_h}} e^{-\frac{d_w}{2\lambda_h}} \quad (4)$$

The first term represents the van der Waals attraction, the second term the hydration repulsion and the third term the steric repulsion due to bilayer undulations, with  $H$  being the Hamaker constant,  $P_h$  a scaling constant,  $\lambda_h$  the decay constant of the hydration forces and  $K_C$  the bilayer bending rigidity (128). A second form for the fluctuation contribution has been proposed, which differs essentially from the present form by using a separate decay constant,  $\lambda_{fl}$  (129). However, its application requires the evaluation of Bragg peak line shapes, which is impeded by the overlapping reflections of the phase separated

system. It has been demonstrated that this has little effect on the bending rigidity, (130, 131).

#### Geometric Model for Ion Channels

Changes of the bending rigidity result in alterations within the lateral pressure profile of the bilayer (Fig.3.8). This can affect the activity of membrane proteins.

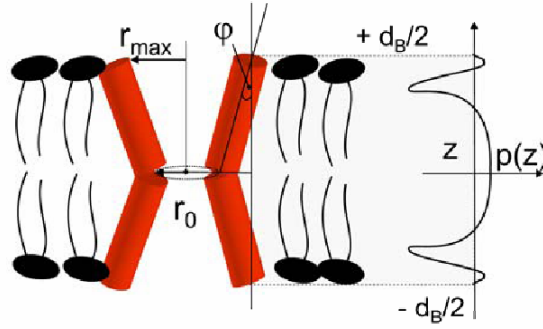


Figure 3.8 Effect of present lateral pressure changes on the activity of ion channels. Pore radius  $r_0$  and maximum radius  $r_{max}$ . Opening is achieved by decreasing the angle  $\phi$ , while keeping  $r_{max}$  constant. A schematic of the lateral pressure profile is presented on the right side.

A conformational change of membrane proteins depends on the volume change of the protein and the lateral pressure density  $p(z)$  of the lipid bilayer along the bilayer normal  $z$ , against which the protein either expands or contracts laterally (132). The fraction  $f$  of active states at a given  $p(z)$  relative to an initial lateral pressure density  $p_0(z)$  can be calculated as follows (133):

$$f = \frac{1 + K_0}{(1 + K_0 e^\alpha)} \quad (5)$$

where

$$\alpha = (k_B T)^{-1} \int_{-d_B/2}^{d_B/2} \Delta p(z) \Delta A(z) dz \quad (6)$$

$K_0 = [r]_0/[a]_0$  is the conformational equilibrium of the initial protein state, i.e. the fraction of the resting protein  $[r]_0$  with respect to the fraction of proteins in the open state  $[t]_0$ , prior to the change of the lateral pressure profile.  $\Delta A(z)$  is the involved lateral change of the protein area. For smoothly varying cross-sectional changes Eq. 7 can be further simplified to

$$\alpha = (k_B T)^{-1} \sum_j \Delta a_j \Delta P_j \quad (7)$$

where  $\Delta a_j$  refers to the coefficients in a power expansion of  $\Delta A$  in  $z$ , and  $\Delta P_j = \int_0^{d_B/2} z^j \Delta p(z) dz$  is the change in the  $j^{\text{th}}$  integral moment of the lateral pressure density  $p(z)$ . For the given geometric model of an hourglass-shaped ion-channel with a central pore-opening, we thus arrive at

$$\alpha = \frac{2\pi}{k_B T} \left[ (2r_{\max} \Delta \tan \varphi - d_B \Delta \tan^2 \varphi) \Delta P_1 + \Delta \tan^2 \varphi \Delta P_2 \right] \quad (8)$$

where  $r_{\max}$  is the outer radius of the pore,  $\varphi$  the angle of the bend helix with the bilayer normal (Fig. 4A) and  $\Delta P_1$  and  $\Delta P_2$  are the changes of the first and second integral moments of  $p(z)$ .

### 3.6 Fluorescence microscopy

Rhodamine-dipalmitoyl phosphatidylethanolamine from Invitrogen (San Diego, CA) was added to the POPC/SM/Cer mixture at a concentration of 0.5 mol%, and giant unilamellar vesicles (GUVs) were prepared by electroformation (121). Fluorescence imaging was performed on a Leica DMIRE2 inverted microscope (Solms, Germany) using a metal halide lamp for sample illumination. Images were captured using a CoolSNAP ES<sub>2</sub> camera from Photometrics (Tucson, AZ). The fluorescence microscopy experiments were done in cooperation with Bibhu R. Sarangi and Velayudhan A. Raghunathan at the Raman Research Institute, Bangalore, India.

### 3.7. Attenuated Total Reflection Fourier Transform Infrared Spectroscopy (ATR-FTIR)

Experiments with ATR-FTIR spectroscopy were performed in collaboration with Zoran Arsov from the Jozef Stefan Institute, Ljubljana, Slovenia. The IR spectra, which result from the resonant absorption of IR radiation by the sample, give information about the vibrational modes within the molecules. The penetration depth of infrared light into the sample is a few hundred nanometers. ATR-FTIR measurements allow to study the lipid acyl chain



conformation (methylene band) and the properties at the water-lipid interface (amide and carbonyl band) can be studied. ATR-FTIR spectra were recorded on a Vertex 70 infrared spectrometer (Bruker Optics, Ettlingen, Germany) equipped with a liquid nitrogen cooled mercury-cadmium telluride detector and fitted to a Horizon ATR unit (Harrick Scientific, Pleasantville, NY, USA). The internal reflection element (IRE) was a trapezoidal germanium ATR plate (50 x 10 x 2 mm) with an incidence angle of 45° yielding 25 internal reflections (New Era Enterprises, Vineland, NJ, USA). 16 scans were averaged for each spectrum. Spectra were recorded at a nominal resolution of 2 cm<sup>-1</sup>. The spectrometer and the ATR unit were continuously purged with dry nitrogen gas. The holder for the IRE was placed in contact with an aluminum block and the temperature was controlled by a circulating water bath connected to the sample mount. The germanium IRE was cleaned just before use sequentially with distilled water and ethanol. After that, 200 µl of liposome suspension were added onto the IRE and spread over the whole area. Thin lipid stacks were obtained by evaporating water. Dried lipid stacks were rehydrated by the addition of 300 µl of pure deuterated water (D<sub>2</sub>O) and incubated at a temperature that ensured the lipids to be in the fluid phase to allow a complete hydrogen-deuterium exchange as judged from the complete disappearance of the amide II band. Analysis of ATR-FTIR spectra was done using the software package OPUS, Version 5.5 (Bruker Optics, Ettlingen, Germany). To examine a particular region of the ATR-FTIR the spectra were cut to an appropriate frequency range and subsequently baseline corrected with a straight line. Peak positions were determined as points with the maximum amplitude in the corresponding absorption bands. The half-bandwidth of the absorption bands was determined as the width of the band at half the maximum amplitude.

#### 3.8 Photon Correlation Spectroscopy (PCS)

PCS exploits the principles of dynamic light scattering. The scattered light is detected at an angle of 90° by a photodiode coupled to a correlator. Applying an auto-correlation function leads to the size distribution curve of the particles in the suspension and the obtained parameters are the average particle size ( $Z_{AV}$ ) and the size distribution (PDI) of the particles. Changes of these parameters during the enzyme reaction were determined with a zetasizer 3000 HAS (Malvern Instruments, Herrenberg, Germany). The instrument

is equipped with a 10 mW helium-neon laser operating at 632.8 nm. All samples were filtered through a 0.02  $\mu\text{m}$  membrane filter unit (Anotop 25, Whatman International Ltd. Maidstone, U.K.) before measurement to avoid artifacts from dust particles. During the enzyme reaction PCS measurements were performed every 10 minutes.

#### 3.9 High Performance Thin Layer Chromatography (HPTLC)

HPTLC leads to separation of the different analytes on the plate due to different ascending rates at the plate. The analytes were assigned in the presence of standard substances and quantified according to the peak size and area.

HPTLC was performed on a fully automated system from CAMAG (Muttensz, Switzerland). HPTLC-plates (silica gel 60 F 254) were from Merck (Germany) and samples were sprayed automatically with 150 nL/s. During the experiment, well-defined amounts of the aqueous reaction batch were transferred into organic stop-solution ( $\text{CHCl}_3/\text{MeOH} = 2/1$ ) and rigorously vortex mixed for at least 3 min. Enzymatic hydrolysis of SM was started by adding 30  $\mu\text{L}$  of the LUV dispersion to 70  $\mu\text{L}$  enzyme solution (see 3.4.3). This gave a reaction-batch with a lipid concentration of 27.3 mM and an enzyme activity of 100 U/mL (7.3 U/ $\mu\text{mol}$  SM).

The HPTLC plates were developed with  $\text{CHCl}_3$ : MeOH:  $\text{H}_2\text{O}$ :  $\text{CH}_3\text{COOH}$  (65/25/4/1 vol/vol) and post-chromatographic derivatization was performed with  $\text{CuSO}_4$  (10%) in  $\text{H}_3\text{PO}_4$  (4%), followed by 10 min incubation at 190°C. The Peaks were scanned at a wavelength of 450 nm and quantified by relating peak-height and area of the unknown lipid bands to those of POPC, SM and C16:0-Cer standards. The minimum and maximum lipid amounts detected on the plate were about 0.1  $\mu\text{g}$  and 1  $\mu\text{g}$ , respectively. A hyperbolic growth function  $C(t) = C_0 + Pt/(\tau_H + t)$  was fitted to the inverted SM hydrolysis and the Cer formation curves.  $C_0$  is the constant offset,  $P$  the saturation level of the enzymatic turnover and  $\tau_H$  corresponds to the time at which half of the fragmentation is achieved.

## 4 Results

This thesis contains three papers, which are:

### **I Characterization of the Fluid-Gel Phase Coexistence Regime in an Apoptotic Model Membrane**

Boulgaropoulos, B., Arsov, Z., Laggner, P. and Pabst, G., (manuscript)

### **II Effect of Ceramide on Non-Raft Proteins**

Pabst, G., Boulgaropoulos, B., Gander, E., Sarangi, B. R., Amenitsch, H., Raghunathan, V. A. and Laggner, P., (2009) *J. Membr. Biol.* **231**,125-132

### **III Implication of Sphingomyelin/Ceramide Molar Ratio on the Biological Activity of Sphingomyelinase**

Boulgaropoulos, B., Amenitsch, H., Laggner, P. and Pabst, G., (submitted to Biophysical Journal, (submitted to Biophysical Journal, March 2010)

This chapter is divided into two parts. Section 4.1 deals with the biophysical characterization of the lipid model system composed of POPC/SM/Cer, performed under equilibrium conditions by the use of several biophysical techniques (paper I and II).

The non-equilibrium, time-resolved study of the enzymatic SM conversion within the model membrane is presented in section 4.2 (paper III).

### 4.1 Equilibrium study

The samples used in this section exhibit a well defined lipid composition and were measured under equilibrium conditions.

#### 4.1.1 Characterization of the Fluid-Gel Phase Coexistence Regime in an Apoptotic Model Membrane

A biophysical characterization of the multi lamellar lipid system, composed of POPC/SM was performed under equilibrium conditions by a combination of biophysical techniques, namely SWAXS, DSC and ATR-FTIR (paper I). SM was substituted gradually by Cer, and the POPC/sphingolipid (SL) ratio was kept constant at one.

The phase transition temperatures of the samples with different Cer contents were revealed by the DSC data, structural specifications were derived from the SWAXS data, and the IR data shed light on the vibrational dynamics within the lipid systems.

##### Thermotropic behaviour

Pure POPC exhibited a melting transition at  $-3.3^{\circ}\text{C}$ , and egg-SM a narrow transition at  $39.2^{\circ}\text{C}$  in agreement with previous studies (134-136). Pure Cer shows an endothermic transition at  $90^{\circ}\text{C}$ , according to (39). The melting behaviour of a multi lamellar POPC/SM/Cer suspension was recorded by DSC. SM was replaced by Cer in the range from 0 to 20 mol% (Fig.4.1).

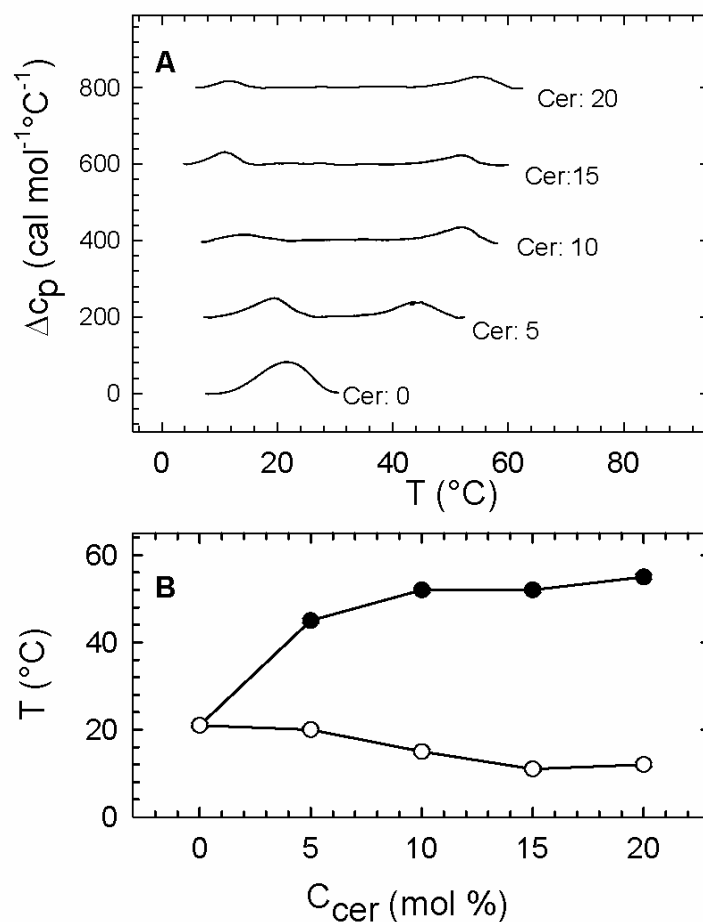


Figure 4.1 Melting of POPCSM/Cer-mixtures. Panel A shows DSC heating scans of MLVs composed of POPCSM/Cer (50/50-x/x, molar ratio,  $x = 0$  to 20 mol%). The heat capacity curves were shifted vertically for better graphic representation. Panel B shows the phase transition temperatures as a function of Cer content. Error bars are within the size of the symbols.

The binary lipid system POPC/SM showed a single broad melting transition from lamellar gel ( $L_\beta$ ) to lamellar fluid ( $L_\alpha$ ) at 21.3°C. In the presence of 5 mol% Cer, this peak was split into two phase transition peaks, which clearly indicates the coexistence of two phases, namely a gel and a fluid phase, denoted as  $L_\alpha^c$  and  $L_\beta^c$  in the following. Upon decreasing the SM/Cer ratio, the transition peaks separated further on the temperature axis causing the coexistence region to broaden with increasing Cer content. The areas (enthalpies) of the endothermic peaks decreased at the same time. This effect has also been observed upon Cer addition to pure POPC vesicles (134).

### Structural Characterization of the coexistence region

We focussed on the changes of the structural parameters in the phase coexistence region applying SWAXS measurements. The wide angle data are discussed only with respect to the gel phase of the lipid system in the gel fluid coexistence region. The WAXS peak exhibited a gel phase with hexagonal packing of the hydrocarbon chains in the presence of Cer (see also Fig.4.7). The induction of a gel phase in PC bilayers by Cer has also been reported previously (134, 137). The WAXS gel peak intensity increased with increasing Cer concentration and decreased with temperature.

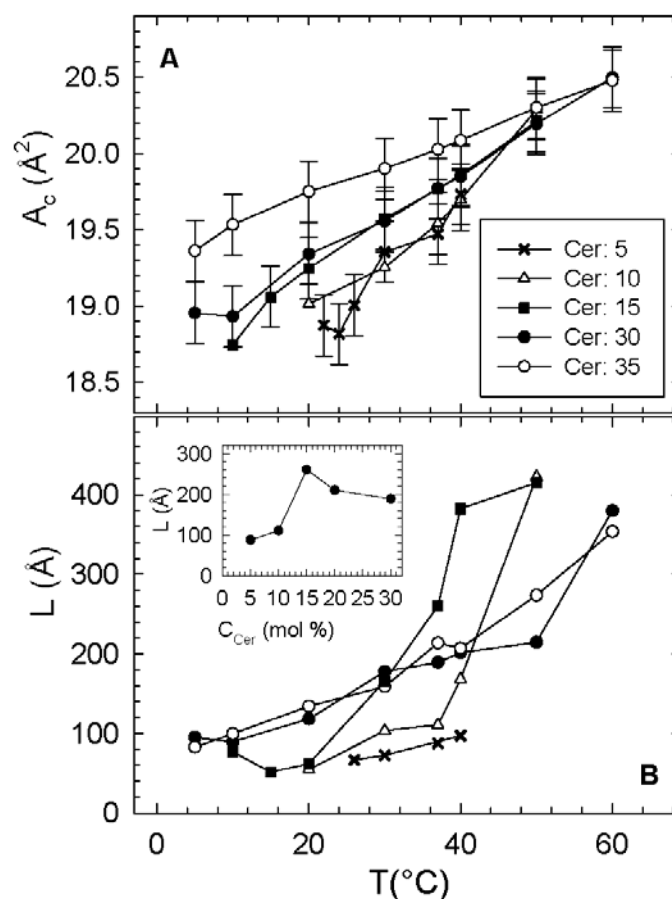


Figure 4.2 Area per lipid chain  $A_c$  (A) and domain size  $L$  (B) as a function of temperature for Cer concentrations from 5 to 35 mol%. B: Error bars are within the symbol size. B, Inset: Domain size as a function of Cer concentration at 37°C.

The area per lipid chain within the gel domains generally increased upon heating for all Cer concentrations and decreased with Cer content at 37°C (Fig.4.2 A). This signifies a lateral expansion of the membrane with temperature and upon Cer addition. The slopes of the  $A_c$  versus T curves decreased upon Cer addition suggesting a stabilization of the gel phase. This trend also pertained for the sample with 35 mol% Cer, where besides the fluid POPC-rich and the gel SL-rich, an additional pure Cer phase exists.

The gel domain sizes did not show a monotonic increase with temperature with respect to the Cer concentrations. The largest domain at physiological temperature was found for a Cer content of 15 mol%. This corresponds to a SM to Cer ratio of 2.3 (Fig.4.2 B, insert) and suggests that this is the preferred stoichiometry of the gel domains, in agreement with (138).

The SAXS patterns are superimpositions of the scattering curves of the coexisting phases. Hence, the d-spacing values within the two phase coexistence regime correspond to the weighted average of the lamellar repeat distances of the two phases. All SAXS patterns revealed lamellar phases. In the presence of Cer the SAXS Bragg peaks broadened due to the overlapping lattices of the coexisting phases. The two coexisting phases were a fluid phase enriched in POPC, and a gel phase enriched in SL, as it was confirmed by additional SAXS measurements in combination with an applied osmotic pressure (86), presented in section 4.1.2. The changes of the lamellar repeat distances of the bilayer stacks as a function of temperature for several Cer concentrations and as a function of Cer for selected temperatures are shown in Fig.4.3.

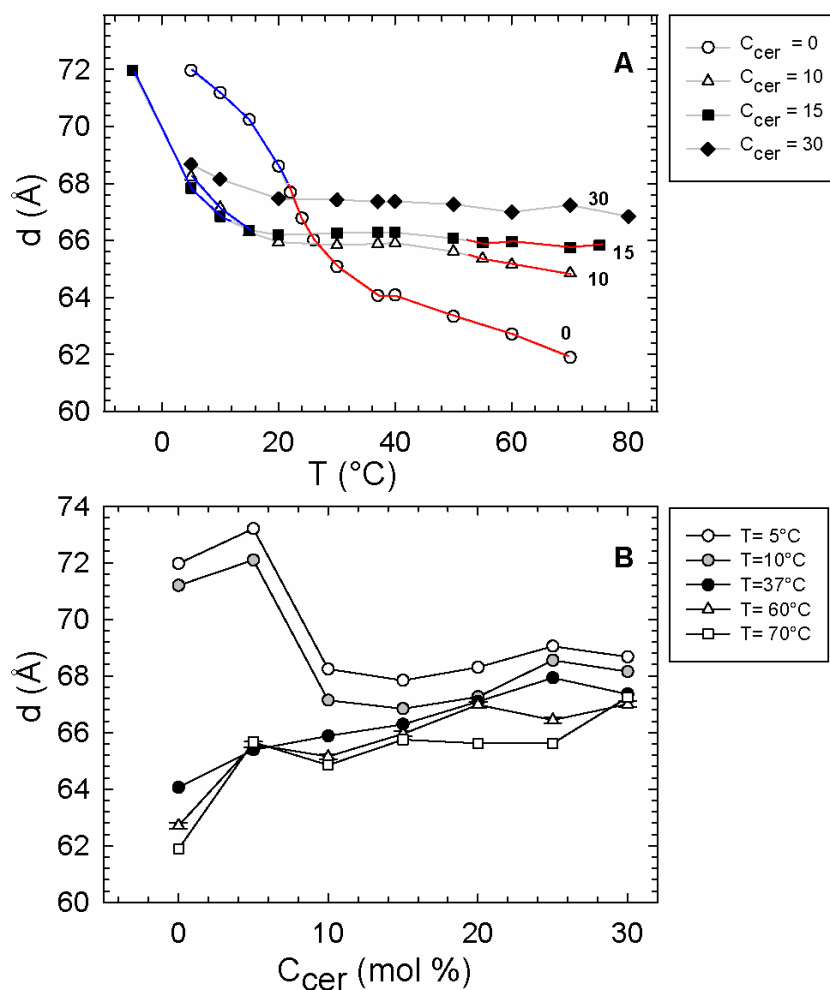


Figure 4.3 A: Lamellar repeat distance  $d$  as a function of the temperature for samples with different Cer contents. Blue: gel phase region, grey: gel-fluid coexistence region and red: fluid phase. B: Lamellar repeat distance  $d$  versus Cer concentration for selected temperatures.

Within the phase coexistence regime, the increase of the lamellar repeat distances reflects the growing proportion of gel domains. The distinct phase regimes were labelled with different colours, according to the phase transitions derived from the DSC data (Fig.4.1 A). The melting transition of POPC/SM was clearly seen in a  $d$ -spacing decrease from  $\sim 72.0$  Å ( $L_\beta^c$  phase) to  $\sim 62.0$  Å ( $L_\alpha^c$  phase), (Fig.4.3 A). This difference between the lamellar repeat distances of the two phases of about 10 Å is in agreement with (136) and clearly appears also in Fig.4.3 B. In the upper plot of Fig.4.3, the  $d$ -values at 5 and 10°C for the binary system (Cer: 0 mol%) and for the ternary system with 5 mol% Cer exhibit a pure gel phase in agreement with the DSC data (Fig.4.1 A). The slope of the  $d$ -values versus temperature curves was decreased with



increasing Cer content, which again signifies a stabilization of the gel phase upon Cer addition. Fig.4.3 B explicitly shows the increase of the d-value with Cer due to the generation of the  $L^c_\beta$  phase. At a Cer content of 35 mol%, an additional SAXS peak occurred with a corresponding d-value of 43.6 Å. (Fig.4.4 B)

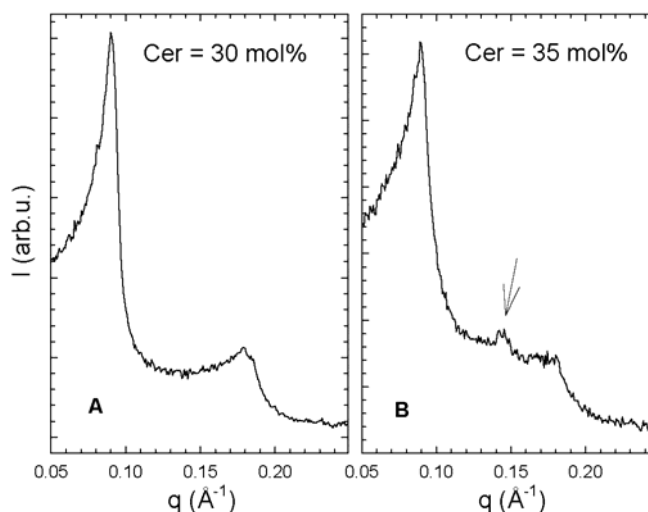


Figure 4.4 SAXS patterns of MLVs with 30 mol% (A) and 35 mol% (B), respectively. The arrow indicates the additional peak, which originates from a pure Cer phase. Both patterns were recorded at 37°C.

This peak was best developed at around 37°C but existed over the whole temperature range from 5 to 60°C. Shah et al. (39) found a d-value of 46.9 Å for pure C16:0-Cer at 26°C and a about 5 Å smaller d-value for anhydrous Cer ( $d = 42.1 \text{ \AA}$ ). The d-value of 43.6 Å suggests therefore pure, partially hydrated Cer. Thus, the solubility limit of Cer for this system lies between 30 and 35 mol%.

#### Vibrational dynamics

The changes of the lipid acyl chain conformation (methylene band) and the changes at the water-lipid interface (amide and carbonyl band) upon Cer addition were observed by IR-spectroscopy (Fig.4.5).

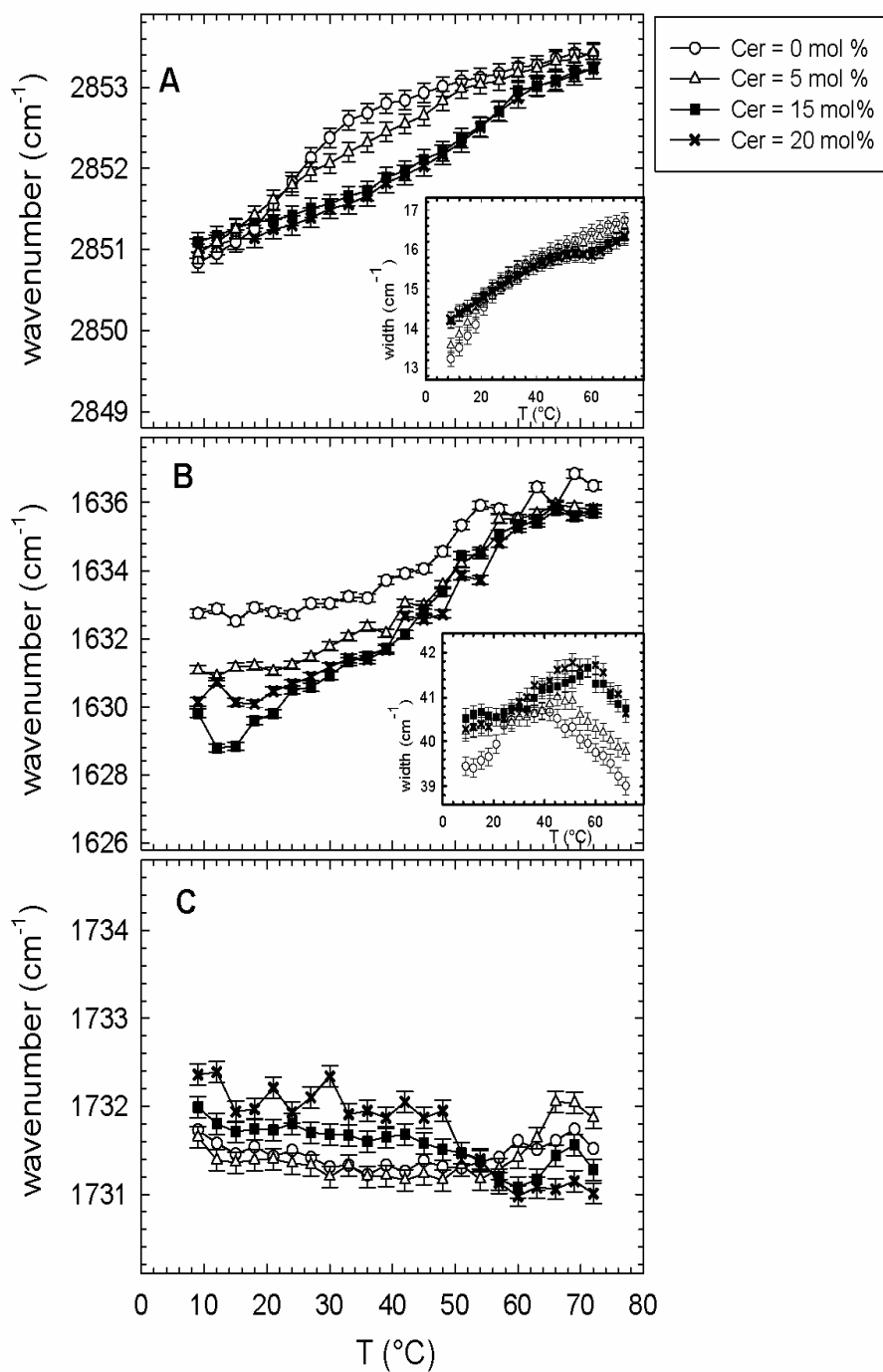


Figure 4.5 Temperature dependence of the methylene- (A), the amide- (B) and the carbonyl- (C) band peak position. The inserts give the course of the half-bandwidths of the methylene- (A) and the amide-peak (B). Samples were hydrated multi lamellar POPC/SM/Cer mixtures with different Cer contents.

All IR spectra were recorded as a function of the temperature for samples with different Cer contents from 0 to 20 mol%. The anti-symmetric and the symmetric stretching bands showed similar behaviour. Therefore, only the symmetric ones which overlap less with other vibration modes will be discussed in the following.

The course of the methylene peak positions (Fig.4.5 A) reflects the behaviour of the acyl chain conformations of all lipids within the bilayers and showed increased order above  $\sim 20^{\circ}\text{C}$  in the presence of Cer, seen as a shift to lower wave numbers for the samples with 15 and 20 mol% Cer, respectively. Below about  $20^{\circ}\text{C}$ , which corresponds with the phase transition temperature for the binary system, the peaks appeared at higher wavenumbers upon Cer addition. Thus Cer promotes disorder below the phase transition temperature of the binary lipid system and has an ordering effect above it.

Similar to the peak positions, lower methylene bandwidths indicate more ordered and higher values less ordered lipids (Fig.4.5 A, insert). The behaviour of the temperature dependence of the methylene bandwidth for the samples with 15 and 20 mol% Cer gave evidence of the presence of coexisting phases. Below about  $20^{\circ}\text{C}$  the lower values for the binary sample indicated a more ordered system, as was revealed also by the peak shifts upon Cer addition and heating. Above about  $20^{\circ}\text{C}$ , the width would be expected to shift to lower values upon Cer addition. But in the temperature range of the coexistence regime the bandwidth-values for all samples showed about the same behaviour with increasing temperature. One explanation is that the methylene bandwidth is composed of two parts, namely a contribution from POPC and a contribution from the SLs. If these two have different peak values, the overall methylene band broadens. Instead of reflecting the ordering effect induced by Cer above  $20^{\circ}\text{C}$  by decreased width-values for the samples with more than 15 mol% Cer, the phase coexistence leads to an increased methylene band width in the presence of Cer.

With the addition of Cer, the amide band peak, which only refers to the behaviour of the SLs, shifted to lower wavenumbers (Fig.4.5 B). The reason is an increase of the overall hydrogen bonding involving carbonyl and N-H groups and indicated the growing SL hydrogen bonding with increasing Cer content.

The changes of the width of the amide band (Fig.4.5 B, insert) reflect the phase transitions derived from the DSC data. The width for the POPC/SM sample decreased above  $36^{\circ}\text{C}$ , and oppositely the width for the sample with 15 mol% Cer increased. This correlates with the data

derived from the methylene band. But as the amide band only shows the behaviour of the sphingolipids, this again indicated the presence of a phase separation.

The carbonyl peak positions (Fig.4.5 C) as well as the carbonyl bandwidths (data not shown) did not show any significant change for the different samples upon heating. POPC itself is therefore not influenced significantly by the SLs at least for SM/Cer ratios  $\geq 1.5$ .

#### Phase diagram for POPC/SM/Cer

On the basis of these results, a phase diagram was constructed, which shows the different phase regimes depending on temperature and Cer concentration (Fig.4.6).

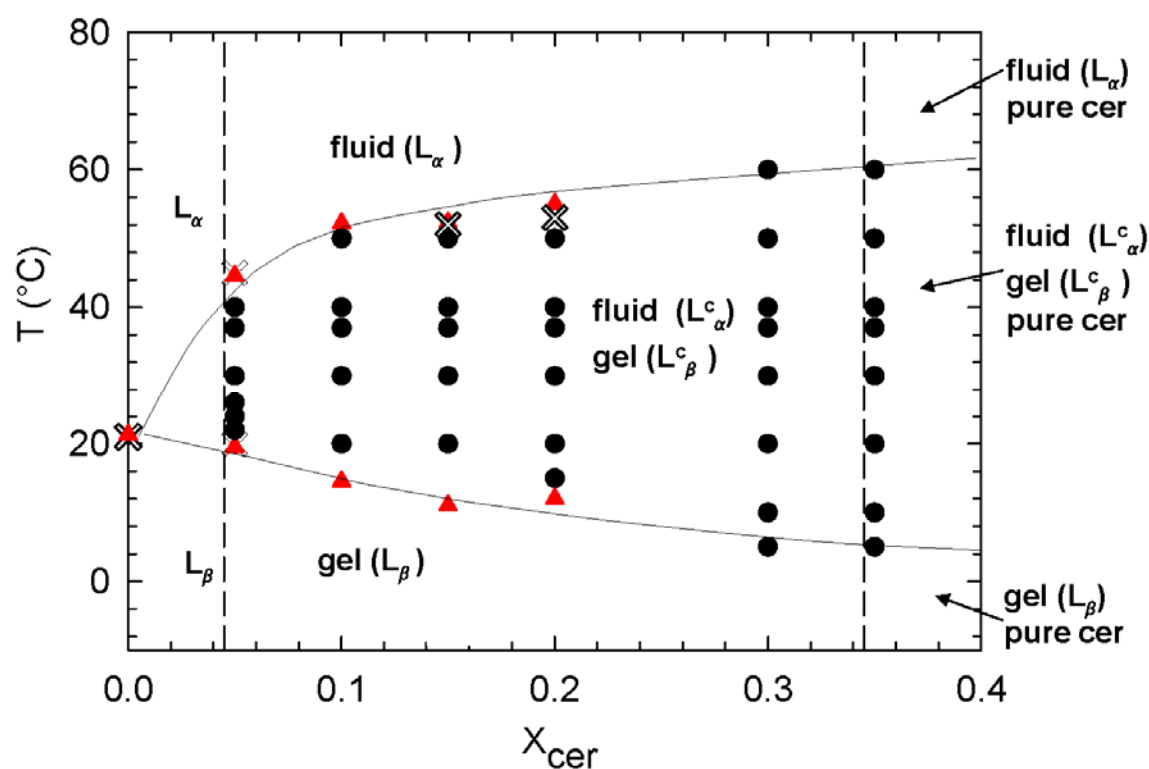


Figure 4.6 Partial phase diagram of fully hydrated POPC/SM/Cer bilayers. SM is substituted by Cer from  $X_{cer} = 0$  to  $X_{cer} = 0.35$  and the molar ratio POPC to sphingolipid is kept constant at one. Black circles: WAXS gel peaks; red triangles: DSC phase transition temperatures and crosses: phase transition temperatures estimated from the IR spectra. The lines are drawn as guide to the eye. Legend:  $L_\alpha$ : lamellar fluid phase,  $L_\beta$ : lamellar gel phase, pure cer: pure C16:0-Cer phase.  $L_\beta^c$  and  $L_\alpha^c$ : lamellar gel and lamellar fluid phase within the phase coexistence region.

The following regimes within the phase diagram were clearly distinguished: Uniform phases of the binary lipid system without Cer, a gel-fluid coexistence regime and a three phase coexistence regime with an additional pure Cer phase. The coexisting phases in the presence of Cer were denoted as  $L^c_\alpha$  and  $L^c_\beta$  in the following and were subject to further studies (86), section 4.1.2.

#### 4.1.2 Effect of Ceramide on Non-Raft Proteins

The two phases within the coexistence region of the POPC/SM/Cer system were additionally characterized by X-ray scattering experiments in combination with osmotic pressures. Besides the splitting of the DSC transition peaks and the results from the IR measurements, the shape of the SAXS Bragg peak of the fully hydrated lamellar system, which are slightly broadened due to overlapping reflections in the presence of Cer gave a strong indication of phase coexistence (previous section). Upon application of an osmotic pressure, the two phases were clearly resolved (Fig.4.7). Additionally, fluorescence microscopy imaging visualized the two distinct domains (Fig.4.7, insert).

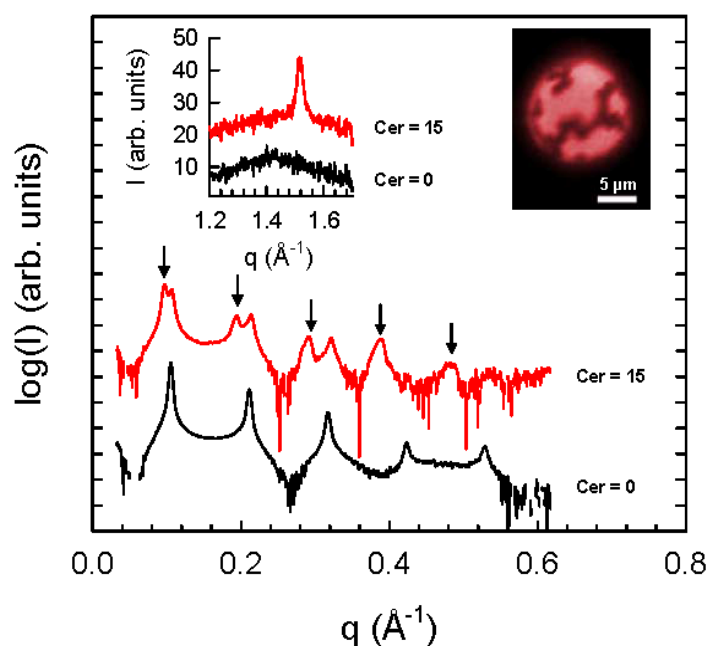


Figure 4.7 SAXS patterns of MLVs composed of POPC/SM (Cer = 0 mol%) and POPC/SM/Cer (Cer = 15 mol%) at 37°C and under an osmotic pressure of 2 atm. Arrows indicate the lamellar diffraction orders of the gel phase. The inserts show the corresponding WAXS patterns (Red: fluid phase, black: gel phase) and a fluorescence microscopy image of a GUV with coexisting lipid domains fluid-gel domains.

## 4 Results

The SAXS pattern of the binary lipid system exhibited a single phase with a lamellar repeat distance of  $d = 59.4 \text{ \AA}$ . The corresponding WAXS pattern showed a diffuse peak at  $q \sim 1.4 \text{ \AA}^{-1}$ , which indicated short-range order within the plane of the bilayer, typical for the lamellar fluid  $L_\alpha$  phase. The SAXS pattern of the sample with 15 mol% Cer clearly reveals the phase coexistence of two lamellar phases with  $d = 65.3 \text{ \AA}$  and  $d = 58.8 \text{ \AA}$ . The corresponding wide-angle data shows an additional sharp peak at  $q = 1.52 \text{ \AA}^{-1}$ . Calculation of the electron density profiles (120) leads to the values for the membrane thicknesses,  $d_B$  and the head-to-headgroup distances  $d_{HH}$  of all observed phases (Tab.4.1).

Table 4.1 Experimental interaction parameters for POPC/SM MLVs at 37°C and under an osmotic pressure of 2 atm in the absence and presence of Cer

Cer (mol%)	Phase	$d_B$ (Å)	$d_{HH}$ (Å)	$P_h$ (atm)	$\lambda_h$ (Å)	$K_C$ ( $k_B T$ )
0	$L_\alpha$	48.4	38.4	1585	1.7	57.7
15	$L_\alpha$	48.6	38.6	616	1.7	15.7
15	$L_\beta$	53.3	43.3	5000	1.6	~100

The head-to-headgroup distance of the fluid phase of the POPC/SM/Cer mixture is slightly larger than reported for pure POPC membranes (139), which gives an indication that this phase is not a pure POPC domain. However, the difference in membrane thickness of the coexisting phases is consistent with the gel–fluid phase separation.

To study the membrane interactions and mechanical properties of the different domains, both lipid systems were exposed to a range of osmotic pressures from  $\Pi = 0 \text{ atm}$  up to  $\Pi = 0.725 \text{ atm}$  in combination with SAXS. The lamellar repeat distances and the membrane thicknesses stem from the calculated electron density profiles from the SAXS patterns. The corresponding isotherms,  $\Pi(d_w)$ , are presented in Fig.4.8.

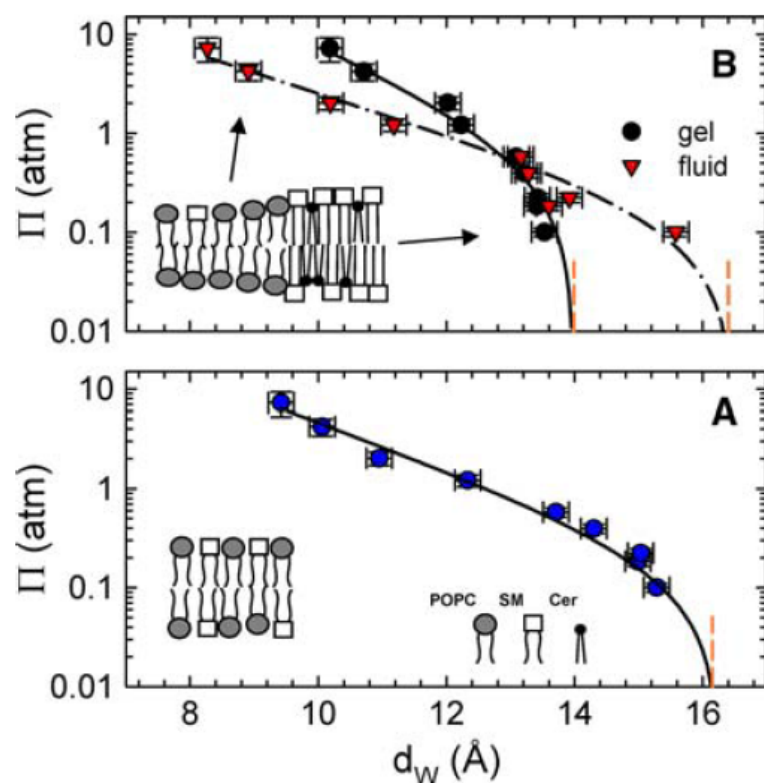


Figure 4.8  $\Pi(d_W)$  isotherms for POPC/SM membranes (A) and POPC/SM/Cer bilayers (B) at 37°C. Solid/dashed-dotted lines correspond to fits and dashed lines indicate the equilibrium bilayer separation for  $\Pi = 0$ . Inserts sketch the molecular organization.

The values for the bilayer separation  $d_W$  were obtained by taking the membrane thickness  $d_B$  as a constant and subtracting it from the particular lamellar repeat distance at a given osmotic pressure. Hydration forces dominate at the highest osmotic pressures. As  $\Pi$  decreases, steric repulsion due to thermal undulations comes increasingly into play until the system attains its equilibrium separation at  $\Pi = 0$  due to balancing van der Waals attraction. At zero osmotic pressure  $d_W$  of the  $L_\beta^c$  phase is significantly smaller than the bilayer separation of the fluid phases (Fig 4.8 B), because of the negligible steric repulsions in the  $L_\beta^c$  phase due to insignificant membrane undulations.

The isotherms of the coexisting phases cross each other at  $\Pi \sim 0.6$  atm, upon which the gel phase is more difficult to compress than the  $L_\alpha^c$  phase. This signifies the independent behaviour of the coexisting phases under osmotic pressure, as expected for a macroscopically phase separated system.

These isotherms were analyzed as described in section 3.5 with a Hamaker constant of  $4.3 \times 10^{-21}$  J (140). The parameters, which needed to be adjusted, were the scaling constant  $P_h$  and the decay length of  $\lambda_h$  of hydration forces, as well as the bilayer bending rigidity  $K_C$ . Fluctuation pressures were neglected for the  $L_\beta$  phase, because of its large bending rigidity. The isotherms were fitted and optimized iteratively until satisfactory fits were obtained (Fig.4.7). The resulting parameters are listed in Tab.4.1. The values for the scaling constant  $P_h$ , and the decay lengths of  $\lambda_h$  of hydration forces are within the typical ranges for the fluid phase (129), with  $\lambda_H = 1.3\text{--}2.1$  Å and  $P_h = 500\text{--}1,000$  atm, and the  $P_h$  values are up to about one order of magnitude higher in the gel phase (128). Hydration forces decayed with similar constants for all studied systems. The  $L_\beta^c$  phase exhibited the largest  $P_h$  value and consequently requires the largest work for dehydration. The  $L_\alpha^c$  phase exhibited the lowest  $P_h$ , which means that water can be removed most easily from this phase.

Regarding the bending rigidities of the different lipid phases (Tab.4.1) the  $L_\alpha^c$  phase at Cer = 15 mol% turns out to be much softer than the homogeneous POPC/SM membrane. Its bending rigidity of  $\sim 16$   $k_B T$  closely resembles that of pure POPC (141). This softening of the remaining POPC-rich membrane fraction is due to the strong hydrogen bonding activity between Cer and SM, which was clearly shown by the IR data in the previous section. Cer recruits SM molecules with a SM/Cer enriched gel phase formation as consequence and thus SM is depleted from the coexisting fluid phase. The remaining  $L_\alpha^c$  phase is then mainly composed of POPC and hence has a lower  $K_C$  than the POPC/SM mixture. SM itself, which would be in the gel phase at 37°C, stiffens the POPC membrane, which results in a  $K_C$  increase from about 20  $k_B T$  to nearly 60  $k_B T$ .

Integration of the pressure isotherms yields the interaction potentials, which are presented in Fig 4.9.



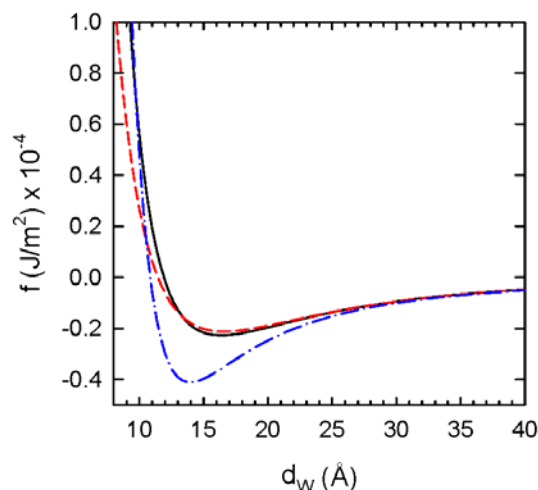


Figure 4.10 Interaction potentials for POPC/SM bilayers (black) and for the  $L_{\alpha}^c$  (red) and  $L_{\beta}^c$  (blue) phases coexisting in POPC/SM/Cer membranes.

The  $L_{\beta}^c$  phase has the steepest increase of the potential upon further compression and the deepest free energy minimum. Further, the interaction potential of the fluid phase ( $L_{\alpha}^c$ ) of the POPC/SM/Cer mixture is clearly softer than that of the homogenous POPC/SM mixture, seen in the smoother ascent of the potential as the bilayers come closer to each other. The absolute value of the minimum for the fluid phases is about two times smaller.

Cantor et al (142) introduced the lateral pressure profile concept (Fig.3.8) to study its effect on membrane proteins. The lateral pressure profile deals with the changes within the lateral pressure along the bilayer normal  $z$ . Lateral pressures are negative at the water/lipid interface and exhibit mainly positive contributions in the head group and the hydrocarbon tails regimes. In a tensionless membrane the integral over all pressures along the bilayer normal is zero. However, the first and second moments ( $P_1$  and  $P_2$ ) of the lateral pressure may differ from zero. The first integral moment  $P_1$  is defined by  $P_1 = K_C^m c_0$ . The second integral moment gives the Gaussian curvature modulus  $\kappa_G$  (143). We estimated the changes of the first integral moment due to SM depletion and came to an upper and lower limit of  $\Delta P_1/P_1$ , with -0.4 and  $\Delta P_1/P_1 = -0.730$ , respectively. This means that the increase of membrane flexibility induced a net shift of lateral pressures within the hydrocarbon region toward the lipid/water interface.

It is possible to relate the above estimated change of  $P_1$  to the pore sizes of ion channels (see Fig.3.8), which are not located in membrane rafts. First order approximation calculations show that the activation of such an ion-channel may be inhibited.

## 4.2 Non-equilibrium study

The non-equilibrium studies were performed on a model system consisting of a lipid part, which was an equimolar mixture of POPC and egg-SM to model the mammalian membranes and a bacterial nSMase from *Bacillus cereus* (*Bc*-SMase), which was taken as a model for the mammalian SMase. The implicated hierarchical levels were addressed by a combination of high performance thin layer chromatography (HPTLC), synchrotron time-resolved X-ray diffraction and photon correlation spectroscopy (PCS). All experiments were performed at 37°C.

The following figure shows the reaction progress in terms of SM-fragmentation and generation of C16:0-Cer, which was determined by HPTLC on several reaction batches.

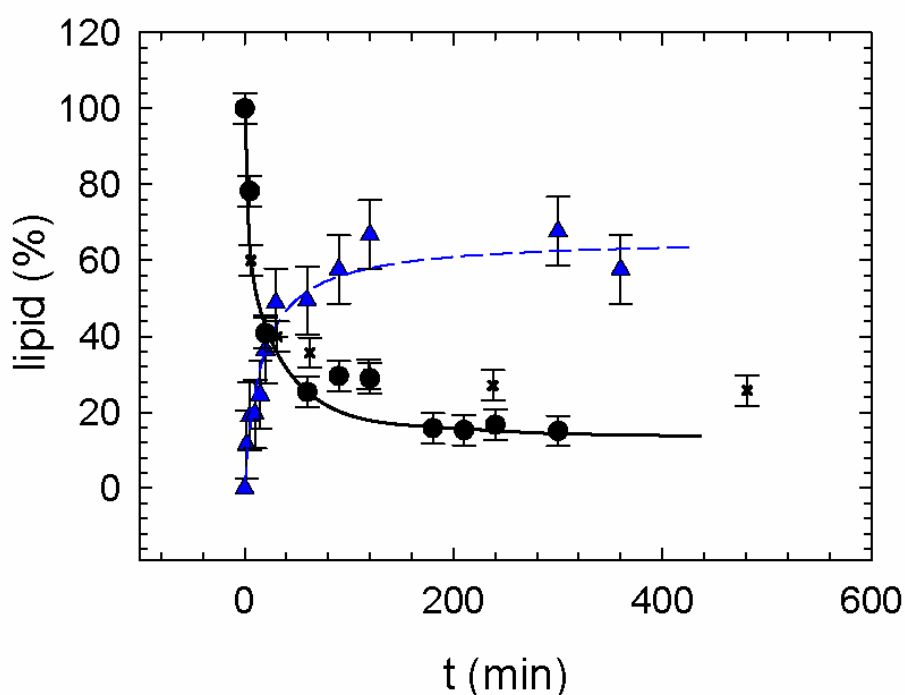


Figure 4.11 SM hydrolysis and generation of C16:0-Cer by *Bc*-SMase in POPC/SM bilayers as determined by HPTLC (black circles). Crosses show SM-fragmentation data from human leukaemia cells undergoing apoptosis (2). Lines refer to hyperbolic fits.

The Cer generation follows hyperbolic growth behaviour and exhibits a plateau value of  $65 \pm 8$  mol% C16:0-Cer. About 86 % of the total SM molecules were hydrolyzed during the reaction,

which was determined from a hyperbolic fit to the SM fragmentation data. These values make sense, considering that the fraction of C16:0 acyl chains of egg-SM is 84 %. The time needed for the half maximum conversion  $\tau_H$  was about 12 min for both of the hyperbolic fits. Comparison of both kinetics and final SM levels of these findings to SM degradation measurements of a biological system undergoing apoptosis showed a highly remarkable agreement (2) (Fig.4.11). The reaction stopped after the hydrolyzation of 86 % of the total SM molecules

Structural characterization of the binary lipid system before enzyme addition and of the ternary lipid system more than 15 hours after enzyme addition was done by SWAXS measurements.

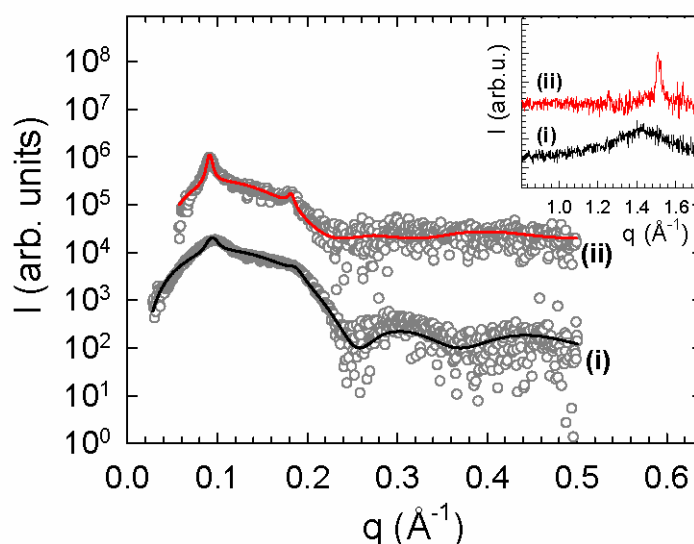


Figure 4.12 SAXS patterns of POPC/SM bilayers before (black) and 930 min after enzyme addition (red). The patterns were fitted by applying a full  $q$ -range model (144) and are horizontally shifted for better graphical presentation.

SAXS data show very broad first and second order Bragg reflections (Fig.4.11) prior to the addition of SMase. These broad SAXS peaks indicate the presence of oligo lamellar vesicles (OLVs) with about three positional correlated bilayers and a lamellar repeat distance of  $d = 64.6 \text{ \AA}$ , although ULVs are the initial major population of vesicles according to the PCS data. The reason for this is that correlated bilayers have a significantly stronger scattering signal than ULVs and therefore OLVs are much more apparent in SAXS patterns than LUVs. During the enzymatic reaction the Bragg peaks sharpened considerably, and the SAXS pattern recorded

930 minutes after enzyme addition (Fig.4.11 ii) exhibited positional correlated bilayers with  $d = 68.7 \text{ \AA}$ . Both SAXS patterns were fitted with a full  $q$ -range model (144, 145) assuming uniform membranes. These fits gave the head-to-headgroup distances  $d_{HH}$  of the bilayers. Prior to the addition of SMase we found a fluid phase with  $d_{HH} = 40.8 \text{ \AA}$ . The final SAXS pattern showed a gel phase with  $d_{HH} = 45.2 \text{ \AA}$ . Thus although the system enters the phase coexistence region due to Cer generation (Fig.4.6), the SAXS patterns are dominated by the  $L^c_\beta$  phase. Apparently, the  $L^c_\alpha$  phase bilayers do not become positionally correlated during the enzyme reaction.

The corresponding WAXS patterns exhibited a diffuse chain correlation peak centered at  $q = 1.43 \text{ \AA}^{-1}$  indicating fluid hydrocarbon chain packing before enzyme addition and a sharp peak at  $q = 1.51 \text{ \AA}^{-1}$ , that belongs to a  $L_\beta$  gel phase with a 2D hexagonal packing of the acyl chains. The lateral area per lipid  $A$  was  $40.0 \text{ \AA}^2$  after about 15 hours of reactions. From the peak width we further estimate that about 200 lipids contribute on average to a gel phase domain. The WAXS peaks are in agreement with the ones recorded for samples with zero and 15 mol% Cer under an osmotic pressure (previous section, Fig.4.7).

Structural changes occurring on the membrane level during the enzymatic hydrolysis of SM were followed by time-resolved synchrotron SWAXS measurements (Fig.4.13).

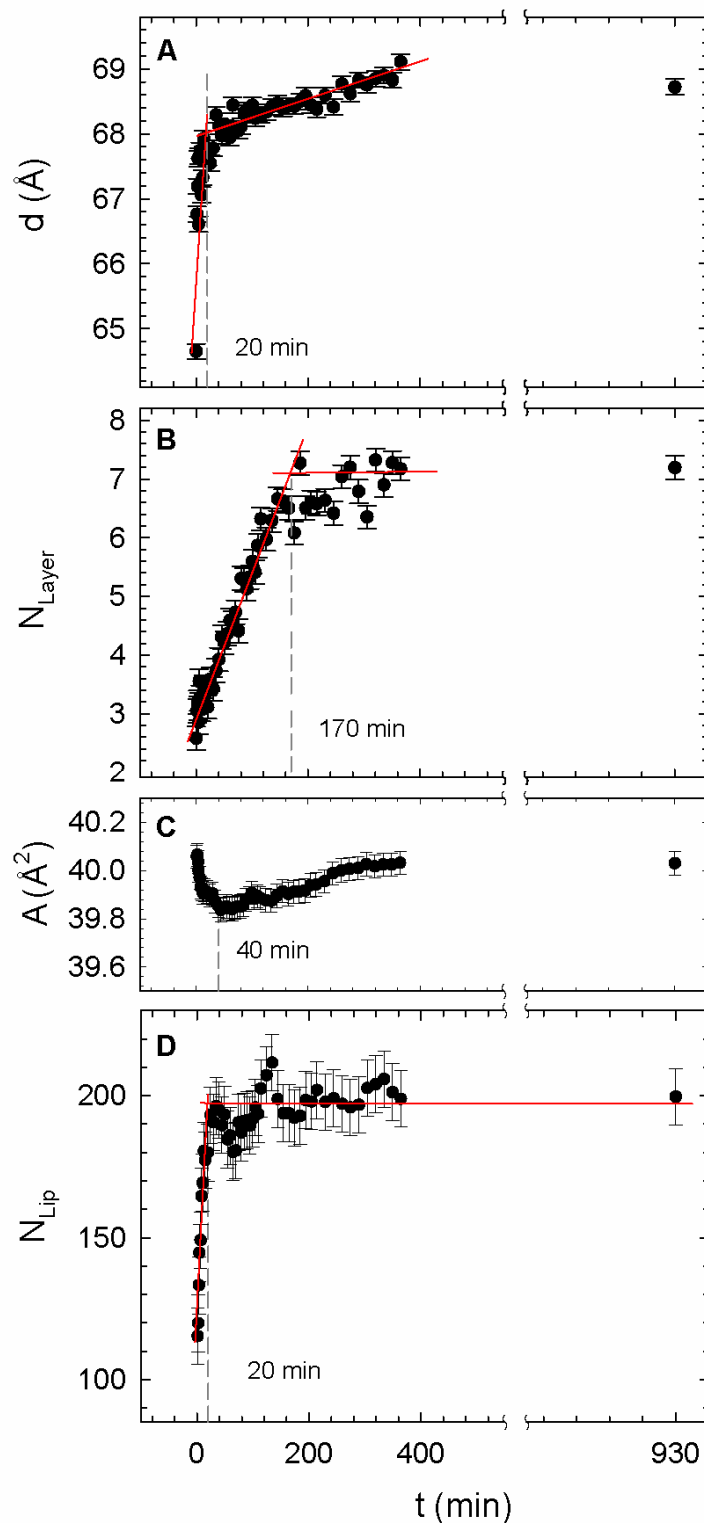


Figure 4.13 Evolution of lamellar repeat distance (A), average number of positional correlated layers (B), lateral area per lipid in the gel phase (C) and average number of lipids per gel phase domain (D) during the enzyme reaction. Panel A and B show parameters derived from SAXS data and panel C and D those, coming from WAXS data.

Panels A and B of Fig.4.13 are related to the small angle regime and show the corresponding time evolutions of the lamellar repeat distance  $d$  and the number of correlated bilayers  $N_{\text{layer}}$ , respectively, during the hydrolysis reaction. We found a time constant of  $\tau_H \sim 2$  min for the course of the  $d$ -values. After about 20 minutes the slope of the  $d$ -value versus time curve decreased significantly. Contemporaneously, we observed a significantly slower ( $\tau_H \sim 50$  min) initial linear increase of  $N_{\text{layer}}$ , which leveled off after  $\sim 170$  min.

WAXS data (panels C and D of Fig.4.13) revealed the presence of a gel phase already 70 s after the addition of SMase and the lateral area per lipid was  $40 \text{ \AA}^2$  at this time and equaled the final  $A$ . The minimum value of  $A$  was  $39.8 \text{ \AA}^2$  after about 30 - 40 min and the curve then increased in a sigmoidal fashion back to  $40 \text{ \AA}^2$ . This value is about  $20 \text{ \AA}^2 - 25 \text{ \AA}^2$  smaller than the area estimated for the POPC/SM mixture in the  $L_\alpha$  phase. Therefore mechanical strains are built up and may lead to bilayer disruption. Additional mechanical strain is imposed by the spontaneous negative curvature of Cer. The number of lipids per domain  $N_{\text{lip}}$  was initially about 100 and reached its final value of about 200 after  $\sim 20$  min. The time constant  $\tau_H \sim 3$  min of this growth is comparable to the one found for the changes of the SAXS  $d$ -values and shows that this occurs about four times faster than Cer generation (Fig.4.11). This demonstrates that the SAXS results are not dominated by the few OLVs present prior to the addition of SMase, but by the generation of the  $L_\beta$  phase.

The membrane aggregation itself is clearly indicated by these data (Fig.4.13 B). However, growth of positional correlated bilayers proceeded significantly slower than gel phase formation and bilayer swelling. This is because removal of interstitial water and membrane diffusion processes will proceed on a slower time scale than gel phase formation. Since the lamellar SAXS peak is dominated by the  $L_\beta$  phase and hence also the course of the  $N_{\text{layer}}$  value, we can follow the coupling of the gel phase domains.

The lateral area per gel phase lipid decreased nearly as fast as  $N_{\text{lip}}$  and  $d$  increased. The  $L_\beta^c$  phase was formed within the first minutes of the enzyme reaction and the domain size of the gel phase grows about four times faster than Cer is generated by SMase (Fig.4.13 C). This can be understood by the ability of SM to form hydrogen bonds with Cer, which leads to a recruitment of SM to gel phase domains. The rapid gel phase formation stops after  $\sim 20$  min. Further, also bilayer swelling, which proceeded initially with about the same kinetics as the formation of gel-phase domains slowed down after  $\sim 20$  min (Fig.4.13 A). According to the fit to our HPTLC data (Fig.4.11) after 20 min of reaction time, the molar SM/Cer ratio is about

one. Thus, as long as Cer levels do not exceed those of SM, progression of the gel phase is faster than Cer generation.

In order to gain deeper insight into the lamellar swelling occurring during the reaction (Fig.4.13), we compared the d-values found by the in-situ measurements to the d-values of the MLVs of defined POPC/SM/Cer ratios under equilibrium conditions (Fig.4.14).

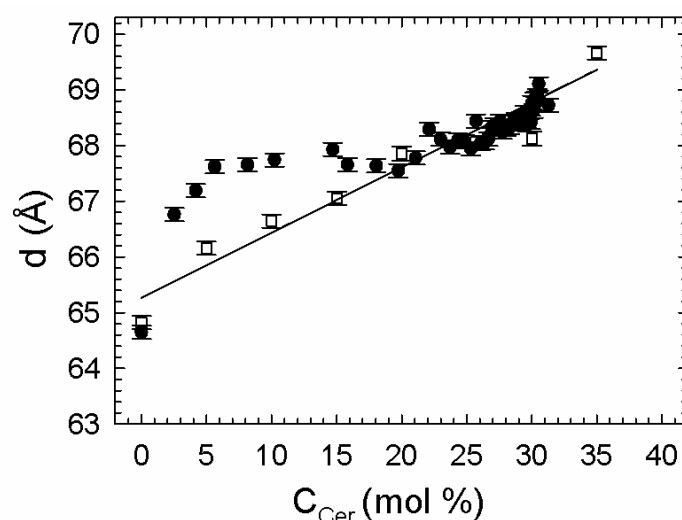


Figure 4.14 Comparison of the d-values of enzymatic reaction to equilibrium values of MLVs composed of POPCSM/Cer (50/50-x/x, molar ratio)

We have to keep in mind that the d-spacings correspond to the weighted average of the lamellar repeat of fluid and the gel phases at each Cer concentration at full hydration. Thus the roughly linear increase of the equilibrium d-values increased with Cer content and reflects the increase of the gel phase fraction (Fig.4.14). With a solubility limit of Cer in the present system between 30 and 35 mol% (see section 4.1.), it is remarkable that we did not observe any pure Cer aggregates. Hence, catalytic turnover seems to stop just before a pure Cer phase forms. This can be due to a mechanical feedback mechanism induced by changes of lateral pressures at the lipid/water interface. Indeed, SMase activity has been reported to depend on the mechanical membrane properties (45, 85, 116).

The comparison of the d-values from the time-resolved study with the d-values from the equilibrium mixtures of various Cer concentrations was done by the generation of a Cer

concentration axis by the use of the fits to the C16:0-Cer generation data (Fig.4.11). Before about 20 min the d-values of the dynamic experiment deviate significantly from the linear increase under equilibrium condition. At later times the dynamic changes essentially pursues the equilibrium d-values. The molar SM/Cer ratio after about 20 minutes of reaction is about one according to the HPTLC data. Even above this ratio the amount of  $L^c_\beta$  phase continues to grow as evidenced by the continued increase of the d-spacing (Fig.4.13 A). This growth is slow enough to follow equilibrium d-values (Fig.4.14). However, at SM/Cer ratios smaller than one, POPC is increasingly incorporated into the gel domains. This is substantiated by the pickup of the lateral area per lipid after 40 min (Fig.4.13 C) that may be related to the larger lateral size of POPC compared to SM due to its monounsaturated acyl chain.

The morphological changes of the vesicles were studied by time-resolved PCS experiments. Fig.4.15 shows the results for two different enzyme/lipid ratios.

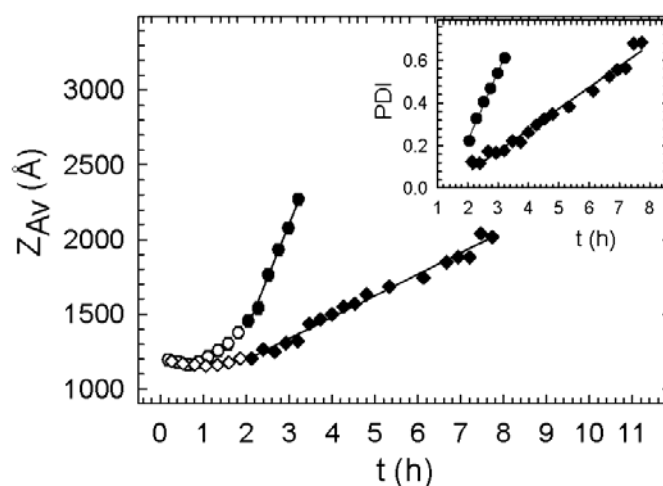


Figure 4.15 Changes of the average particle size,  $Z_{AV}$  and the PDI during the enzymatic hydrolysis of SM for 20.5 U/ $\mu\text{mol}$  SM (diamonds) and 41 U/ $\mu\text{mol}$  SM (circles). Filled symbols indicate the range of linear vesicle growth.

During the first  $\sim 60$  min the average particle size  $Z_{av}$  of about 1200 Å remained constant for both systems as well as the PDI of about 0.085. After this lag period  $Z_{av}$  and the PDI both started to increase substantially and exhibited a linear increase above  $\sim 120$  min. Hence, the vesicle growth goes in hand with size heterogeneity. We were following these changes for  $\text{PDI} < 0.7$ , upon which  $Z_{av}$ -values become unreliable. Vesicular growth confirms that the



equilibration process involves fusion processes, as reported previously (83) and the vesicle growth is significantly faster for the higher enzyme/lipid ratio. However, the final particle sizes are about equal for the data sets presented. This indicates that enzyme concentration correlates only with the speed of morphological rearrangements, but not the final vesicle aggregation size.

## 5 Discussion

### 5.1 Equilibrium study

The phase diagram for the system POPC/SM/Cer revealed distinct phase regimes, namely uniform lamellar phases ( $L_\alpha$  and  $L_\beta$ ), a gel-fluid coexistence regime in the presence of Cer ( $L_\beta^c$  and  $L_\alpha^c$ ), and a three phase coexistence regime with an additional pure Cer phase in the presence of more than 30 mol% Cer (Fig.4.6).

A big variety of biophysical studies on lipid mixtures containing PCs and SLs exists –using well defined synthetic lipids as well as lipid extracts with a large variety of different acyl chains. The lipid mixtures, we studied were composed of synthetic POPC, synthetic C16:0-Cer and egg-SM, which contain around 84% C16:0 acyl chains. We found uniform phases for the binary equimolar POPC/SM mixture with a phase transition from lamellar gel ( $L_\beta$ ) to lamellar fluid ( $L_\alpha$ ) at  $\sim 20^\circ\text{C}$  (Fig.4.1).

Lipid systems can mix ideally with randomly distributed lipids within the membrane, without any phase separation, or the mixing can be non-ideally, which means that compositional fluctuations exist. This occurs mainly in binary lipid systems, whereas in ternary lipid systems macroscopic phase separation with the formation of micron-sized stable lipid domains can be observed (146). By comparing the results from different studies on lipid phases one has to keep in mind that the different experimental techniques look through different time-windows during the experiment. X-ray scattering techniques need exposure times of seconds to minutes to yield a scattering pattern of significant quality. Therefore, with this technique, stable macroscopic phases are detected. However, compositional fluctuations within the bilayer occur on timescales of ms to ns and can not be seen by the X-ray measurements. To detect these so-called liquid ordered ( $l_o$ ) and liquid disordered ( $l_d$ ) phases, spectroscopic techniques are required (147). Further, X-rays are scattered by the electrons of the sample molecules itself, which results in a scattering pattern, whereas the information from fluorescence or electron spin resonance (ESR) spectroscopy is an indirect one -transferred via reporter molecules that are incorporated into the lipid membrane. These labels may also have influence on the observed phase behaviour (148-150).

With fluorescence spectroscopy, phase separations can easily be detected, but the differentiation between macroscopic or microscopic phases and compositional fluctuations is not possible. The results from X-ray scattering and fluorescence spectroscopy experiments are therefore complementary to each other and by combining the results it is possible to assign the different phases.

Untracht et al. (151) detected lateral phase separation in a lipid mixture composed of egg-POPC and bovine-brain-SM, applying X-ray diffraction, scanning calorimetry, and light microscopy. They observed a SM-enriched gel phase and a gel phase containing both SM and PC upon cooling to 20°C in the presence of more than 33 mol% SM, which is in contrast to our observations. The formation of this macroscopic phase separation can be due to the use of two natural lipids, which contain a variety of different acyl chains in contrast to well synthetic lipids with a well defined molecular structure.

Degovics et al. (138) studied an equimolar synthetic-POPC/egg-SM mixture in HEPES buffer with X-ray scattering and DSC. The DSC data showed two weakly resolved peak maxima for the equimolar POPC/SM-mixture but the X-ray data did not show any macroscopic phase separation. This is in agreement with our results. Nevertheless, they assumed that these two lipids might have differences in their lateral organization. Indeed, studies exist, where microscopic phase separation, differences in the order parameters of the single lipids within the binary lipid sample and/or compositional fluctuations were observed (152, 153).

Bunge et al. (154) studied a binary lipid system, composed of synthetic POPC/C16:0-SM with fluorescence microscopy, <sup>2</sup>H-NMR and ESR. They found microdomains with a minimal radius of 45–70 nm, which had also been observed previously (155). Such domains could not be detected by fluorescence microscopy, where a uniform phase has been observed. The same lipid system was studied by de Almeida et al. (153) with photophysical methods (fluorescence anisotropy, lifetime and quenching), who found a broad gel/fluid phase coexistence region and confirmed the existence of a gel-gel phase separation. Microscopic differences in the lateral organization of the lipids were also indicated by fluorescence measurements (152).

Upon addition of Cer we observed phase separation into a lamellar gel phase ( $L^c_\beta$ ), enriched in SLs and a POPC-rich lamellar fluid phase ( $L^c_\alpha$ ) in the temperature range within the coexisting region (Fig.4.6). In the presence of Cer, but outside of this phase coexistence region we did not find a clear indication of phase separation within the ternary lipid system.

To clearly resolve a gel-gel or fluid-fluid phase coexistence by X-ray scattering, experiments with an applied osmotic pressure would have to be performed (86). Our results show that the temperature range of the phase coexisting region broadens with increasing Cer concentration and also the observed phase transition peaks for the ternary lipid systems broaden in the presence of Cer (Fig.4.1), which agrees with (135). Already at 5 mol% Cer a gel phase is formed due to the tight interaction between the SLs. This was also confirmed by our IR data that show increased hydrogen bonding upon Cer addition (Fig.4.5), which is in agreement with (138, 156, 157). In the presence of Cer the binary POPC/SM mixture showed a macroscopic phase separation into two different phases (Fig.4.7), which were assigned to be a POPC-rich fluid ( $L^c_\alpha$ ) and a SL-rich gel phase ( $L^c_\beta$ ) recently (86). This phase separation was already observed for the smallest measured Cer content of 5 mol% Cer. The phase coexistence was confirmed by the IR measurements, which indicated a two phase regime, because of the high bandwidth value in an ordered regime and the fact that POPC was not much influenced for SM/Cer ratios down to 1.5 (Fig.4.5). We detected an additional pure Cer phase between 30 and 35 mol% Cer (Fig.4.4).

Castro et al. (152) built up a phase diagram for the ternary model system composed of POPC, C16:0-SM and C16:0-Cerby the use of fluorescence membrane probes and at 24°C (Fig.5.1).

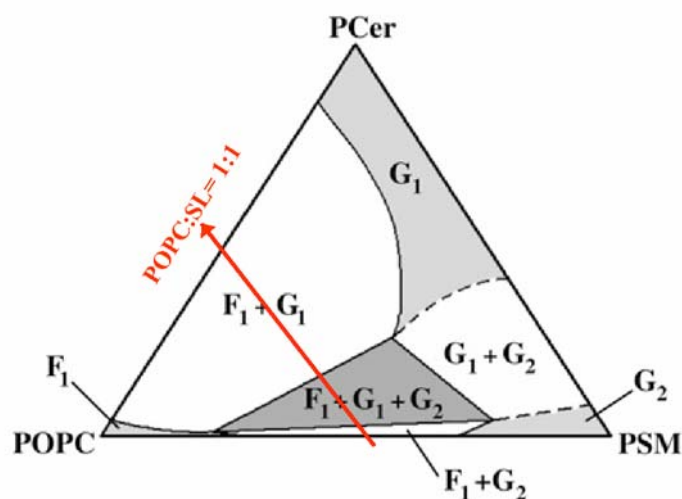


Figure 5.1 Phase diagram for the ternary lipid system POPC/SM/Cer at 24°C, determined by Castro et al. (152). The red arrow follows a POPC/SL ratio of 1 towards increasing Cer content. Legend:  $F_1$ : POPC-rich fluid phase;  $G_1$ : Cer-rich gel phase and  $G_2$ : SM-rich gel phase.

In the following, we will compare the phase regimes found by Castro et al. (152), (Fig.5.1) with the ones detected in this study (Fig.4.6) to shed light on the stability and life time of the different phases.

Following the imaginary line given by a POPC/SL ratio of one towards increasing Cer content (red arrow in Fig.5.1), the following phase regimes were detected by Castro et al. (152). Until 2 mol% Cer, a two phase regime was found, consistent of a fluid POPC- rich and a gel SM-rich phase. Above a Cer content of 2 mol% Cer an additional gel phase enriched in Cer was observed up to 15 mol% Cer (SM/Cer ratio of 2.3). At ratios below 2.3, the SM-rich gel phase vanished to reveal a two phase coexistence with a gel Cer-rich and a fluid POPC-rich phase upon increasing Cer content. The existence of a SM-rich gel phase for SM/Cer ratios above 2.3 up to about 15 can be explained by the interplay between SM and Cer in the system. Cer recruits SM for gel domain formation and excess SM would mix again with POPC in a non ideal way, thereby showing compositional phase fluctuations by fluorescence spectroscopy. For SM/Cer ratios smaller than 2.3, all SM molecules are recruited by Cer. The preferential SM/Cer ratio for the gel domain formation has been shown also in kinetic studies of the enzymatic hydrolysis of SM (see section 5.2.). Below a ratio of one Cer lacks a SM partner and is forced to recruit POPC or to segregate as pure Cer phase, which is energetically unfavourable (section 5.2.). Castro et al did not find the SM rich gel phase for SM/Cer ratios below 2.3, because at this ratio Cer couples all SM molecules. Above 15 mol% Cer a two phase coexistence region, consisting of a fluid POPC-rich and a gel Cer-rich phase continues at 24°C. They did not observe a pure, crystalline Cer phase.

Following the line at constant temperature of  $T = 24^{\circ}\text{C}$  in direction of increasing Cer content in our phase diagram (Fig.4.6), a uniform lamellar fluid phase has been observed until a Cer content of about 2 mol%, which is in contrast to Castro et al. (152), who detected an additional SM-rich gel phase, which is therefore not a macroscopic stable one. The SM-rich and Cer-rich gel phases, which coexist with the fluid phase in the concentration range from ~2 to 15 mol% Cer, according to (152), were not detected by X-ray measurements and thus refer to compositional fluctuations as well. X-ray scattering revealed a two-phase coexistence of a fluid POPC-rich and a gel SL-rich phase (Fig.4.7) and at Cer concentrations between 30 and 35 mol% Cer an additional pure Cer phase (Fig.4.4).

SWAXS measurements were applied to observe the dynamic structural changes within the coexistence region. The area per lipid chain within the gel domains was generally increasing upon heating for all Cer concentrations and increasing with decreasing SM/Cer ratio at 37°C (Fig.4.2 A). This signifies a lateral expansion upon heating and Cer addition. Similar behaviour has been found previously with peptides inducing disorder into bilayers (130). The growing of the area per lipid chain within the gel domains upon decreasing SM/Cer ratio suggests the incorporation of POPC into the gel domains at SM/Cer molar ratios  $< 1$ . The area per lipid chain is growing because of the bigger lateral area requirement of POPC due to its kinked chain. Additionally, Cer with its conical molecular shape can lead to an increased area. Stabilization of these domains with increasing Cer is clearly indicated by the decreased lateral expansion upon addition of Cer, which is in agreement with Veiga et al. (158). They found with mainly DSC studies with additional support from infrared and nuclear magnetic resonance (NMR) spectroscopy that Cers favour the stability of the gel over the fluid lamellar phase in phospholipid bilayers. Another indication of the stabilization of these gel domains is given by the decreasing ascent of the lamellar repeat distances upon heating for a given Cer concentration (Fig.4.3 A). With combined X-ray and osmotic pressure experiments we were able to derive interaction potentials (Fig.4.10) between POPC/SM bilayers and for the fluid and gel phases coexisting in POPC/SM/Cer membranes. It was shown, that the  $L^c_\beta$  phase is the most stable one and has strongly coupled corresponding bilayers (86).

The domain sizes of the gel domains are generally increasing with increasing temperature. This can be explained with the fact, that heating accelerates the lateral diffusion and therefore, the probability for Cer to meet and recruit SM is growing. Interestingly, the biggest domain at physiological temperature was found for a Cer content of 15 mol% (SM/Cer ratio: 2.3). This confirms the preferred number of SM molecules recruited by Cer for gel domain formation is around 2.3. These results are in agreement with Silva et al. (138), who found that Cer added to a ternary lipid system composed of POPC/SM/Chol recruits two to three SM molecules for the formation of highly ordered gel domains. This is an optimum ratio also in the absence of Chol, as was further confirmed by the finding of dependency of structural rearrangement from the SM/Cer ratio (section 4.2.) and by Goni et al. recently (159).

Our X-ray measurements revealed lamellar phases for all samples and the course of the  $d$ -values versus temperature and Cer content are in good agreement with the phase boundaries

seen from the DSC data. Within the gel-fluid domain coexistence region, the SAXS peaks slightly broaden, which indicates the coexistence of two lamellar phases, as has also been observed previously (69, 86, 134, 152).

The d-values are average values of the overlapping lattices of the coexisting phases. The proportion of the gel phase is increasing upon decreasing SM/Cer ratio, which is reflected in higher d-values (Fig 4.3). The lamellar repeat distance at 37°C is increasing upon Cer addition down to an equimolar SM/Cer ratio (Fig.4.3 B). For Cer contents bigger than 25 mol%, the lamellar repeat distance shrinks, which suggests the incorporation of POPC into the  $L^c_\beta$  phases. The IR data also confirm that the POPC molecules remain unaffected from the SM/Cer ratio for values down to 1.5 (Fig.4.5).

By applying an osmotic pressure to two different samples (POPC/SM, binary lipid mixture and POPC/SM/Cer = 50/35/15 molar ratio) at physiological temperature and performing a theoretical analysis, it was shown that the addition of Cer to POPC/SM model membranes leads to a four times smaller bending rigidity of the fluid phase within the phase coexisting regime. The reason is a depletion of SM, which gets recruited by Cer to the gel phase. This results in a redistribution of repulsive lateral pressures from the bilayer interior toward the lipid/water interface within the  $L^c_\alpha$  phase, which could significantly affect the function of membrane proteins, which are not associated to raft structures, like ion channels.

### 5.3 Non-equilibrium study

On the basis of our results we are able link the microscopic events occurring in the course of SMase action in an apoptotic model membrane system to effects on the macroscopic level. The initiation of the enzyme reaction is the attachment of the enzyme to the vesicles, where it starts to hydrolyze the SM lipids of the outer membrane-leaflet which leads to the formation of an  $L_{\beta}$  gel phase. As these domains grow in size trans-bilayer coupling might occur at some point (160), leading to the formation of a gel phase in both monolayers, which may be further supported by Cer flip-flop (161). Asymmetric gelification of the outer membrane leaflet builds up a large mechanical strain due to difference in lateral areas per lipid in the fluid and gel phase. We found  $A = 40 \text{ \AA}^2$  for the gel phase already 70 s after the start of the enzyme reaction, which is about  $20 - 25 \text{ \AA}^2$  smaller than the area estimated for the POPC/SM mixture in the  $L_{\alpha}$  phase (162, 163). The spontaneous negative curvature of Cer given by their small headgroup size (71) imposes additional strain. This results in an invagination of the membrane, budding and finally shedding of vesicles in combination with transient pore formation (13, 35, 79, 164).

We found an induction of the  $L_{\beta}^c$  phase right at the onset of the enzyme reaction and, interestingly, this domain size grows about four times faster than Cer is generated (Fig.4.13 D). This can be understood by the ability of SM to form hydrogen bonds with Cer, which leads to a recruitment of SM to gel phase domains, as has been found in equilibrium studies (152). The rapid gel phase formation stops after  $\sim 20$  min (Fig.4.13 D). The associated bilayer swelling proceeded initially at the same rate as gel-phase formation and also slowed down at this time (Fig.4.13 A). Comparison to HPTLC data shows that the fast changes occur until the SM/Cer molar ratio of about 1 is reached. Thus, as long as Cer levels do not exceed those of SM, progression of the gel phase is faster than Cer generation. For SM/Cer  $< 1$  the growth of gel domains stop. Thus, the biological activity of SMase is highly dependent on the evolving SM/Cer molar ratio within the membrane (Fig.5.2).



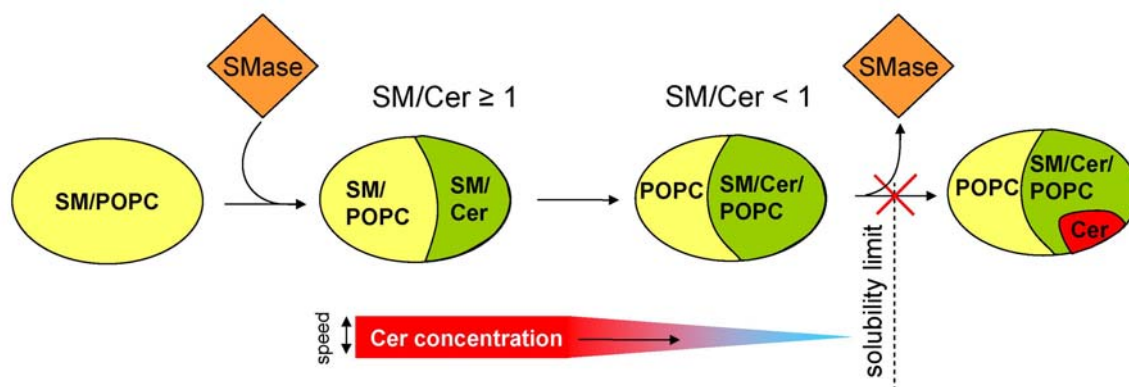


Figure 5.2 Schematic of SMase-activity as a function of the SM/Cer molar ratio. The addition of SMase to SM/POPC vesicles induces a macroscopic phase separation into SM/Cer-rich gel and SM/POPC-rich fluid domains. As long as  $SM/Cer \geq 1$ , each Cer can pair with at least one SM and progress of gel phase formation is faster than Cer generation. For  $SM/Cer < 1$ , kinetics slow down, because POPC, which has a lower affinity to Cer, needs to be incorporated into the growing gel domains in order to avoid precipitation of Cer crystallites. The reaction stops just at the solubility limit of Cer within the membrane.

The growth of domain size stops for  $SM/Cer$  ratios  $< 1$ . This can be rationalized by:

- (i) the low affinity of POPC/Cer interactions (138) and
- (ii) the entropic penalty of pairwise Cer interactions which lead to segregation of membrane insoluble Cer crystallites

Still the amount of the the  $L_{\beta}^c$  phase continues to grow as evidenced by the continued increase of the average d-spacing (Fig.4.13 A). This growth is slow enough to follow equilibrium d-values (Fig.4.14). However, because Cer levels are larger than those of SM ( $SM/Cer < 1$ ), POPC is increasingly incorporated into the gel domains in agreement with previous reports that show the induction of a gel phase in POPC bilayers by Cer (134, 137). This scenario is substantiated by the recovery of the lateral area per lipid after 40 min (Fig.4.13 C), which is related to the larger lateral size of POPC compared to SM due to its monounsaturated acyl chain.

In agreement with previous biophysical studies (79, 164) we also found an aggregation of membranes (Fig.4.13 B). However, growth of regularly stacked bilayers proceeded

significantly slower than gel phase formation and bilayer swelling. This is expected, because the removal of interstitial water and membrane diffusion processes proceeds on a slower time scale than gel phase formation. The increasing number of correlated layers corresponds to the growth of the  $L_{\beta}^c$  phase. The correlation of the gel domains proceeds much slower than all the other observed structural changes. The reason lies in membrane diffusion processes and the additional time needed for the removal of the interstitial water. The adhesion of the gel domains can be explained by the negligible bilayer undulations and the consequently increased attraction of adjacent membranes. Additionally thicker gel membranes experience also increased van der Waals attraction.

Since the SAXS signal is dominated by the  $L_{\beta}^c$  phase, our data shed light on the physical origin of vesicle aggregation during the action of SMase. The gel phase macroscopically separates from the coexisting  $L_{\alpha}^c$  phase. Gel phase bilayers are rigid and exhibit negligible bending undulations, which are the source of a long-range repulsive force in fluid membranes (86). In the absence of this force, adhesion between gel phase membranes increases. Additionally, the thicker gel membranes also experience increased van der Waals attraction. In turn, attractive interactions between macroscopically phase separated  $L_{\alpha}^c$  domains are much weaker. Hence, they may remain positionally uncorrelated, accounting for the absence of their signature in the SAXS data (Fig.4.12).

Comparing the present results to previous studies on SMase activity (69, 79, 164), we generally find differences in time scales on the order of one magnitude. Aggregation of vesicles (79, 164) was found to proceed on the time scale of seconds, whereas we observed a growth rate of bilayers stacks of several minutes. Most likely this is related to differences in enzyme/SM ratios and/or composition of lipid model membranes as the physical state of membranes was demonstrated to influence SM hydrolysis (45, 85).

Finally, we focussed on the saturation level of Cer, which is at ~86 % of all SM molecules, although SMase has full access to all SM upon entry into the vesicles. One of the more obvious reasons could be that the enzyme gets entrapped during the various vesiculation processes. Another possibility is that the affinity of the SMase to the lipid surface decreases with an increase of POPC relative to SM (87). However, it is also remarkable that we did not observe any pure Cer aggregates. C16:0-Cer aggregates are readily detectable by SAXS in equilibrium systems (Fig.4.4). Hence, catalytic turnover stops just at the solubility limit of Cer in

POPC/SM membranes. Indeed, SMase activity has been reported to depend on the fluidity of model membranes (45, 85) and we have demonstrated that Cer affects the bending rigidity of both coexisting phases (86).

Interestingly SM hydrolysis stopped at about the same Cer concentration in different cell biology experiments (2, 165, 166). This suggests that a similar feedback system may be also present in cells, which could be a natural control mechanism to reduce toxic risks of pure Cer aggregates (167).

# 6 Conclusions and Outlook

The effect of Cer on the lateral membrane structure has been studied extensively, for reviews see (26, 35, 63). Cer induces lateral phase separation into coexisting fluid and gel domains (52, 135, 152) and thereby may stabilize membrane rafts (152). This is confirmed by our data, which clearly show the stabilization of a gel phase upon increasing Cer content.

In SM mixtures this gel phase is formed due to the coordination of up to 3 SM molecules per Cer molecule. Consequently, this alters the mechanical properties of the fluid domains and could strongly affect the function of non-raft proteins. The increase of membrane flexibility induced a net shift of lateral pressures within the hydrocarbon region toward the lipid/water interface, which is the opposite effect, Chol is known to exert in membranes (168). Hence, we expect that the addition of cholesterol would counteract the inhibition of the ion-channel. In support of this argument cholesterol has been reported to be an essential membrane component for the activation of nicotinic acetylcholine receptors (169). Because of the large differences in the cholesterol content between the two sites, where Cer is generated (170), i.e. endoplasmic reticulum and plasma membrane, these effects will be specific to the given membrane.

Our time-resolved study of the effects of enzymatic generated Cer showed that the activity of the SMase is directly influenced by the membrane properties, which are strongly influenced by the SM/Cer ratio.

This biophysical regulation of SMase activity based on the SM/Cer ratio is further suggested by the remarkable correlation of the model data to those from cell biology experiments (2, 165), in terms of the kinetics as well as the level of SM fragmentation. This may indicate the existence of a natural control mechanism to reduce toxic risks of pure Cer aggregates in living systems (167).

Chol is an ubiquitous component of biological membranes (7) and the addition of Chol to the lipid model system is therefore the next logical step, as has been done by several workgroups (74, 134, 152-154, 171-176). London and co-workers (172) observed that Cer stabilizes domain formation in SM/PC/Chol mixtures and they suggested that Cer competes with Chol for the presence within these ordered domains. This can lead to a Chol displacement by Cer (177), while high cholesterol concentrations are able to dissolve the

## 6 Conclusion & Outlook

Cer-enriched gel domains (172, 178). These domains contain lipids with large headgroups and are therefore able to accommodate such lipids with small polar head groups, like Chol and Cer. Chol and Cer do not only have similar headgroup sizes and therefore similar preferential places of residence but they seem to have similar effects on membrane properties, too. It was shown by our IR results that Cer promotes disorder below the phase transition of the binary lipid system, whereas above this temperature, it exhibits an ordering effect. The presence of Chol was also found to strongly affect the SMase activity (175). Future work will therefore focus on the role of Chol on the kinetics of Cer formation.

Additionally there is a gap of 70 s after mixing (Fig.4.13), where we were not able to record X-ray scattering data of the enzyme reaction. Further work should therefore focus also on the technological improvement of the time-resolution of the experiment, using an automated mixing device to study the lag-time (time between enzyme addition and catalytic action) of the enzyme reaction.

## 7 Bibliography

1. Kroemer, G, Zamzami, N, Susin, S A (1997) Mitochondrial control of apoptosis. *Immunol. Today* **18**: 44-51.
2. Tepper, A D, Ruurs, P, Wiedmer, T, Sims, P J, Borst, J, van Blitterswijk, W J (2000) Sphingomyelin hydrolysis to ceramide during the execution phase of apoptosis results from phospholipid scrambling and alters cell-surface morphology. *J. Cell Biol.* **150**: 155-164.
3. Elmore, S (2007) Apoptosis: a review of programmed cell death. *Toxicol. Pathol.* **35**: 495-516.
4. Andrieu-Abadie, N, Levade, T (2002) Sphingomyelin hydrolysis during apoptosis. *Biochim. Biophys. Acta* **1585**: 126-134.
5. van Blitterswijk, W J, van der Luit, A H, Veldman, R J, Verheij, M, Borst, J (2003) Ceramide: second messenger or modulator of membrane structure and dynamics? *Biochem. J.* **369**: 199-211.
6. Riboni L., T G (1997) The role of Sphingolipids in the process of signal transduction. *Prog. Lipid Res.* **35**: 153-157.
7. Yeagle, P. L. (2005) *The structure of biological membranes* (CRC Press, New York).
8. Koval M., P R (1991) Intracellular transport and metabolism of sphingomyelin. *Biochim Biophys Acta* **1082**: 113-125.
9. van Meer, G, Voelker, D R, Feigenson, G W (2008) Membrane lipids: where they are and how they behave. *Nat. Rev. Mol. Cell Biol* **9**: 112-124.
10. Ikeda, M, Kihara, A, Igarashi, Y (2006) Lipid asymmetry of the eukaryotic plasma membrane: functions and related enzymes. *Biol. Pharm. Bull.* **29**: 1542-1546.
11. Merrill, A H, Jones, D (1990) An update of the enzymology and regulation of sphingomyelin metabolism. *Biochim. Biophys. Acta* **1044**: 1-12.
12. Gulbins, E, Dreschers, S, Wilker, B, Grassme, H (2004) Ceramide, membrane rafts and infections. *J. Mol. Med.* **82**: 357-363.
13. Goni, F M, Alonso, A (2009) Effects of ceramide and other simple sphingolipids on membrane lateral structure. *Biochim. Biophys. Acta* **1788**: 169-177.
14. Ganesan, V, Perera, M N, Colombini, D, Datskovskiy, D, Chadha, K, Colombini, M (2010) Ceramide and activated Bax act synergistically to permeabilize the mitochondrial outer membrane. *Apoptosis*.
15. Colombini, M (2010) Ceramide channels and their role in mitochondria-mediated apoptosis. *Biochim Biophys Acta*.

16. Siskind, L J, Kolesnick, R N, Colombini, M (2006) Ceramide forms channels in mitochondrial outer membranes at physiologically relevant concentrations. *Mitochondrion* **6**: 118-125.
17. van Blitterswijk, W J, van der Luit, A H, Caan, W, Verheij, M, Borst, J (2001) Sphingolipids related to apoptosis from the point of view of membrane structure and topology. *Biochem. Soc. Trans.* **29**: 819-824.
18. Van Cruchten, S, Van den, B W (2002) Morphological and biochemical aspects of apoptosis, oncosis and necrosis. *Anat. Histol. Embryol.* **31**: 214-223.
19. Rudolf, E, Cervinka, M (2005) Membrane blebbing in cancer cells treated with various apoptotic inducers. *ACTA MEDICA* **48**: 29-34.
20. Coleman, M L, Sahai, E A, Yeo, M, Bosch, M, Dewar, A, Olson, M F (2001) Membrane blebbing during apoptosis results from caspase-mediated activation of ROCK I. *Nat. Cell Biol.* **3**: 339-345.
21. Shiratsuchi, A, Mori, T, Nakanishi, Y (2002) Independence of plasma membrane blebbing from other biochemical and biological characteristics of apoptotic cells. *J. Biochem.* **132**: 381-386.
22. Rudolf, E, Cervinka, M (2005) membrane blebbing in cancer cells treated with various apoptotic inducers. *ACTA MEDICA* **48**: 29-34.
23. Rudolf, E, Cervinka, M (2005) membrane blebbing in cancer cells treated with various apoptotic inducers. *ACTA MEDICA* **48**: 29-34.
24. Goldkorn, T, Balaban, N, Shannon, M, Chea, V, Matsukuma, K, Gilchrist, D, Wang, H, Chan, C (1998) H<sub>2</sub>O<sub>2</sub> acts on cellular membranes to generate ceramide signaling and initiate apoptosis in tracheobronchial epithelial cells. *J. Cell Sci.* **111**: 3209-3220.
25. Deigner, H P, Claus, R, Bonaterra, G A, Gehrke, C, Bibak, N, Blaess, M, Cantz, M, Metz, J, Kinscherf, R (2001) Ceramide induces aSMase expression: implications for oxLDL-induced apoptosis. *Faseb Journal* **15**: 807-814.
26. Goni, F M, Alonso, A (2006) Biophysics of sphingolipids I. Membrane properties of sphingosine, ceramides and other simple sphingolipids. *Biochim. Biophys. Acta* **1758**: 1902-1921.
27. Obeid, L M, Linardic, C M, Karolak, L A, Hannun, Y A (1993) Programmed cell death induced by ceramide. *Science* **259**: 1769-1771.
28. Cremesti, A, Paris, F, Grassme, H, Holler, N, Tschopp, J, Fuks, Z, Gulbins, E, Kolesnick, R (2001) Ceramide enables Fas to cap and kill. *J. Biol. Chem.* **276**: 23954-23961.
29. Hannun, Y A a L M O (1995) Ceramide: an intracellular signal for apoptosis. *Trends Biochem. Sci.* **20**: 73-77.

30. Hannun Y.A. and Lina M.Obeid (2002) The Ceramide-centric Universe of Lipid-mediated Cell Regulation: Stress Encounters of the Lipid Kind\*. *THE JOURNAL OF BIOLOGICAL CHEMISTRY* **277**: 25847-25850.
31. Hannun, Y A, Luberto, C (2000) Ceramide in the eukaryotic stress response. *Trends in Cell Biology* **10**: 73-80.
32. Hannun, Y A (1994) The Sphingomyelin Cycle and the Second Messenger Function of Ceramide . *Journal of Biological Chemistry* **269**: 3125-3128.
33. Hannun, Y A, Obeid, L M (2008) Principles of bioactive lipid signalling: lessons from sphingolipids. *Nature Rev.* **9**: 139-150.
34. Schurer, N Y, Elias, P M (1991) The biochemistry and function of stratum corneum lipids. *Adv. Lipid Res.* **24**: 27-56.
35. Kolesnick, R N, Goni, F M, Alonso, A (2000) Compartmentalization of ceramide signaling: Physical foundations and biological effects. *J. Cell. Phys.* **184**: 285-300.
36. Ballou, L R, Lauderkind, S J, Rosloniec, E F, Raghov, R (1996) Ceramide signalling and the immune response. *Biochim. Biophys. Acta* **1301**: 273-287.
37. Carrer, D C, Hartel, S, Monaco, H L, Maggio, B (2003) Ceramide modulates the lipid membrane organization at molecular and supramolecular levels. *Chem. Phys. Lipids* **122**: 147-152.
38. Sprong, H, van der Sluijs, P, van Meer, G (2001) How proteins move lipids and lipids move proteins. *Nature Rev.* **2**: 504-513.
39. Shah, J, Atienza, J M, Rawlings, A V, Shipley, G G (1995) Physical properties of ceramides: effect of fatty acid hydroxylation. *J. Lipid Res.* **36**: 1945-1955.
40. Hannun, Y A, Luberto, C (2000) Ceramide in the eukaryotic stress response. *Trends Cell Biol.* **10**: 73-80.
41. Spiegel, S, Foster, D, Kolesnick, R (1996) Signal transduction through lipid second messengers. *Curr. Opin. Cell Biol* **8**: 159-167.
42. Merrill A (2002) De Novo Sphingolipid Biosynthesis: A Necessary, but Dangerous, Pathway. *THE JOURNAL OF BIOLOGICAL CHEMISTRY* **277**: 25843-25846.
43. Weiss, B, Stoffel, W (1997) Human and murine serine-palmitoyl-CoA transferase--cloning, expression and characterization of the key enzyme in sphingolipid synthesis. *Eur J Biochem* **249**: 239-247.
44. Hannun, Y A (1994) The Sphingomyelin Cycle and the Second Messenger Function of Ceramide . *Journal of Biological Chemistry* **269**: 3125-3128.
45. Goni, F M, Alonso, A (2002) Sphingomyelinases: enzymology and membrane activity . *FEBS Lett.* **531**: 38-46.



46. Levade, T, Jaffrezou, J P (1999) Signalling sphingomyelinases: which, where, how and why? *Biochim. Biophys. Acta* **1438**: 1-17.
47. Spiegel, S, Sheldon, M (2009) Sphingosine 1-Phosphate, a Key Cell Signaling Molecule. *J. Biol. Chem.* **277**: 25851-25854.
48. Taha, T A, Mullen, T D, Obeid, L M (2006) A house divided: Ceramide, sphingosine, and sphingosine-1-phosphate in programmed cell death. *Biochim. Biophys. Acta* **1758**: 2027-2036.
49. Hannun, Y A, Obeid, L M (2002) The Ceramide-centric universe of lipid-mediated cell regulation: stress encounters of the lipid kind. *J. Biol. Chem.* **277**: 25847-25850.
50. Hannun, Y A, Obeid, L M, Wolff, R A (1993) The novel second messenger ceramide: identification, mechanism of action, and cellular activity. *Adv. Lipid Res.* **25**: 43-64.
51. Hannun, Y A (1994) The sphingomyelin cycle and the second messenger function of ceramide. *J. Biol. Chem.* **269**: 3125-3128.
52. Venkataraman, K, Futerman, A H (2000) Ceramide as a second messenger: sticky solutions to sticky problems. *Trends Cell Biol* **10**: 408-412.
53. Futerman, A H, Hannun, Y A (2004) The complex life of simple sphingolipids. *EMBO Rep.* **5**: 777-782.
54. Hannun, Y A, Obeid, L M (1995) Ceramide: an intracellular signal for apoptosis. *Trends Biochem. Sci.* **20**: 73-77.
55. Hannun, Y A, Obeid, L M (1997) Mechanisms of ceramide-mediated apoptosis. *Adv. Exp. Med. Biol* **407**: 145-149.
56. Hannun, Y A (1996) Functions of ceramide in coordinating cellular responses to stress. *Science* **274**: 1855-1859.
57. Hofmann, K, Dixit, V M (1998) Ceramide in apoptosis--does it really matter? *Trends Biochem Sci.* **23**: 374-377.
58. Zhang, Y, Yao, B, Delikat, S, Bayoumy, S, Lin, X H, Basu, S, McGinley, M, Chan-Hui, P Y, Lichenstein, H, Kolesnick, R (1997) Kinase suppressor of Ras is ceramide-activated protein kinase. *Cell* **89**: 63-72.
59. Diaz-Meco, M T, Municio, M M, Frutos, S, Sanchez, P, Lozano, J, Sanz, L, Moscat, J (1996) The product of par-4, a gene induced during apoptosis, interacts selectively with the atypical isoforms of protein kinase C. *Cell* **86**: 777-786.
60. Huwiler, A, Johansen, B, Skarstad, A, Pfeilschifter, J (2001) Ceramide binds to the CaLB domain of cytosolic phospholipase A2 and facilitates its membrane docking and arachidonic acid release. *FASEB J* **15**: 7-9.

61. van Blitterswijk, W J (1998) Hypothesis: ceramide conditionally activates atypical protein kinases C, Raf-1 and KSR through binding to their cysteine-rich domains. *Biochem J* **331**: 679-680.
62. Heinrich, M, Wickel, M, Winoto-Morbach, S, Schneider-Brachert, W, Weber, T, Brunner, J, Saftig, P, Peters, C, Kronke, M, Schutze, S (2000) Ceramide as an activator lipid of cathepsin D. *Adv. Exp. Med. Biol* **477**: 305-315.
63. Cremesti, A E, Goni, F M, Kolesnick, R (2002) Role of sphingomyelinase and ceramide in modulating rafts: do biophysical properties determine biologic outcome? *FEBS Lett.* **531**: 47-53.
64. Goni, F M, Alonso, A (2009) Effects of ceramide and other simple sphingolipids on membrane lateral structure. *Biochim Biophys Acta* **1788**: 169-177.
65. Huang, H W, Goldberg, E M, Zidovetzki, R (1998) Ceramides perturb the structure of phosphatidylcholine bilayers and modulate the activity of phospholipase A2. *Eur. Biophys. J.* **27**: 361-366.
66. Carrer, D C, Maggio, B (1999) Phase behavior and molecular interactions in mixtures of ceramide with dipalmitoylphosphatidylcholine. *J. Lipid Res.* **40**: 1978-1989.
67. Moore, D (1997) FTIR spectroscopy studies of the conformational order and phase behavior of ceramides. *J. Phys. Chem. B.* **101**: 8933-8940.
68. Huang, H W, Goldberg, E M, Zidovetzki, R (1996) Ceramide induces structural defects into phosphatidylcholine bilayers and activates phospholipase A2. *Biochem. Biophys. Res. Commun.* **220**: 834-838.
69. Holopainen, J M, Subramanian, M, Kinnunen, P K (1998) Sphingomyelinase induces lipid microdomain formation in a fluid phosphatidylcholine/sphingomyelin membrane. *Biochemistry* **37**: 17562-17570.
70. Holopainen, J M, Lemmich, J, Richter, F, Mouritsen, O G, Rapp, G, Kinnunen, P K (2000) Dimyristoylphosphatidylcholine/C16:0-ceramide binary liposomes studied by differential scanning calorimetry and wide- and small-angle x-ray scattering. *Biophys. J.* **78**: 2459-2469.
71. Veiga, M P, Arrondo, J L, Goni, F M, Alonso, A (1999) Ceramides in phospholipid membranes: effects on bilayer stability and transition to nonlamellar phases. *Biophys. J.* **76**: 342-350.
72. Holopainen, J M, Lehtonen, J Y, Kinnunen, P K (1997) Lipid microdomains in dimyristoylphosphatidylcholine-ceramide liposomes. *Chem. Phys. Lipids* **88**: 1-13.
73. Hsueh, Y W, Giles, R, Kitson, N, Thewalt, J (2002) The effect of ceramide on phosphatidylcholine membranes: A deuterium NMR study. *Biophys. J.* **82**: 3089-3095.
74. Massey, J B (2001) Interaction of ceramides with phosphatidylcholine, sphingomyelin and sphingomyelin/cholesterol bilayers. *Biochim. Biophys. Acta* **1510**: 167-184.

75. Ruiz-Arguello, M B, Goni, F M, Alonso, A (1998) Vesicle membrane fusion induced by the concerted activities of sphingomyelinase and phospholipase C. *J. Biol. Chem.* **273**: 22977-22982.
76. Sot, J, Arada, F J, Collado, M I, Goni, F M, Alonso, A (2005) Different effects of long- and short-chain ceramides on the gel-fluid and lamellar-hexagonal transitions of phospholipids: a calorimetric, NMR, and x-ray diffraction study. *Biophys. J.* **88**: 3368-3380.
77. Siegel, D P (1999) The modified stalk mechanism of lamellar/inverted phase transitions and its implications for membrane fusion. *Biophys. J.* **76**: 291-313.
78. Siegel, D P, Burns, J L, Chestnut, M H, Talmon, Y (1989) Intermediates in membrane fusion and bilayer/nonbilayer phase transitions imaged by time-resolved cryo-transmission electron microscopy. *Biophys. J.* **56**: 161-169.
79. Ruiz-Arguello, M B, Basanez, G, Goni, F M, Alonso, A (1996) Different effects of enzyme-generated ceramides and diacylglycerols in phospholipid membrane fusion and leakage. *J. Biol. Chem.* **271**: 26616-26621.
80. Montes, L R, Ruiz-Arguello, M B, Goni, F M, Alonso, A (2002) Membrane restructuring via ceramide results in enhanced solute efflux. *J. Biol. Chem.* **277**: 11788-11794.
81. Kiessling, V, Crane, J M, Tamm, L (2006) Transbilayer Effects of Raft-Like Lipid Domains in Asymmetric Planar Bilayers Measured by Single Molecule Tracking. *Biophys. J.* **91**: 3313-3326.
82. Contreras, F X, Villar, A V, Alonso, A, Kolesnick, R N, Goni, F M (2003) Sphingomyelinase activity causes transbilayer lipid translocation in model and cell membranes. *J. Biol. Chem.* **278**: 37169-37174.
83. Goni, F M, Alonso, A (2000) Membrane fusion induced by phospholipase C and sphingomyelinases. *Biosci. Rep.* **20**: 443-463.
84. Honger, T, Jorgensen, K, Biltonen, R L, Mouritsen, O G (1996) Systematic relationship between phospholipase A2 activity and dynamic lipid bilayer microheterogeneity. *Biochemistry* **35**: 9003-9006.
85. Ruiz-Arguello, M B, Veiga, M P, Arrondo, J L R, Goni, F M, Alonso, A (2002) Sphingomyelinase cleavage of sphingomyelin in pure and mixed lipid membranes. Influence of the physical state of the sphingolipid. *Chem. Phys. Lipids* **114**: 11-20.
86. Pabst, G, Boulgaropoulos, B, Gander, E, Sarangi, B R, Amenitsch, H, Raghunathan, V A, Laggner, P (2009) Effect of Ceramide on Nonraft Proteins. *J. Membr. Biol.* **231**: 125-132.
87. Yu, B Z, Zakim, D, Jain, M K (2002) Processive interfacial catalytic turnover by *Bacillus cereus* sphingomyelinase on sphingomyelin vesicles. *Biochim. Biophys. Acta* **1583**: 122-132.

88. Berg, O G, Yu, B Z, Rogers, J, Jain, M K (1991) Interfacial Catalysis by Phospholipase A2: Determination of the Interfacial KineticRate Constants. *Biochemistry* **30**: 7283-7297.
89. Berg, O. G. & Jain, M. K. (2002) *Interfacial Enzyme Kinetics* (Wiley, London).
90. Israelachvili, J. N. (1985) *Intermolecular and Surface Force*, (Academic Press, London).
91. Luzzati V (1968) in *Biological Membranes*, ed. Chapman, D. (Academic Press, London, New York,), pp. 71-123.
92. Parsegian, V A, Rand, R P (1995) in *Structure and Dynamics of Membranes*, eds. Lipowsky, R., Sackmann, E. pp. 643-690.
93. Helfrich, W (1973) Elastic properties of lipid bilayers: theory and possible experiments. *Z. Naturforsch. C* **28**: 693-703.
94. Chatterjee, S (1999) Neutral sphingomyelinase: past, present and future. *Chem. Phys. Lipids* **102**: 79-96.
95. Samet, D, Barenholz, Y (1999) Characterization of acidic and neutral sphingomyelinase activities in crude extracts of HL-60 cells. *Chem. Phys. Lipids* **102**: 65-77.
96. Goni, F M, Alonso, A (2002) Sphingomyelinases: enzymology and membrane activity. *FEBS Lett.* **531**: 38-46.
97. Schneider, P B, Kennedy, E P (1967) Sphingomyelinase in normal human spleens and in spleens from subjects with Niemann-Pick disease. *J Lipid Res.* **8**: 202-209.
98. Schissel, S L, Jiang, X, Tweedie-Hardman, J, Jeong, T, Camejo, E H, Najib, J, Rapp, J H, Williams, K J, Tabas, I (1998) Secretory sphingomyelinase, a product of the acid sphingomyelinase gene, can hydrolyze atherogenic lipoproteins at neutral pH. Implications for atherosclerotic lesion development. *J Biol Chem.* **273**: 2738-2746.
99. Goni, F M, Alonso, A (2002) Sphingomyelinases: enzymology and membrane activity. *FEBS Lett.* **531**: 38-46.
100. Okazaki, T, Bielawska, A, Domae, N, Bell, R M, Hannun, Y A (1994) Characteristics and partial purification of a novel cytosolic, magnesium-independent, neutral sphingomyelinase activated in the early signal transduction of 1 alpha,25-dihydroxyvitamin D3-induced HL-60 cell differentiation. *J Biol Chem.* **269**: 4070-4077.
101. Jung, S Y, Suh, J H, Park, H J, Jung, K M, Kim, M Y, Na, D S, Kim, D K (2000) Identification of multiple forms of membrane-associated neutral sphingomyelinase in bovine brain. *J Neurochem.* **75**: 1004-1014.
102. Yamada, A, Tsukagoshi, N, Udaka, S, Sasaki, T, Makino, S, Nakamura, S, Little, C, Tomita, M, Ikezawa, H (1988) Nucleotide sequence and expression in Escherichia

- coli of the gene coding for sphingomyelinase of *Bacillus cereus*. *Eur. J. Biochem.* **175**: 213-220.
103. Clarke, C J, Snook, C F, Tani, M, Matmati, N, Marchesini, N, Hannun, Y A (2006) The extended family of neutral sphingomyelinases. *Biochemistry* **45**: 11247-11256.
  104. Coleman, D C, Arbuthnott, J P, Pomeroy, H M, Birkbeck, T H (1986) Cloning and expression in *Escherichia coli* and *Staphylococcus aureus* of the beta-lysin determinant from *Staphylococcus aureus*: evidence that bacteriophage conversion of beta-lysin activity is caused by insertional inactivation of the beta-lysin determinant. *Microb. Pathog.* **1**: 549-564.
  105. Ago, H, Oda, M, Takahashi, M, Tsuge, H, Ochi, S, Katunuma, N, Miyano, M, Sakurai, J (2006) Structural basis of the sphingomyelin phosphodiesterase activity in neutral sphingomyelinase from *Bacillus cereus*. *J. Biol. Chem.* **281**: 16157-16167.
  106. Tomita, M, Ueda, Y, Tamura, H, Taguchi, R, Ikezawa, H (1993) The role of acidic amino-acid residues in catalytic and adsorptive sites of *Bacillus cereus* sphingomyelinase. *Biochim. Biophys. Acta* **1203**: 85-92.
  107. Ikezawa, H, Mori, M, Ohyabu, T, Taguchi, R (1978) Studies on sphingomyelinase of *Bacillus cereus*. I. Purification and properties. *Biochim. Biophys. Acta* **528**: 247-256.
  108. Milhas, D, Clarke, C J, Hannun, Y A (2009) Sphingomyelin metabolism at the plasma membrane: Implications for bioactive sphingolipids. *FEBS Lett.*
  109. Montes, L R, Goñi, F M, Johnston, N C, Goldfine, H, Alonso, A (2004) Membrane Fusion Induced by the Catalytic Activity of a Phospholipase C/Sphingomyelinase from *Listeria monocytogenes*. *Biochemistry* **43**: 3688-3695.
  110. Jungner, M, Ohvo, H, Slotte, J P (1997) Interfacial regulation of bacterial sphingomyelinase activity. *Biochim. Biophys. Acta* **1344**: 230-240.
  111. McElhaney, R N (1982) The use of differential scanning calorimetry and differential thermal analysis in studies of model and biological membranes. *Chem. Phys. Lipids* **30**: 229-259.
  112. Ohura, K S K a M H (1972) The crystal and molecular structure of p-bromobenzoic acid. *Bull. Chem. Soc. Japan* **45**: 2651-2652.
  113. Pabst, G (2006) Global properties of biomimetic membranes. *Biophys. Rev. Lett.* **1**: 57-84.
  114. Warren, B E (1941) X-ray diffraction methods. *J. Appl. Phys.* **12**: 375-383.
  115. McIntosh, T J, Magid, A D, Simon, S A (1987) Steric repulsion between phosphatidylcholine bilayers. *Biochemistry* **26**: 7325-7332.
  116. Pabst, G, Danner, S, Karmakar, S, Deutsch, G, Raghunathan, V A (2007) On the propensity of phosphatidylglycerols to form interdigitated phases. *Biophys J* **93**: 513-525.

117. McIntosh, T J, Simon, S A (1986) Area per molecule and distribution of water in fully hydrated dilauroylphosphatidylethanolamine bilayers. *Biochemistry* **25**: 4948-4952.
118. Parsegian, V A, Rand, R P (1995) in Handbook of biological physics., eds. Lipowsky, R., Sackmann, E. e. (Elsevier, Amsterdam), pp. 643-690.
119. Petrache, H I, Gouliaev, N, Tristram-Nagle, S, Zhang, R T, Suter, R M, Nagle, J F (1998) Interbilayer interactions from high-resolution X-ray scattering. *Phys. Rev. E* **57**: 7014-7024.
120. Pabst, G, Danner, S, Podgornik, R, Katsaras, J (2007) Entropy-driven softening of fluid lipid bilayers by alamethicin. *Langmuir* **23**: 11705-11711.
121. Pan, J, Tieleman, D P, Nagle, J F, Kucerka, N, Tristram-Nagle, S (2009) Alamethicin in lipid bilayers: combined use of X-ray scattering and MD simulations. *Biochim Biophys Acta* **1788**: 1387-1397.
122. Cantor, R S (1999) The influence of membrane lateral pressures on simple geometric models of protein conformational equilibria. *Chem. Phys. Lipids* **101**: 45-56.
123. Cantor, R S (1997) Lateral Pressures in Cell Membranes: A Mechanism for Modulation of Protein Function. *J. Phys. Chem.* **101**: 1723-1725.
124. Fidorra, M, Duelund, L, Leidy, C, Simonsen, A C, Bagatolli, L A (2006) Absence of fluid-ordered/fluid-disordered phase coexistence in ceramide/POPC mixtures containing cholesterol. *Biophys. J.* **90**: 4437-4451.
125. Sot, J, Bagatolli, L A, Goni, F M, Alonso, A (2006) Detergent-resistant, ceramide-enriched domains in sphingomyelin/ceramide bilayers. *Biophys. J.* **90**: 903-914.
126. Degovics, D, Latal, A, Prenner, E, Kriechbaum, M, Lohner, K (1997) Structure and Thermotropic Behaviour of Mixed Choline Phospholipid Model Membranes. *J. Appl. Cryst.* **30**: 776-780.
127. Silva, L, De Almeida, R F M, Fedorov, A, Matos, A P A, Prieto, M (2006) Ceramide-platform formation and -induced biophysical changes in a fluid phospholipid membrane. *Molecular Membrane Biology* **23**: 137-1U2.
128. Silva, L C, de Almeida, R F, Castro, B M, Fedorov, A, Prieto, M (2007) Ceramide-domain formation and collapse in lipid rafts: membrane reorganization by an apoptotic lipid. *Biophys. J.* **92**: 502-516.
129. Sun, W, Suter, R M, Knewton, M A, Worthington, C R, Tristram-Nagle, S, Zhang, R, Nagle, J F (1994) Order and disorder in fully hydrated unoriented bilayers of gel-phase dipalmitoylphosphatidylcholine. *Phys. Rev. E Stat. Phys. Plasmas. Fluids Relat Interdiscip. Topics* **49**: 4665-4676.
130. Kucerka, N, Tristram-Nagle, S, Nagle, J F (2005) Structure of fully hydrated fluid phase lipid bilayers with monounsaturated chains. *J Membr. Biol* **208**: 193-202.

131. Podgornik, R, French, R H, Parsegian, V A (2006) Nonadditivity in van der Waals interactions within multilayers. *J Chem. Phys.* **124**: 044709.
132. Kucerka, N, Tristram-Nagle, S, Nagle, J F (2005) Structure of fully hydrated fluid phase lipid bilayers with monounsaturated chains. *J Membr. Biol* **208**: 193-202.
133. Cantor, R S (1999) Lipid composition and the lateral pressure profile in bilayers. *Biophys. J.* **76**: 2625-2639.
134. Ben Shaul, A (1995) in Handbook of biological physics, eds. Lipowsky, R., Sackmann, E. (Elsevier, Amsterdam), pp. 359-401.
135. Pabst, G, Rappolt, M, Amenitsch, H, Laggner, P (2000) Structural information from multilamellar liposomes at full hydration: full q-range fitting with high quality x-ray data. *Phys. Rev. E.* **62**: 4000-4009.
136. Pabst, G, Katsaras, J, Raghunathan, V A, Rappolt, M (2003) Structure and Interactions in the Anomalous Swelling Regime of Phospholipid Bilayers. *Langmuir* **19**: 1716-1722.
137. Pellkofer, R, Sandhoff, K (1980) Halothane increases membrane fluidity and stimulates sphingomyelin degradation by membrane-bound neutral sphingomyelinase of synaptosomal plasma membranes from calf brain already at clinical concentrations. *J. Neurochem.* **34**: 988-992.
138. Baumgart, T, Hess, S T, Webb, W W (2003) Imaging coexisting fluid domains in biomembrane models coupling curvature and line tension. *Nature* **425**: 821-824.
139. Ipsen, J H, Karlstrom, G, Mouritsen, O G, Wennerstrom, H, Zuckermann, M J (1987) Phase equilibria in the phosphatidylcholine-cholesterol system. *Biochim Biophys Acta* **905**: 162-172.
140. Ayuyan, A G, Cohen, F S (2006) Lipid peroxides promote large rafts: effects of excitation of probes in fluorescence microscopy and electrochemical reactions during vesicle formation. *Biophys. J.* **91**: 2172-2183.
141. Zhao, J, Wu, J, Shao, H L, Kong, F, Jain, N, Hunt, G, Feigenson, G (2007) Phase studies of model biomembranes: Macroscopic coexistence of L $\alpha$  plus L $\beta$ , with light-induced coexistence of L $\alpha$  plus L $\alpha$  Phases. *Biochim. Biophys. Acta* **1768**: 2777-2786.
142. Veatch, S L, Leung, S S, Hancock, R E, Thewalt, J L (2007) Fluorescent probes alter miscibility phase boundaries in ternary vesicles. *J. Phys. Chem. B* **111**: 502-504.
143. Untracht, S H, Shipley, G G (1977) Molecular interactions between lecithin and sphingomyelin. *J. Biol. Chem.* **252**: 4449-4457.
144. Castro, B M, de Almeida, R F, Silva, L C, Fedorov, A, Prieto, M (2007) Formation of ceramide/sphingomyelin gel domains in the presence of an unsaturated phospholipid: a quantitative multiprobe approach. *Biophys. J.* **93**: 1639-1650.

145. de Almeida, R F, Fedorov, A, Prieto, M (2003) Sphingomyelin/phosphatidylcholine/cholesterol phase diagram: boundaries and composition of lipid rafts. *Biophys. J.* **85**: 2406-2416.
146. Bunge, A, Muller, P, Stockl, M, Herrmann, A, Huster, D (2008) Characterization of the ternary mixture of sphingomyelin, POPC, and cholesterol: support for an inhomogeneous lipid distribution at high temperatures. *Biophys J* **94**: 2680-2690.
147. de Almeida, R F, Loura, L M, Fedorov, A, Prieto, M (2005) Lipid rafts have different sizes depending on membrane composition: a time-resolved fluorescence resonance energy transfer study. *J Mol. Biol* **346**: 1109-1120.
148. Niemela, P S, Hyvonen, M T, Vattulainen, I (2006) Influence of chain length and unsaturation on sphingomyelin bilayers. *Biophys. J.* **90**: 851-863.
149. Staneva, G, Chachaty, C, Wolf, C, Koumanov K., Quinn, P J (2008) The role of sphingomyelin in regulating phase coexistence in complex lipid model membranes: Competition between ceramide and cholesterol. *Biochim. Biophys. Acta* **1778** : 2727-2739.
150. Veiga, M P, Arrondo, J L, Goni, F M, Alonso, A (1999) Ceramides in phospholipid membranes: effects on bilayer stability and transition to nonlamellar phases. *Biophys J* **76**: 342-350.
151. Páli, T, Bartucci, R, Horváth, L, Marsh, D (1993) Kinetics and dynamics of annealing during sub-gel phase formation in phospholipid bilayers A saturation transfer electron spin resonance study. *Biophys. J.* **64**: 1781-1788.
152. Tristram-Nagle, S, Suter, R M, Sun, W J, Nagle, J F (1994) Kinetics of subgel formation in DPPC: X-ray diffraction proves nucleation-growth hypothesis. *Biochim Biophys Acta* **1191**: 14-20.
153. Katsaras, J, Raghunathan, V A (2000) in *Lipid Bilayers Structure and Interactions* Berlin), pp. 26-30.
154. Busto, J V, Fanani, M L, De Tullio, L, Sot, J, Maggio, B, Goni, F M, Alonso, A (2009) Coexistence of immiscible mixtures of palmitoylsphingomyelin and palmitoylceramide in monolayers and bilayers. *Biophys J* **97**: 2717-2726.
155. May, S (2009) Trans-monolayer coupling of fluid domains in lipid bilayers. *Soft Matter* **5**: 3148-3156.
156. Contreras, F X, Basanez, G, Alonso, A, Herrmann, A, Goni, F M (2005) Asymmetric addition of ceramides but not dihydroceramides promotes transbilayer (flip-flop) lipid motion in membranes. *Biophys. J.* **88**: 348-359.
157. Chiu, S W, Vasudevan, S, Jakobsson, E, Mashl, R J, Scott, H L (2003) Structure of sphingomyelin bilayers: a simulation study. *Biophys. J.* **85**: 3624-3635.



158. Pabst, G, Hodzic, A, Strancar, J, Danner, S, Rappolt, M, Laggner, P (2007) Rigidification of neutral lipid bilayers in the presence of salts. *Biophys. J.* **93**: 2688-2696.
159. Holopainen, J M, Angelova, M I, Kinnunen, P K (2000) Vectorial budding of vesicles by asymmetrical enzymatic formation of ceramide in giant liposomes. *Biophys. J.* **78**: 830-838.
160. Andrieu, N, Salvayre, R, Levade, T (1996) Comparative study of the metabolic pools of sphingomyelin and phosphatidylcholine sensitive to tumor necrosis factor. *Eur. J. Biochem.* **236**: 738-745.
161. Ohvo, H, Olsio, C, Slotte, J P (1997) Effects of sphingomyelin and phosphatidylcholine degradation on cyclodextrin-mediated cholesterol efflux in cultured fibroblasts. *Biochim. Biophys. Acta* **1349**: 131-141.
162. Shabbits, J A, Mayer, L D (2003) Intracellular delivery of ceramide lipids via liposomes enhances apoptosis in vitro. *Biochim Biophys Acta* **1612**: 98-106.
163. Cantor, R S (1999) Lipid composition and the lateral pressure profile in bilayers. *Biophys. J.* **76**: 2625-2639.
164. Rankin, S E, Addona, G H, Kloczewiak, M A, Bugge, B, Miller, K W (1997) The cholesterol dependence of activation and fast desensitization of the nicotinic acetylcholine receptor. *Biophys. J.* **73**: 2446-2455.
165. van Meer, G, Voelker, D R, Feigenson, G W (2008) Membrane lipids: where they are and how they behave. *Nat. Rev. Mol. Cell Biol.* **9**: 112-124.
166. Castro, B M, Silva, L C, Fedorov, A, de Almeida, R F, Prieto, M (2009) Cholesterol-rich fluid membranes solubilize ceramide domains: implications for the structure and dynamics of mammalian intracellular and plasma membranes. *J Biol Chem.* **284**: 22978-22987.
167. Megha, London, E (2004) Ceramide selectively displaces cholesterol from ordered lipid domains (rafts): implications for lipid raft structure and function. *J Biol Chem.* **279**: 9997-10004.
168. Veiga, M P, Arrondo, J L, Goni, F M, Alonso, A, Marsh, D (2001) Interaction of cholesterol with sphingomyelin in mixed membranes containing phosphatidylcholine, studied by spin-label ESR and IR spectroscopies. A possible stabilization of gel-phase sphingolipid domains by cholesterol. *Biochemistry* **40**: 2614-2622.
169. de Almeida, R F, Loura, L M, Fedorov, A, Prieto, M (2005) Lipid rafts have different sizes depending on membrane composition: a time-resolved fluorescence resonance energy transfer study. *J Mol. Biol* **346**: 1109-1120.
170. Contreras, F X, Sot, J, Ruiz-Arguello, M B, Alonso, A, Goni, F M (2004) Cholesterol modulation of sphingomyelinase activity at physiological temperatures. *Chem. Phys. Lipids* **130**: 127-134.

171. Arsov, Z, Quaroni, L (2008) Detection of lipid phase coexistence and lipid interactions in sphingomyelin/cholesterol membranes by ATR-FTIR spectroscopy. *Biochim. Biophys. Acta* **1778**: 880-889.
172. Sot, J, Ibarguren, M, Busto, J V, Montes, L R, Goni, F M, Alonso, A (2008) Cholesterol displacement by ceramide in sphingomyelin-containing liquid-ordered domains, and generation of gel regions in giant lipidic vesicles. *FEBS Lett.* **582**: 3230-3236.
173. Castro, B M, Silva, L C, Fedorov, A, de Almeida, R F, Prieto, M (2009) Cholesterol-Rich Fluid Membranes Solubilize Ceramide Domains. Implications for the Structure and Dynamics of Mammalian Intracellular and Plasma Membrane. *J. Biol. Chem.*
174. Fruhwirth, G O, Hermetter, A (2008) Mediation of apoptosis by oxidized phospholipids. *Subcell. Biochem* **49**: 351-367.
175. Pike, L J (2006) Rafts defined: a report on the Keystone Symposium on Lipid Rafts and Cell Function. *J Lipid Res* **47**: 1597-1598.
176. Lingwood, D, Simons, K (2010) Lipid rafts as a membrane-organizing principle. *Science* **327**: 46-50.
177. Pabst, G, Boulgaropoulos, B, Gander, E, Sarangi, B R, Amenitsch, H, Raghunathan, V A, Laggner, P (2009) Effect of ceramide on nonraft proteins. *J. Membr. Biol.* **231**: 125-132.
178. Chao, L, Gast, A P, Hatton, T A, Jensen, K F (2010) Sphingomyelinase-induced phase transformations: causing morphology switches and multiple-time-domain ceramide generation in model raft membranes. *Langmuir* **26**: 344-356.
179. Ayuyan, A G, Cohen, F S (2006) Lipid peroxides promote large rafts: effects of excitation of probes in fluorescence microscopy and electrochemical reactions during vesicle formation. *Biophys. J.* **91**: 2172-2183.
180. Zhao, J, Wu, J, Shao, H L, Kong, F, Jain, N, Hunt, G, Feigenson, G (2007) Phase studies of model biomembranes: Macroscopic coexistence of L alpha plus L beta, with light-induced coexistence of L alpha plus Lo Phases. *Biochim. Biophys. Acta* **1768**: 2777-2786.
181. Veatch, S L, Leung, S S, Hancock, R E, Thewalt, J L (2007) Fluorescent probes alter miscibility phase boundaries in ternary vesicles. *J. Phys. Chem. B* **111**: 502-504.
182. Pabst, G, Boulgaropoulos, B, Gander, E, Sarangi, B R, Amenitsch, H, Raghunathan, V A, Laggner, P (2009) Effect of ceramide on nonraft proteins. *J. Membr. Biol.* **231**: 125-132.
183. Pabst, G, Boulgaropoulos, B, Gander, E, Sarangi, B R, Amenitsch, H, Raghunathan, V A, Laggner, P (2009) Effect of ceramide on nonraft proteins. *J. Membr. Biol.* **231**: 125-132.

184. Pabst, G, Boulgaropoulos, B, Gander, E, Sarangi, B R, Amenitsch, H, Raghunathan, V A, Laggner, P (2009) Effect of ceramide on nonraft proteins. *J. Membr. Biol.* **231**: 125-132.
185. Pabst, G, Boulgaropoulos, B, Gander, E, Sarangi, B R, Amenitsch, H, Raghunathan, V A, Laggner, P (2009) Effect of ceramide on nonraft proteins. *J. Membr. Biol.* **231**: 125-132.
186. Pabst, G, Boulgaropoulos, B, Gander, E, Sarangi, B R, Amenitsch, H, Raghunathan, V A, Laggner, P (2009) Effect of ceramide on nonraft proteins. *J. Membr. Biol.* **231**: 125-132.
187. Pabst, G, Boulgaropoulos, B, Gander, E, Sarangi, B R, Amenitsch, H, Raghunathan, V A, Laggner, P (2009) Effect of ceramide on nonraft proteins. *J. Membr. Biol.* **231**: 125-132.
188. Pabst, G, Boulgaropoulos, B, Gander, E, Sarangi, B R, Amenitsch, H, Raghunathan, V A, Laggner, P (2009) Effect of ceramide on nonraft proteins. *J. Membr. Biol.* **231**: 125-132.
189. Pabst, G, Boulgaropoulos, B, Gander, E, Sarangi, B R, Amenitsch, H, Raghunathan, V A, Laggner, P (2009) Effect of ceramide on nonraft proteins. *J. Membr. Biol.* **231**: 125-132.
190. Busto, J V, Fanani, M L, De Tullio, L, Sot, J, Maggio, B, Goni, F M, Alonso, A (2009) Coexistence of immiscible mixtures of palmitoylsphingomyelin and palmitoylceramide in monolayers and bilayers. *Biophys. J.* **97**: 2717-2726.
191. Pabst, G, Boulgaropoulos, B, Gander, E, Sarangi, B R, Amenitsch, H, Raghunathan, V A, Laggner, P (2009) Effect of ceramide on nonraft proteins. *J. Membr. Biol.* **231**: 125-132.
192. Pabst, G, Boulgaropoulos, B, Gander, E, Sarangi, B R, Amenitsch, H, Raghunathan, V A, Laggner, P (2009) Effect of ceramide on nonraft proteins. *J. Membr. Biol.* **231**: 125-132.
193. Alley, S H, Ces, O, Templer, R H, Barahona, M (2008) Biophysical regulation of lipid biosynthesis in the plasma membrane. *Biophys J* **94**: 2938-2954.
194. Pabst, G, Boulgaropoulos, B, Gander, E, Sarangi, B R, Amenitsch, H, Raghunathan, V A, Laggner, P (2009) Effect of ceramide on nonraft proteins. *J. Membr. Biol.* **231**: 125-132.
195. Chao, L, Gast, A P, Hatton, T A, Jensen, K F (2010) Sphingomyelinase-induced phase transformations: causing morphology switches and multiple-time-domain ceramide generation in model raft membranes. *Langmuir* **26**: 344-356.
196. Fanani, M L, De Tullio, L, Hartel, S, Jara, J, Maggio, B (2008) Sphingomyelinase-induced domain shape relaxation driven by out-of-equilibrium changes of composition. *Biophys. J.*

197. Chao, L, Gast, A P, Hatton, T A, Jensen, K F (2010) Sphingomyelinase-induced phase transformations: causing morphology switches and multiple-time-domain ceramide generation in model raft membranes. *Langmuir* **26**: 344-356.

## **8 Publications**

### **8.1 Paper I** Characterization of the Fluid-Gel Phase Coexistence Regime in an Apoptotic Model Membrane (manuscript)

**Characterization of the Fluid-Gel Phase Coexistence  
Regime in an Apoptotic Model Membrane**

Beate Boulgaropoulos, Zoran Arsov, Peter Laggner, Georg Pabst

**Abstract:** Ceramide (Cer), which is generated in the cells through the enzymatic hydrolysis of Sphingomyelin (SM) is known as lipid second messenger molecule, having influence on the death or the survival of the cell. Cer is a lipid molecule with unique biophysical properties and it is a potent modulator of the membrane structure. For this reason we were carrying out a biophysical characterization of the lipid model system POPC/SM/Cer.

We further focussed on the change of the membrane properties upon Cer addition within the phase coexistence region, which is induced in the model system palmitoyl-oleoyl-phosphatidylcholine (POPC)/SM in the presence of Cer. A variety of techniques, namely small- and wide-angle X-ray scattering (SWAXS), differential scanning calorimetry (DSC) and attenuated total reflection Fourier transform infrared (ATR-FTIR) spectroscopy allowed a thorough biophysical characterization. We started with the equimolar binary system POPC/SM and added Cer up to 35 mol% with a concomitant decrease of SM to keep the ratio of sphingolipid (SL) to POPC constant and therefore be able to mimic the action of SMase on the membrane. The Cer/SM-rich domains form a gel phase with hexagonally packed acyl chains and the POPC-rich domains exhibit fluid behaviour. We found a stabilization of the gel domains by Cer and a preferential SM/Cer ratio of 2.3 for domain formation at 37°C. POPC remains unaffected for SM/Cer ratios down to 1.5. The solubility limit of Cer in this lipid mixture lies between 30 and 35 mol%.

## Introduction

In plasma membranes SM is a major component, can cover up to 20 % of the total phospholipid content (7, 179) and is located extensively in the outer leaflet of the bilayer (9-11, 180). During enzymatic hydrolysis SM is cleaved to water soluble phosphocholine and Cer. Cer does not only function as a metabolic regulator molecule (11, 35, 40, 49, 181), but has outstanding physical properties and strongly influences the bilayer structure itself (5, 17, 35, 36, 38). Pure Cer and Cer in mixtures with various lipids were therefore studied by several groups with a variety of biophysical techniques. They found that the presence of Cer in lipid bilayers leads to several structural changes, like Cer-enriched domain formation (65, 66, 71, 152, 182, 183), increased ordering of the acyl chains (69, 73, 137, 152), induction of transbilayer lipid movement (75, 81-83) and membrane defects and leakage (65, 79, 80). Further, due to its molecular shape Cer is able to induce negative curvature, which can result in non lamellar phase formation (134). Pure C16:0-Cer exhibits a metastable bilayer phase at room temperature (39). Upon increasing the temperature, an exothermic transition occurs at 64.2°C and further heating reveals an endothermic transition at about 90°C (39).

This work contains a systematic biophysical characterization of a POPC/SM/Cer model system, keeping the POPC to sphingolipid ratio constant at one. Several biophysical techniques namely small- and wide angle x-ray scattering (SWAXS), differential scanning calorimetry (DSC), and attenuated total reflection- Fourier transform infrared (ATR-FTIR) spectroscopy were used. Our data show that the domain sizes of the Cer rich domains are highly dependent on the lipid composition. The preferential SM/Cer ratio for gel domain formation at 37°C was 2.3 in our lipid system. Similar values for SM/Cer ratios have been found in the presence of Chol (138) and in binary SM/Cer mixtures (184). Interestingly Castro et al. (152) observed additional to a POPC-rich fluid and a Cer-rich gel phase, a gel phase enriched in SM at 24 ° C from SM/Cer ratios from nearly 20 down to 2.3 by the use of fluorescence probes.

Our data clearly show a stabilization of the gel phase upon increasing Cer content with a preferential SM/Cer ratio for domain formation of 2.3. Cer molecules recruit SM molecules from the POPC/SM-rich fluid phase, which leads to a softening of the fluid phase within the coexistence region in the presence of Cer (86). We found the solubility limit of Cer within this membrane between 30 and 35 mol% Cer. The POPC molecules remain unaffected for SM/Cer ratio  $\geq 1.5$ .



## Materials and Methods

Lipids: POPC (1-palmitoyl-2-oleoyl-sn-glycero-3-phosphocholine), egg-sphingomyelin ((2S,3R,4E)-2-acylaminoctadec-4-ene-3-hydroxy-1-phosphocholine) and synthetic C16:0-ceramide ((2S,3R,4E)-2-palmitoylaminoctadec-4-ene-1,3-diol) were purchased from Avanti Polar Lipids (Birmingham, AL) and used without further purification.

Preparation of the liposomes: Lipid stock solutions were prepared by dissolving weighted amounts of dry lipid powder in chloroform/methanol (2/1, v/v). After mixing the appropriate volumes of the stock solutions, the organic solvent was evaporated at room temperature under a gentle stream of nitrogen and placed under vacuum for at least 12 h to form a thin lipid film on the bottom of glass vials. The dry lipid films were suspended in buffer (16 mM Na<sub>2</sub>HPO<sub>4</sub>, 4 mM NaH<sub>2</sub>PO<sub>4</sub>, 130 mM NaCl, pH = 7.4, aqueous solution with 18 MV/cm water (UHQ PS, USF Elga, Wycombe, UK)) and incubated for 4 h in the fluid phase of the system with vigorous intermittent vortex-mixing. At least 8 freeze-thaw circles were supplied. The total lipid concentrations of the samples were 1 mg/ml for DSC, 200 mg/mL for steal-capillary DSC experiments, 20 mg/ml for the IR and 50 mg/ml for X-ray diffraction experiments.

DSC: DSC measurements were performed on a MicroCal VP-DSC high-sensitivity differential scanning calorimeter (MicroCal, Northampton, MA). The samples with Cer were performed with steal capillary inserts. 10 µl of the lipid dispersion was poured into stainless steel capillaries, which were sealed with nylon plugs and subsequently inserted into the calorimeter cell containers. The cell containers were filled with a glycerol solution to prevent freezing of the cell content. Each DSC experiment consisted of three heating and three cooling scans. Samples were tempered for 30 min before each heating and cooling scan, respectively. The scan rate for all experiments was 0.5°C/min. MicroCal's Origin software (MicroCal) was used for data acquisition and analysis throughout. The phase-transition temperatures were derived from the temperatures at the peak maximum of the heat capacity ( $c_p$ ) versus temperature curve (118). The total lipid concentrations of the samples were 1 mg/ml for the DSC measurements without steal capillary and 200 mg/mL for steal- capillary DSC experiments.

X-ray-diffraction experiments: SWAXS experiments were performed on a SWAXS camera (System 3, Hecus X-ray Systems, Graz, Austria). The X-ray camera was mounted on a sealed-tube generator (GE-Seifert, Ahrensburg, Germany) operating at 2 kW. CuK<sub>α</sub> radiation ( $\lambda = 1.542 \text{ \AA}$ ) was selected using a Ni filter in combination with a pulse height discriminator. The X-ray beam size was set to 0.5 mm x 3.5 mm (V x H). The SWAXS patterns were recorded using two linear, one-dimensional, position-sensitive detectors (PSD 50, Hecus X-ray Systems, Graz, Austria) for the wave vector ( $q = 4\pi \sin\theta/\lambda$ ) of  $10^{-3} \text{ \AA}^{-1} < q < 1 \text{ \AA}^{-1}$  (SAXS) and  $1.2 \text{ \AA}^{-1} < q < 2.7 \text{ \AA}^{-1}$  (WAXS). Samples were filled in 1-mm thin-walled quartz-glass capillaries in thermal contact with a programmable Peltier unit and were equilibrated

for 10 min at each temperature before measurement. Exposure times were 3600 s simultaneously for SAXS and WAXS. Calibration in the wide-angle region was performed with para bromo-benzoic acid (119) and in the small-angle region by the use of silver-stearate ( $d = 48.68 \text{ \AA}$ ). Diffraction patterns were corrected for background scattering. From the SAXS peak position the lamellar repeat distances were derived. The background corrected WAXS peaks were fitted with Lorentzians, from which we took the full width at half maximum ( $\Delta q$ ) and the center of the peak ( $q_{11}$ ) to calculate the area per lipid chain, given by  $A_c = 8\pi^2 / (\sqrt{3} \cdot q_{11}^2)$  and the domain size:  $L = 2\pi / \sqrt{\Delta q_{corr}}$ .  $\Delta q_{corr}$  is the full width at half maximum (FWHM) of the WAXS peak corrected for the width of the vertical beam profile.

ATR-FTIR: IR spectra were recorded on a Vertex 70 infrared spectrometer (Bruker Optics, Ettlingen, Germany) equipped with a liquid nitrogen cooled mercury-cadmium telluride detector and fitted with a Horizon ATR unit (Harrick Scientific, Pleasantville, NY, USA). The internal reflection element (IRE) was a trapezoidal germanium ATR plate (50 x 10 x 2 mm) with an incidence angle of  $45^\circ$  yielding 25 internal reflections (New Era Enterprises, Vineland, NJ, USA). 16 scans were averaged for each spectrum. Spectra were recorded at a nominal resolution of  $2 \text{ cm}^{-1}$ . The spectrometer and the ATR-unit were continuously purged with dry nitrogen gas. The holder for the IRE was placed in contact with an aluminum block and the temperature was controlled by a circulating water bath connected to the sample mount. The germanium IRE was cleaned just before use sequentially with distilled water and ethanol. After that, 200  $\mu\text{l}$  of liposome suspension were added onto the IRE and spread over the whole area. Thin lipid stacks were obtained by evaporating water. Dried lipid stacks were rehydrated by the addition of 300  $\mu\text{l}$  of pure deuterated water and incubated at a temperature that ensures the lipids to be in the fluid phase to allow a complete hydrogen-deuterium exchange as judged from the complete disappearance of the amide II band. Analysis of ATR-FTIR spectra was done using the OPUS software package, Version 5.5 (Bruker Optics, Ettlingen, Germany). To examine a particular region of the ATR-FTIR the spectra were cut to an appropriate frequency range and subsequently baseline corrected with a straight line. Peak positions were determined as points with the maximum amplitude in the corresponding absorption bands. The half-bandwidth of the absorption bands was determined as the width of the band at half the maximum amplitude.

### Results:

A biophysical characterization of the multi lamellar lipid system, composed of POPC/SM was performed under equilibrium conditions by a combination of biophysical techniques, namely SWAXS, DSC and ATR-FTIR. SM was substituted gradually by Cer and the POPC/sphingolipid (SL) ratio was kept constant at one for all samples.

Thermotropic behaviour:

Pure POPC exhibited a melting transition at  $-3.3^{\circ}\text{C}$  and egg-SM a narrow transition at  $39.2^{\circ}\text{C}$  in agreement with previous studies (134-136). The melting behaviour of a multi lamellar POPC/SM/Cer suspension was recorded by DSC. SM was replaced by Cer in the range from 0 to 20 mol% (Fig.1).

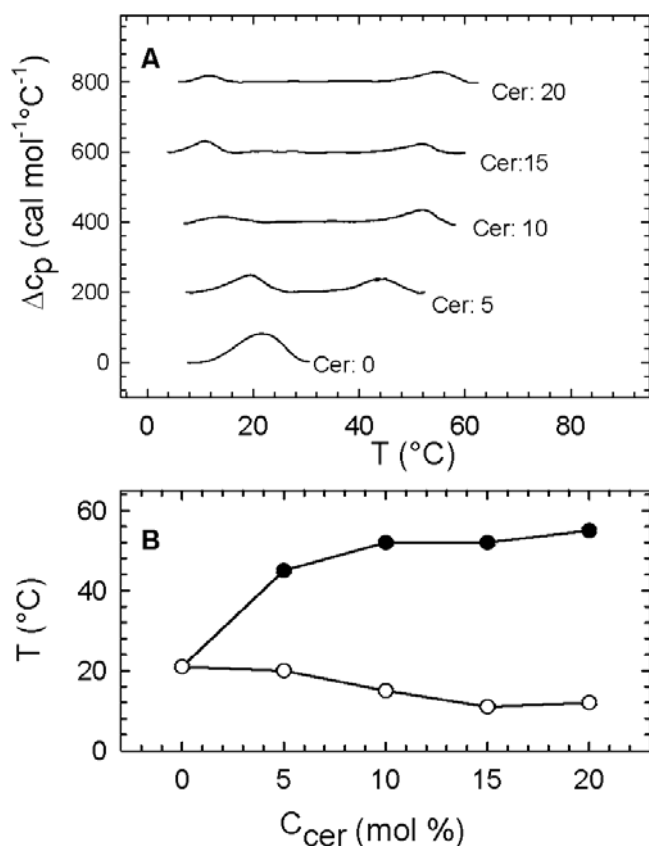


Figure 1 Melting of POPCSM/Cer-mixtures. Panel A shows DSC heating scans of MLVs composed of POPCSM/Cer (50/50-x/x, molar ratio,  $x = 0$  to 20 mol%). The heat capacity curves were shifted vertically for better graphic representation. Panel B shows the phase transition temperatures as a function of Cer content. Error bars are within the size of the symbols.

The binary lipid system POPC/SM showed a single broad melting transition from lamellar gel ( $L_{\beta}$ ) to lamellar fluid ( $L_{\alpha}$ ) at  $21.3^{\circ}\text{C}$ . In the presence of 5 mol% Cer this peak was split into two phase transition peaks, which clearly indicates the coexistence of two phases, namely a gel and a fluid phase, denoted as  $L_{\alpha}^c$  and  $L_{\beta}^c$  in the following. Upon decreasing the SM/Cer ratio, the transition peaks separated further on the temperature axis causing the coexistence region to broaden with increasing Cer content; the areas (enthalpy) of the endothermic peaks decreased at the same time. This effect has also been observed upon Cer addition to pure POPC vesicles (134).

Structural Characterization of the coexistence region:

We focussed on the changes of the structural parameters in the phase coexistence region with increasing Cer content applying SWAXS measurements. The wide angle data are discussed only with respect to the gel phase of the lipid system in the gel fluid coexistence region. The WAXS peak exhibited a gel phase with hexagonal packing of the hydrocarbon chains in the presence of Cer, in agreement with (86). The induction of a gel phase in PC bilayers by Cer has been reported previously (134, 137). The WAXS gel peak intensity increased with increasing Cer concentration and decreased with temperature.

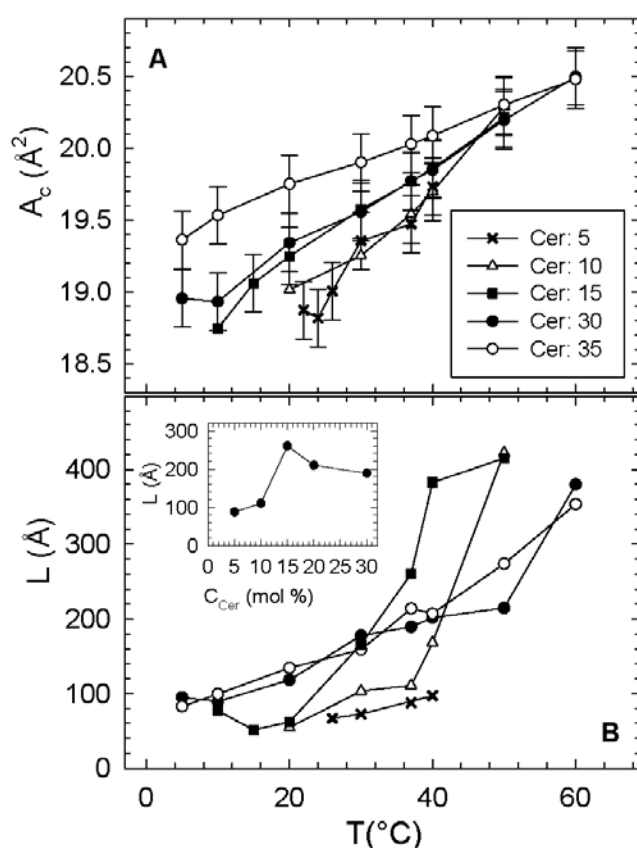


Figure 2 Area per lipid chain  $A_c$  (A) and domain size  $L$  (B) as a function of temperature for Cer concentrations from 5 to 35 mol%. B, Insert: Domain size as a function of Cer concentration at 37°C.

The area per lipid chain within the gel domains generally increased upon heating for all Cer concentrations and decreased with Cer content at 37°C (Fig.2 A). This signifies a lateral expansion of the membrane with temperature and upon Cer addition. The slopes of the  $A_c$  versus T curves decreased upon Cer addition suggesting a stabilization of the gel phase. This

trend also pertained for the sample with 35 mol% Cer, where besides the fluid POPC-rich and the gel SL-rich, an additional pure Cer phase exists.

The gel domain sizes did not show a monotonic increase with temperature with respect to the Cer concentrations. The largest domain at physiological temperature was found for a Cer content of 15 mol%. This corresponds to a SM to Cer ratio of 2.3 (Fig.2 B, insert) and suggests that this is the preferred stoichiometry of the gel domains, in agreement with (138).

The SAXS patterns are superimpositions of the scattering curves of the coexisting phases. Hence, the d-spacing values within two phase coexistence regime correspond to the weighted average of the lamellar repeat distances of the two phases. All SAXS patterns revealed lamellar phases. In the presence of Cer the SAXS Bragg peaks broadened due to the overlapping lattices of the coexisting phases. The two coexisting phases were a fluid phase, enriched in POPC and a gel phase, enriched in SL as it was confirmed by additional SAXS measurements in combination with an applied osmotic pressure and published recently (86). The changes of the lamellar repeat distances of the bilayer stacks were plotted as a function of temperature for several Cer concentrations and as a function of Cer content for selected temperatures and are shown in Fig.3.

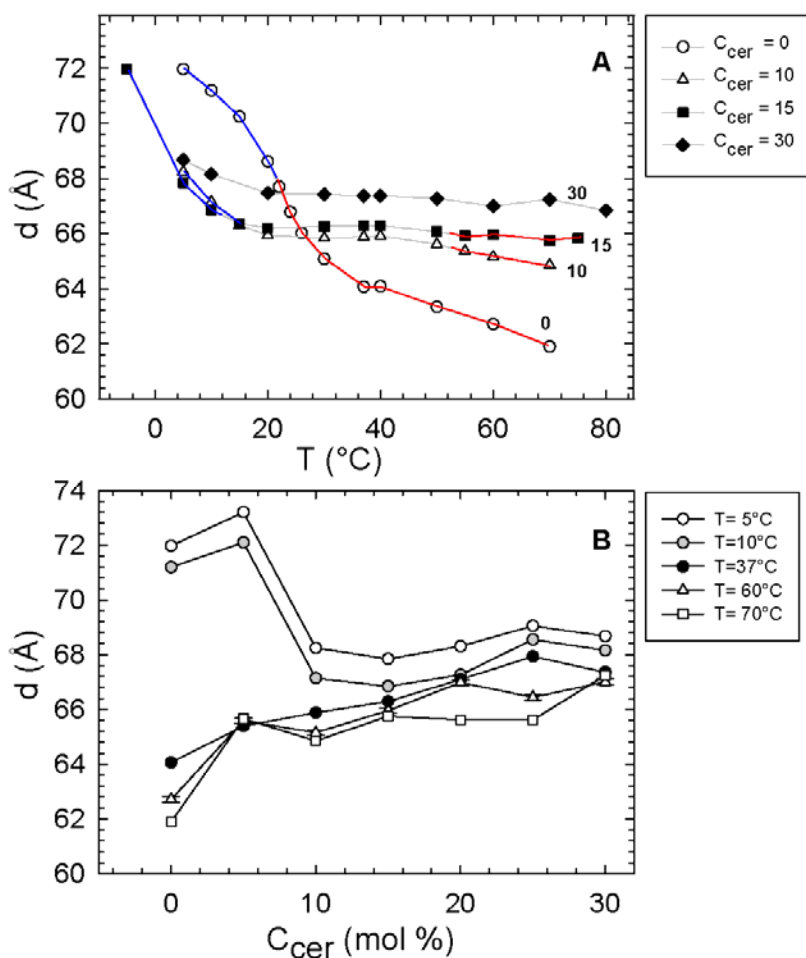


Figure 3 A: Lamellar repeat distance  $d$  as a function of temperature for samples with different Cer contents. Blue: gel phase region, grey: gel-fluid coexistence region and red: fluid phase. B: Lamellar repeat distance  $d$  versus Cer concentration for selected temperatures.

Within the phase coexistence regime, the increase of the lamellar repeat distances reflects the growing proportion of gel domains. The distinct phase regimes were labelled with different colours, according to the phase transitions derived from the DSC data (Fig.1). The melting transition of POPC/SM was clearly seen in a  $d$ -spacing decrease from about  $72.0 \text{ \AA}$  ( $L_\beta^c$ ) to  $\sim 62.0 \text{ \AA}$  ( $L_\alpha^c$ ) (Fig.3 A). This difference between the lamellar repeat distances of the two phases of about  $10 \text{ \AA}$  is in agreement with (136) and clearly appears also in Fig.3 B. In this plot the  $d$ -values at  $5$  and  $10^\circ\text{C}$  for the binary system (Cer:  $0 \text{ mol}\%$ ) and for the ternary system with  $5 \text{ mol}\%$  Cer exhibit a pure gel phase, in agreement with the DSC data (Fig.1 A). The slope of the  $d$ -values versus temperature curves was decreased with increasing Cer content, which again signifies a stabilization of the gel phase upon Cer addition. Fig.3 B explicitly shows the increase of  $d$  with Cer due to the generation of the  $L_\beta^c$  phase.

Upon further Cer increase to 35 mol% an additional SAXS peak occurred with a corresponding d-value of 43.6 Å. (Fig.4.4 B)

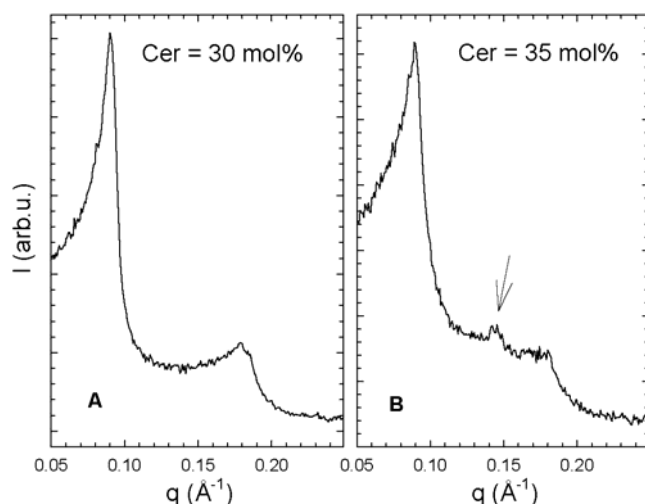


Figure 4 SAXS patterns of MLVs with 30 mol% (A) and 35 mol% (B), respectively. The arrow indicates the additional peak, which originates from a pure Cer phase. Both patterns were recorded at 37°C.

This peak was best developed at around 37°C but existed over the whole temperature range from 5 to 60°C. Considering a methylene distance of 1.27 Å (185), the chain lengths  $d_c$  of the palmitic acids can be assumed with:  $d_c = 2 \cdot n_c \cdot 1.27$ . The resulting 40.64 Å subtracted from the lamellar repeat distance value of 43.6 Å gives 2.96 Å. Thus the length of each headgroup plus water-aliquot is ~1.5 Å and the additional phase seems to be pure nearly dehydrated Cer. Shah et al. (39) found a d-value of 46.9 Å for pure C16:0-Cerat 26°C, which is about 5 Å greater than its anhydrous form ( $d = 42.1$  Å). The value of 43.6 suggests therefore pure partially hydrated Cer. Thus, the solubility limit of Cer for this system lies between 30 and 35 mol%.

#### Vibrational dynamics:

The changes of the lipid acyl chain conformation (methylene band) and the changes at the water-lipid interface (amide and carbonyl band) upon Cer addition were observed by IR spectroscopy (Fig.4.5).

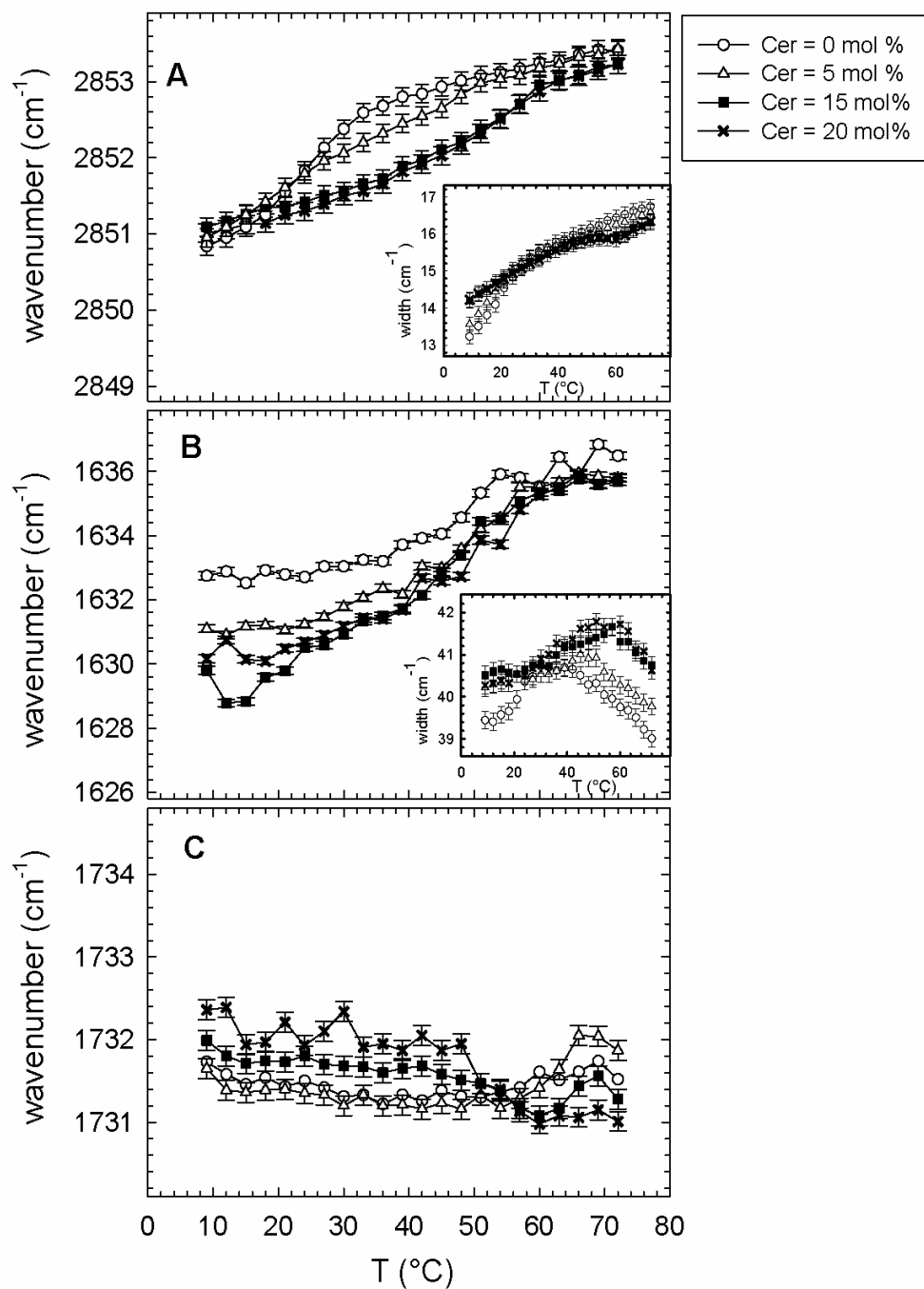


Figure 5 Temperature dependence of the methylene- (A), the amide- (B) and the carbonyl- (C) band peak position. The inserts give the course of the half-bandwidths of the methylene- (A) and the amide-peak (B). Samples were hydrated multi lamellar POPC/SM/Cer mixtures with different Cer contents.

All IR spectra were recorded as a function of temperature for samples with different Cer contents from 0 to 20 mol%. The anti symmetric and symmetric stretching band showed



similar behaviour. Therefore, we accounted for the data analysis only the symmetric ones, which also overlap less with other vibration modes.

The course of the methylene peak positions (Fig.5 A) reflects the behavior of the acyl chain conformations of all lipids within the bilayers and showed increased order above  $\sim 20^{\circ}\text{C}$  in the presence of Cer, seen as a shift to lower wave numbers for the samples with 15 and 20 mol% Cer, respectively. Below about  $20^{\circ}\text{C}$ , which corresponds with the phase transition temperature for the binary system, the peaks appeared at higher wavenumbers upon Cer addition. Thus Cer promotes disorder below the phase transition temperature of the binary lipid system and has an ordering effect above it.

Similar to the peak positions, lower methylene bandwidths indicate more ordered and higher values less ordered lipids (Fig.5 A, insert). The behavior of the temperature dependence of the methylene bandwidth for the samples with 15 and 20 mol% Cer gave strong evidence of phase coexistence. Below about  $20^{\circ}\text{C}$  the lower values for the binary sample indicated a more ordered system, as expected. Above this temperature, the width would be expected to shift to lower values upon Cer addition. But in the temperature range of the coexistence regime the bandwidth-values for all samples showed about the same behaviour with increasing temperature. One explanation is that the methylene bandwidth is composed of two parts, namely a contribution from POPC and a contribution from the SLs. If these two have different peak values, the overall methylene band will broaden. Instead of reflecting the ordering effect induced by Cer above  $20^{\circ}\text{C}$  by decreased width values for samples above 15 mol% Cer, the phase coexistence leads to an increased methylene band width in the presence of Cer.

With the addition of Cer, the amide band peak, which only refers to the behavior of the sphingolipids, shifted to lower wavenumbers (Fig.5 B). The reason is an increase of the overall hydrogen bonding involving carbonyl and N-H groups and indicated the growing SL hydrogen bonding with increasing Cer content. The changes of the width of the amide band (Fig.5 B, insert) reflect the phase transitions derived from the DSC data. The width for the binary POPC/SM sample decreased above  $36^{\circ}\text{C}$ , and oppositely the width for the sample with 15 mol% Cer increased. This correlates with the data derived from the methylene band. But as the amide band only shows the behaviour of the sphingolipids, this again indicated the presence of a phase separation.

The carbonyl peak positions (Fig.5 C) as well as the carbonyl bandwidths (data not shown) did not show any significant change for the different samples upon heating. Thus we conclude that POPC itself is not influenced significantly by the SLs for SM/Cer ratios  $\geq 1.5$ .

On the basis of these results, a phase diagram was constructed, which shows the different phase regimes depending on temperature and Cer concentration (Fig 6).

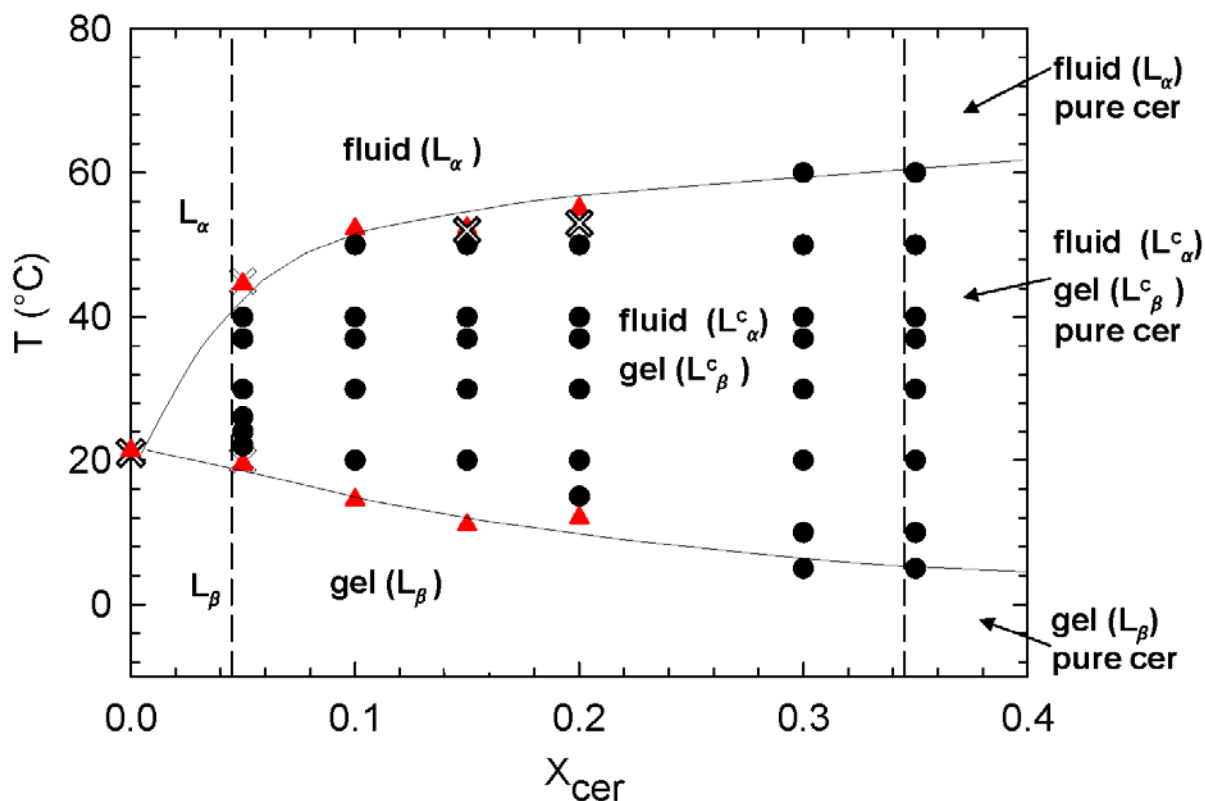


Figure 6 Partial phase diagram of fully hydrated POPC/SM/Cer bilayers. SM is substituted by Cer from  $X_{cer} = 0$  to  $X_{cer} = 0.35$  and the molar ratio POPC to sphingolipid is one. Black circles: WAXS gel peaks; red triangles: DSC phase transition temperatures and crosses: phase transition temperatures estimated from the IR spectra. The lines are drawn as guide to the eye. Legend:  $L_\alpha$ : lamellar fluid phase,  $L_\beta$ : lamellar gel phase, pure cer: pure C16:0-Cer phase.  $L_\beta^c$  and  $L_\alpha^c$ : lamellar gel and lamellar fluid phase within the phase coexistence region.

The following regimes within the phase diagram were clearly distinguished: Uniform gel and fluid lamellar phases, a gel-fluid coexistence regime in the presence of Cer and a three phase coexistence regime with an additional pure Cer phase. The coexisting phases in the presence of Cer were denoted as  $L_\alpha^c$  and  $L_\beta^c$  in the following.

## Discussion

The phase diagram for the system POPC/SM/Cer revealed distinct phase regimes, namely uniform lamellar phases ( $L_\alpha$  and  $L_\beta$ ), a gel-fluid coexistence regime in the presence of Cer and a three phase coexistence regime with an additional pure Cer phase in the presence of more than 30 mol% Cer (Fig.6).

A big variety of biophysical studies of lipid mixtures containing PCs and SLs exists –using well defined synthetic lipids as well as lipid extracts, which contain a large variety of different acyl chains. The lipid mixtures we studied were composed of synthetic POPC and C16:0-Cer and egg-SM, which contains around 84% C16:0 acyl chains. We found uniform phases for the binary equimolar POPC/SM mixture with a phase transition from lamellar gel ( $L_\beta$ ) to lamellar fluid ( $L_\alpha$ ) at  $\sim 20^\circ\text{C}$  (Fig.1).

In general lipid systems can mix ideally with randomly distributed lipids within the membrane and without any phase separation, or the mixing can be non-ideally which means that compositional fluctuations take place. This occurs mainly in binary lipid systems, whereas in ternary lipid systems macroscopic phase separation with the formation of micron-sized stable lipid domains can be observed (146). By comparing the results from different studies on lipid phases one has to keep in mind that the different experimental techniques look through different time-windows during the experiment. X-ray scattering techniques need exposure times of seconds to minutes to yield a scattering pattern of significant quality. Therefore, with this technique, stable macroscopic phases are detected. However, compositional fluctuations within the bilayer occur on timescales of ms to ns and can not be seen by the X-ray measurements. To detect these so-called liquid ordered ( $l_o$ ) and liquid disordered ( $l_d$ ) phases spectroscopic techniques are required (147).

X-rays are scattered by the electrons of the sample molecules itself, which then results in a scattering pattern, whereas the information from fluorescence or electron spin resonance spectroscopy (ESR) methods is an indirect one, transferred via reporter molecules that are incorporated into the lipid membrane. It need to be considered that these labels may also influence the observed phase behaviour (186-188).

With fluorescence spectroscopy, phase separations can easily be detected, but the differentiation between macroscopic or microscopic phases and compositional fluctuations is not possible. The results from X-ray scattering and fluorescence spectroscopic methods are

therefore complementary to each other and by combining the results it is possible to assign the different phases.

Untracht et al. (151) detected lateral phase separation in a lipid mixture composed of egg-POPC and SM from bovine brain applying X-ray diffraction, scanning calorimetry, and light microscopy. They observed gel phase separation into a SM-enriched gel phase and a gel phase containing both SM and PC upon cooling to 20°C in the presence of more than 33 mol% SM, which is in contrast to our observations. The formation of this macroscopic phase separation can be due to the use of two natural lipids, which contain a variety of different acyl chains in contrast to well defined synthetic lipids. Degovics et al. (138) studied an equimolar synthetic-POPC/egg-SM mixture in Hepes buffer by X-ray scattering and DSC. The DSC data showed two weakly resolved peak positions for the equimolar POPC/SM-mixture but the X-ray data did not show any phase separation and therefore they concluded that no macroscopic phase separation is present in this lipid mixture. This is in agreement with our results. Nevertheless, they assumed that these two lipids might have differences in their lateral organization. Indeed, studies exist, where microscopic phase separation, differences in the order parameters of the single lipids within the binary lipid sample and/or compositional fluctuations were observed (152, 153).

Bunge et al. (154) studied the binary lipid system, composed of synthetic POPC/C16:0-SM with fluorescence microscopy, <sup>2</sup>H-NMR, and ESR. They found microdomains with a minimal radius of 45–70 nm, which had also been observed previously (189). Such domains could not be detected by fluorescence microscopy, where a uniform phase has been observed. The same lipid system was studied by de Almeida et al. (153) with photophysical methods, who found a broad gel/fluid phase separation region and confirmed the existence of a gel-gel phase separation. Microscopic differences in the lateral organization of the lipids were also indicated by fluorescence measurements (152) .

Upon addition of Cer we observed phase separation into a lamellar gel phase ( $L^c_\beta$ ), enriched in SLs and a POPC-rich lamellar fluid phase ( $L^c_\alpha$ ) for the temperature range within the coexisting region (Fig.6) in agreement with other studies (134, 135, 138, 152, 154). In the presence of Cer, but outside of this phase coexistence region we did not find a clear indication of phase separation within the ternary lipid system. To clearly resolve a gel-gel or fluid-fluid phase coexistence by X-ray scattering, osmotic pressure experiments would have to be performed, as has been done recently for the domain coexistence region of the herein presented phase diagram (86). Our results show that the temperature range of the phase

coexisting region broadens with increasing Cer concentration and also the observed phase transition peaks for the ternary lipid systems broaden in the presence of Cer (Fig.1), which agrees with (135). Already at 5 mol% Cer a gel phase is formed due to tight interaction between the SLs. This was also confirmed by our IR data that show increased hydrogen bonding upon Cer addition (Fig.5), which is in agreement with (138, 156, 157).

In the presence of Cer the binary POPC/SM mixture showed a macroscopic phase separation into two different phases (Fig.6), which were assigned to be a POPC-rich fluid ( $L^c_\alpha$ ) and a SL-rich gel phase ( $L^c_\beta$ ) by additional experiments combining X-ray scattering and osmotic pressure experiments (86). This phase separation was already observed for the smallest measured Cer content of 5 mol% Cer. The phase coexistence was confirmed by the IR measurements, which indicated a two phase regime, because the high bandwidth value in an ordered regime and the fact that POPC was not much influenced for SM/Cer ratios down to 1.5 (Fig.5). We detected an additional pure Cer phase between 30 and 35 mol% Cer (Fig.4). Castro et al. (152) built up a phase diagram for the ternary model system composed of POPC, C16:0 SM and C16:0-Cer by the use of fluorescence membrane probes and at 24°C (Fig.7).

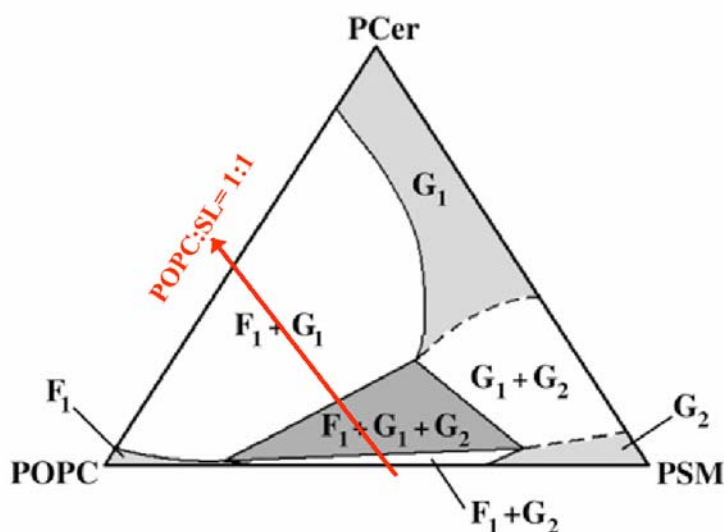


Figure 7 A: Phase diagram for the ternary lipid system POPC/SM/Cer at 24°C, determined by Castro et al. (152). The red arrow follows a POPC/SL ratio of one towards increasing Cer content. Legend: F1: POPC-rich fluid phase; G1: Cer-rich gel phase and G2: SM-rich gel phase.

In the subsequent paragraph we will compare the phase regimes found in his phase diagram (Fig.7) with the ones detected in this study to shed light on the stability and life time of the different phases.

Following the imaginary line given by a POPC/SL ratio of one towards increasing Cer content (red arrow in Fig.7), the following phase regimes were detected by Castro et al. (152). Until 2 mol% Cer a two phase regime was found, consistent of a fluid POPC- rich and a gel SM-rich phase. Above a Cer content of 2 mol% Cer an additional gel phase enriched in Cer was observed up to 15 mol% Cer, which refers to a SM/Cer ratio of 2.3. At ratios below 2.3, the SM-rich gel phase, within a three phase coexistence regime vanished to reveal a two phase coexistence with a gel Cer-rich and a fluid POPC-rich phase upon increasing Cer content. The existence of the SM-rich gel phase for a SM Cer ratio above 2.3 up to about 15 can be explained by the detection of compositional fluctuations by fluorescence spectroscopy. Cer recruits SM for gel domain formation and excess SM would mix again with POPC in a non ideal way. The preferential SM/Cer ratio for the gel domain formation has been shown also in kinetic studies of the enzymatic hydrolysis of SM (Boulgaropoulos et al., submitted). Below a ratio of one Cer lacks a SM partner and is forced to recruit POPC or to segregate as pure Cer phase, which is energetically unfavourable. Castro et al did not find the SM rich gel phase for SM/Cer ratios below 2.3, because at this ratio Cer seems to couple all SM molecules. This again shows that Cer recruits preferentially 2 to 3 SM molecules for gel domain formation.

Above 15 mol% Cer a two phase coexistence region, consisting of a fluid POPC rich and a gel Cer rich phase continues at this temperature. A crystalline pure Cer phase has not been observed in contrast to our results, which clearly revealed that Cer segregates out of the membrane between 30 and 35 mol%.

Following the line at constant temperature of  $T = 24^{\circ}\text{C}$  in direction of increasing Cer content in our phase diagram (Fig.6), a uniform lamellar fluid phase has been observed until a Cer content of about 2 mol%, which is in contrast to Castro et al. (152), who detected an additional SM-rich gel phase. This additional phase is therefore not a macroscopic stable one. The SM-rich and Cer-rich gel phases, which coexist with the fluid phase in the concentration range from  $\sim 2$  to 15 mol% Cer according to (152), were not detected by X-ray measurements and thus refer to compositional fluctuations as well. X-ray scattering revealed a two-phase coexistence of a fluid POPC-rich and a gel SL-rich phase and at 35 mol% Cer an additional pure Cer phase (Fig.4).

In this study, SWAXS measurements were applied to observe the dynamic structural changes within the coexistence region. The area per lipid chain within the gel domains was generally increasing upon heating for all Cer concentrations and increasing with decreasing SM/Cer

ratio at 37°C (Fig.2 A). This signifies a lateral expansion upon heating and Cer addition. Similar behaviour has been found previously with peptides inducing disorder into bilayers (130). The growing of the area per lipid chain within the gel domains upon decreasing SM/Cer ratio suggests the incorporation of POPC into the gel domains at SM to Cer molar ratios smaller than one. The area per lipid chain is growing because of the bigger lateral area requirement of POPC due to its kinked chain. Additionally, Cer with its conical molecular shape can lead to an increased area.

Stabilization of these domains with increasing Cer is clearly indicated by the decreased lateral expansion upon addition of Cer, which is in agreement with Veiga et al. (158). They found with mainly DSC studies with additional support from infrared and nuclear magnetic resonance (NMR) spectroscopy that Cers favour the stability of the gel over the fluid lamellar phase in phospholipid bilayers. Another indication of the stabilization of these gel domains is given by the decreasing ascent of the lamellar repeat distances upon heating for a given Cer concentration (Fig.3 A). With combined X-ray and osmotic pressure experiments we were able to derive interaction potentials between POPC/SM bilayers and for the fluid and gel phases coexisting in POPC/SM/Cer membranes (86).

The domain sizes of the gel domains are generally increasing with increasing temperature. This can be explained with the fact, that heating accelerates the lateral diffusion and therefore, the probability for Cer to meet and recruit SM is growing, which could be comparable to the temperature dependent nucleation and growth in subgel phases (190-192). Interestingly, the biggest domain at physiological temperature was found for a Cer content of 15 mol%. This corresponds to a SM to Cer ratio of 2.3. (Figure 2 B, insert) and this value therefore indicates a preferential ratio in terms of domain formation at physiological temperature.

These results are in agreement with Silva et al. (138), who found that Cer added to a ternary lipid system composed of POPC/SM/Chol recruits two to three SM molecules for the formation of highly ordered gel domains. This is an optimum ratio also in the absence of Chol as was reported recently (86), (193).

Our X-ray measurements revealed lamellar phases for all samples and the course of the  $d$ -values versus temperature and Cer content are in good agreement with the phase boundaries seen from the DSC data. Within the gel-fluid domain coexistence region, the SAXS peaks slightly broaden, which indicates the coexistence of two lamellar phases as has also been observed previously (69, 86, 134, 152).

The d-values are average values of the overlapping lattices of the coexisting phases. Thus the higher the d-value for a given Cer concentration, the bigger is the gel phase proportion. The proportion of the gel phase is increasing upon decreasing SM/Cer ratio, which is reflected in higher d-values (Fig 3). The lamellar repeat distance at 37°C is increasing upon Cer addition down to an equimolar SM/Cer ratio (Fig.3 B). For Cer contents bigger than 25 the lamellar repeat distance shrinks, which suggests the POPC incorporation into the  $L^c_\beta$  phases. The IR data also confirm that the POPC molecules remain unaffected from the SM/Cer ratio for values down to 1.5 (Fig.5).

By applying an osmotic pressure to two different samples (POPC/SM, binary lipid mixture and POPC/SM/Cer = 50/35/15 molar ratio) at a constant temperature of 37°C and performing a theoretical analysis it was shown that the addition of Cer to POPC/SM model membranes leads to a four times smaller bending rigidity of the fluid phase within the phase coexisting regime. The reason is a depletion of SM, which gets recruited by Cer to the gel phase. This results in a redistribution of repulsive lateral pressures from the bilayer interior toward the lipid/water interface within the  $L^c_\alpha$  phase, which could significantly affect the function of membrane proteins, which are not associated to raft structures, like ion channels.

### Conclusions:

We constructed a phase diagram for the lipid system POPC/SL, 1/1 molar ratio with different SM/Cer with the use of DSC, X-ray scattering and IR techniques. By comparing the different phase regimes detected by X-ray scattering, which refer to macroscopic stable phases with the phases found by fluorescence techniques for the same lipid system (152), it was possible to give a statement about the stability of the different phases. For SM/Cer ratios from more than 20 to 2.3 a SM rich phase was found by (152), which refers to compositional fluctuations within the system and disappears just at a SM/Cer ratio of 2.3.

We further focussed on the characterization of the Cer influence on membrane structural parameters within the phase coexistence regime and found that Cer stabilizes the gel phase and at physiological temperature the SM/Cer ratio of 2.3 lead to maximum gel domain sizes and for a SM/Cer ratio down to 1.5, the POPC fraction remains unaffected.



### **Acknowledgements:**

Experiments with ATR-FTIR spectroscopy were conducted at the infrared beamline SISSI at the Sincrotrone Trieste with technical support from Dr. Lisa Vaccari and Dr. Diane Eichert. Z.A. acknowledges the financial support from the state budget by the Slovenian Research Agency (program No. P1-0060).

## Reference List

1. Yeagle, P. L. (2005) *The structure of biological membranes* (CRC Press, New York).
2. Riboni L., T G (1997) The role of Sphingolipids in the process of signal transduction. *Prog. Lipid Res.* **35**: 153-157.
3. van Meer, G, Voelker, D R, Feigenson, G W (2008) Membrane lipids: where they are and how they behave. *Nat. Rev. Mol. Cell Biol* **9**: 112-124.
4. Ikeda, M, Kihara, A, Igarashi, Y (2006) Lipid asymmetry of the eukaryotic plasma membrane: functions and related enzymes. *Biol. Pharm. Bull.* **29**: 1542-1546.
5. Koval M., P R (1991) Intracellular transport and metabolism of sphingomyelin. *Biochim Biophys Acta* **1082**: 113-125.
6. Merrill, A H, Jones, D (1990) An update of the enzymology and regulation of sphingomyelin metabolism. *Biochim. Biophys. Acta* **1044**: 1-12.
7. Hannun, Y A, Obeid, L M (2002) The Ceramide-centric universe of lipid-mediated cell regulation: stress encounters of the lipid kind. *J. Biol. Chem.* **277**: 25847-25850.
8. Hannun, Y A, Luberto, C (2000) Ceramide in the eukaryotic stress response. *Trends Cell Biol.* **10**: 73-80.
9. Kolesnick, R N, Goni, F M, Alonso, A (2000) Compartmentalization of ceramide signaling: Physical foundations and biological effects. *J. Cell. Phys.* **184**: 285-300.
10. Spiegel, S, Merrill, A H, Jr. (1996) Sphingolipid metabolism and cell growth regulation. *FASEB J.* **10**: 1388-1397.
11. van Blitterswijk, W J, van der Luit, A H, Veldman, R J, Verheij, M, Borst, J (2003) Ceramide: second messenger or modulator of membrane structure and dynamics? *Biochem. J.* **369**: 199-211.
12. van Blitterswijk, W J, van der Luit, A H, Caan, W, Verheij, M, Borst, J (2001) Sphingolipids related to apoptosis from the point of view of membrane structure and topology. *Biochem. Soc. Trans.* **29**: 819-824.
13. Sprong, H, van der Sluijs, P, van Meer, G (2001) How proteins move lipids and lipids move proteins. *Nature Rev.* **2**: 504-513.
14. Ballou, L R, Lauderkind, S J, Rosloniec, E F, Raghoebar, R (1996) Ceramide signalling and the immune response. *Biochim. Biophys. Acta* **1301**: 273-287.
15. Arsov, Z, Quaroni, L (2008) Detection of lipid phase coexistence and lipid interactions in sphingomyelin/cholesterol membranes by ATR-FTIR spectroscopy. *Biochim Biophys Acta* **1778**: 880-889.

16. Veiga, M P, Arrondo, J L, Goni, F M, Alonso, A (1999) Ceramides in phospholipid membranes: effects on bilayer stability and transition to nonlamellar phases. *Biophys. J.* **76**: 342-350.
17. Carrer, D C, Maggio, B (1999) Phase behavior and molecular interactions in mixtures of ceramide with dipalmitoylphosphatidylcholine. *J. Lipid Res.* **40**: 1978-1989.
18. Leung, S, Sot, J, Alonso, A, Goni, F M, Thewalt, J (2008) Effects of Ceramide on Sphingomyelin Membranes: Increased Thermal Stability and Chain Order. *Biophys. J.* **94**: 340.
19. Huang, H W, Goldberg, E M, Zidovetzki, R (1998) Ceramides perturb the structure of phosphatidylcholine bilayers and modulate the activity of phospholipase A2. *Eur. Biophys. J.* **27**: 361-366.
20. Castro, B M, de Almeida, R F, Silva, L C, Fedorov, A, Prieto, M (2007) Formation of ceramide/sphingomyelin gel domains in the presence of an unsaturated phospholipid: a quantitative multiprobe approach. *Biophys. J.* **93**: 1639-1650.
21. Silva, L, De Almeida, R F M, Fedorov, A, Matos, A P A, Prieto, M (2006) Ceramide-platform formation and -induced biophysical changes in a fluid phospholipid membrane. *Molecular Membrane Biology* **23**: 137-142.
22. Hsueh, Y W, Giles, R, Kitson, N, Thewalt, J (2002) The effect of ceramide on phosphatidylcholine membranes: A deuterium NMR study. *Biophys. J.* **82**: 3089-3095.
23. Holopainen, J M, Subramanian, M, Kinnunen, P K (1998) Sphingomyelinase induces lipid microdomain formation in a fluid phosphatidylcholine/sphingomyelin membrane. *Biochemistry* **37**: 17562-17570.
24. Kiessling, V, Crane, J M, Tamm, L (2006) Transbilayer Effects of Raft-Like Lipid Domains in Asymmetric Planar Bilayers Measured by Single Molecule Tracking. *Biophys. J.* **91**: 3313-3326.
25. Contreras, F X, Villar, A V, Alonso, A, Kolesnick, R N, Goni, F M (2003) Sphingomyelinase activity causes transbilayer lipid translocation in model and cell membranes. *J. Biol. Chem.* **278**: 37169-37174.
26. Goni, F M, Alonso, A (2000) Membrane fusion induced by phospholipase C and sphingomyelinases. *Biosci. Rep.* **20**: 443-463.
27. Ruiz-Arguello, M B, Goni, F M, Alonso, A (1998) Vesicle membrane fusion induced by the concerted activities of sphingomyelinase and phospholipase C. *J. Biol. Chem.* **273**: 22977-22982.
28. Montes, L R, Ruiz-Arguello, M B, Goni, F M, Alonso, A (2002) Membrane restructuring via ceramide results in enhanced solute efflux. *J. Biol. Chem.* **277**: 11788-11794.

29. Ruiz-Arguello, M B, Basanez, G, Goni, F M, Alonso, A (1996) Different effects of enzyme-generated ceramides and diacylglycerols in phospholipid membrane fusion and leakage. *J. Biol. Chem.* **271**: 26616-26621.
30. Fidorra, M, Duelund, L, Leidy, C, Simonsen, A C, Bagatolli, L A (2006) Absence of fluid-ordered/fluid-disordered phase coexistence in ceramide/POPC mixtures containing cholesterol. *Biophys. J.* **90**: 4437-4451.
31. Shah, J, Atienza, J M, Rawlings, A V, Shipley, G G (1995) Physical properties of ceramides: effect of fatty acid hydroxylation. *J. Lipid Res.* **36**: 1945-1955.
32. Silva, L C, de Almeida, R F, Castro, B M, Fedorov, A, Prieto, M (2007) Ceramide-domain formation and collapse in lipid rafts: membrane reorganization by an apoptotic lipid. *Biophys. J.* **92**: 502-516.
33. Busto, J V, Fanani, M L, De Tullio, L, Sot, J, Maggio, B, Goni, F M, Alonso, A (2009) Coexistence of immiscible mixtures of palmitoylsphingomyelin and palmitoylceramide in monolayers and bilayers. *Biophys J* **97**: 2717-2726.
34. Pabst, G, Boulgaropoulos, B, Gander, E, Sarangi, B R, Amenitsch, H, Raghunathan, V A, Laggner, P (2009) Effect of Ceramide on Nonraft Proteins. *J. Membr. Biol.* **231**: 125-132.
35. McElhaney, R N (1982) The use of differential scanning calorimetry and differential thermal analysis in studies of model and biological membranes. *Chem. Phys. Lipids* **30**: 229-259.
36. Ohura, K, Kashino, S, Haisa, M (1972) The crystal and molecular structure of p-bromobenzoic acid. *Bull. Chem. Soc. Japan* **45**: 2651-2652.
37. Sot, J, Bagatolli, L A, Goni, F M, Alonso, A (2006) Detergent-resistant, ceramide-enriched domains in sphingomyelin/ceramide bilayers. *Biophys. J.* **90**: 903-914.
38. Degovics, D, Latal, A, Prenner, E, Kriechbaum, M, Lohner, K (1997) Structure and Thermotropic Behaviour of Mixed Choline Phospholipid Model Membranes. *J. Appl. Cryst.* **30**: 776-780.
39. Sun, W, Suter, R M, Knewton, M A, Worthington, C R, Tristram-Nagle, S, Zhang, R, Nagle, J F (1994) Order and disorder in fully hydrated unoriented bilayers of gel-phase dipalmitoylphosphatidylcholine. *Phys. Rev. E Stat. Phys. Plasmas. Fluids Relat Interdiscip. Topics* **49**: 4665-4676.
40. Baumgart, T, Hess, S T, Webb, W W (2003) Imaging coexisting fluid domains in biomembrane models coupling curvature and line tension. *Nature* **425**: 821-824.
41. Ipsen, J H, Karlstrom, G, Mouritsen, O G, Wennerstrom, H, Zuckermann, M J (1987) Phase equilibria in the phosphatidylcholine-cholesterol system. *Biochim Biophys Acta* **905**: 162-172.

42. Ayuyan, A G, Cohen, F S (2006) Lipid peroxides promote large rafts: effects of excitation of probes in fluorescence microscopy and electrochemical reactions during vesicle formation. *Biophys. J.* **91**: 2172-2183.
43. Zhao, J, Wu, J, Shao, H L, Kong, F, Jain, N, Hunt, G, Feigenson, G (2007) Phase studies of model biomembranes: Macroscopic coexistence of L alpha plus L beta, with light-induced coexistence of L alpha plus Lo Phases. *Biochim. Biophys. Acta* **1768**: 2777-2786.
44. Veatch, S L, Leung, S S, Hancock, R E, Thewalt, J L (2007) Fluorescent probes alter miscibility phase boundaries in ternary vesicles. *J. Phys. Chem. B* **111**: 502-504.
45. Untracht, S H, Shipley, G (1977) Molecular interactions between lecithin and sphingomyelin. *J. Biol. Chem.* **252**: 4449-4457.
46. de Almeida, R F, Fedorov, A, Prieto, M (2003) Sphingomyelin/phosphatidylcholine/cholesterol phase diagram: boundaries and composition of lipid rafts. *Biophys. J.* **85**: 2406-2416.
47. Bunge, A, Muller, P, Stockl, M, Herrmann, A, Huster, D (2008) Characterization of the ternary mixture of sphingomyelin, POPC, and cholesterol: support for an inhomogeneous lipid distribution at high temperatures. *Biophys J* **94**: 2680-2690.
48. de Almeida, R F, Loura, L M, Fedorov, A, Prieto, M (2005) Lipid rafts have different sizes depending on membrane composition: a time-resolved fluorescence resonance energy transfer study. *J Mol. Biol* **346**: 1109-1120.
49. Niemela, P S, Hyvonen, M T, Vattulainen, I (2006) Influence of chain length and unsaturation on sphingomyelin bilayers. *Biophys. J.* **90**: 851-863.
50. Staneva, G, Chachaty, C, Wolf, C, Koumanov K., Quinn, P J (2008) The role of sphingomyelin in regulating phase coexistence in complex lipid modelmembranes: Competition between ceramide and cholesterol. *Biochim. Biophys. Acta* **1778** : 2727-2739.
51. Pabst, G, Danner, S, Podgornik, R, Katsaras, J (2007) Entropy-driven softening of fluid lipid bilayers by alamethicin. *Langmuir* **23**: 11705-11711.
52. Veiga, M P, Arrondo, J L, Goni, F M, Alonso, A (1999) Ceramides in phospholipid membranes: effects on bilayer stability and transition to nonlamellar phases. *Biophys J* **76**: 342-350.
53. Páli, T, Bartucci, R, Horváth, L, Marsh, D (1993) Kinetics and dynamics of annealing during sub-gel phase formation in phospholipid bilayers A saturation transfer electron spin resonance study. *Biophys. J.* **64**: 1781-1788.
54. Tristram-Nagle, S, Suter, R M, Sun, W J, Nagle, J F (1994) Kinetics of subgel formation in DPPC: X-ray diffraction proves nucleation-growth hypothesis. *Biochim Biophys Acta* **1191**: 14-20.

55. Katsaras, J, Raghunathan, V A (2000) in Lipid Bilayers Structure and Interactions (Berlin), pp. 26-30.
56. Busto, J V, Fanani, M L, De Tullio, L, Sot, J, Maggio, B, Goni, F M, Alonso, A (2009) Coexistence of immiscible mixtures of palmitoylsphingomyelin and palmitoylceramide in monolayers and bilayers. *Biophys J* **97**: 2717-2726.

**8.2 Paper II** Effect of Ceramide on Non-Raft Proteins

Pabst, G, Boulgaropoulos, B, Gander, E, Sarangi, B R, Amenitsch, H, Raghunathan, V A, Laggner, P (2009) Effect of Ceramide on Nonraft Proteins. *J. Membr. Biol.* **231**: 125-132

# Effect of Ceramide on Nonraft Proteins

Georg Pabst · Beate Boulgaropoulos ·  
Edgar Gander · Bibhu R. Sarangi · Heinz Amenitsch ·  
Velayudhan A. Raghunathan · Peter Laggner

Received: 25 August 2009 / Accepted: 8 October 2009 / Published online: 31 October 2009  
© Springer Science+Business Media, LLC 2009

**Abstract** The currently accepted model of biological membranes involves a heterogeneous, highly dynamic organization, where certain lipids and proteins associate to form cooperative platforms (“rafts”) for cellular signaling or transport processes. Ceramides, a lipid species occurring under conditions of cellular stress and apoptosis, are considered to stabilize these platforms, thus modulating cellular function. The present study focuses on a previously unrecognized effect of ceramide generation. In agreement with previous studies, we find that ceramide leads to a depletion of sphingomyelin from mixtures with palmitoyl oleoyl phosphatidylcholine bilayers, forming a ceramide–sphingomyelin-rich gel phase that coexists with a fluid phase rich in palmitoyl oleoyl phosphatidylcholine. Interestingly, however, this latter phase has an almost fourfold smaller bending rigidity compared to a sphingomyelin–palmitoyl oleoyl phosphatidylcholine mixture lacking ceramide. The significant change of membrane bulk properties can have severe consequences for conformational equilibria of membrane proteins. We discuss these effects in terms of the lateral pressure profile concept for a simple geometric model of an ion channel and find a significant inhibition of its activity.

**Keywords** Phospholipid bilayer · Phase separation · Interactions · Bending rigidity · Lateral pressure profile · Ion channel

---

G. Pabst (✉) · B. Boulgaropoulos · E. Gander · H. Amenitsch ·  
P. Laggner  
Institute of Biophysics and Nanosystems Research,  
Austrian Academy of Sciences, Schmiedlstr. 6, 8042 Graz,  
Austria  
e-mail: Georg.Pabst@oeaw.ac.at

B. R. Sarangi · V. A. Raghunathan  
Raman Research Institute, Bangalore 560 080, India

## Introduction

Biological membranes are prime examples of complex self-assembled matter on the nanometer to micrometer scale. They contain thousands of different lipid and protein species, which do not distribute evenly but exhibit diverse phase separation phenomena. Indeed, it has been suggested that certain lipid/protein domains—rafts—dynamically regulate various physiological processes (trafficking, signaling, endo-/exocytosis, etc.) (Brown 2006; Simons and Ikonen 1997).

Although a clear definition of membrane rafts still seems to be elusive (Pike 2006), consensus has been reached in that sphingolipids and sterols are the major lipid components found in these structures. Segregation of raft proteins and their assembly in signaling or receptor complexes are thought to be tightly controlled by lipid–protein and protein–protein interactions. Naturally, changes in lipid composition due to external or internal stimuli may sensitively influence lateral organization of biological membranes and, hence, affect processes on the cellular level.

Considerable research efforts have recently been focused on ceramides (Goni and Alonso 2006; Posse de Chaves 2006; van Blitterswijk et al. 2003). Ceramides belong to the class of sphingolipids and are mainly generated during cellular stress and apoptosis, either by de novo synthesis in the endoplasmic reticulum or through enzymatic hydrolysis of sphingomyelin (SM) by sphingomyelinase in the plasma membrane. Ceramides have very distinct physicochemical properties, such as a very small polar headgroup (only two hydroxyl groups), and have been shown to induce a gel phase that coexists with fluid domains in lipid model membranes (Castro et al. 2007; Fidorra et al. 2006; Holopainen et al. 2000b; Staneva et al. 2008). Additionally, due to its cone-like molecular shape,



asymmetric generation of ceramide in one of the membrane leaflets by sphingomyelinase has been demonstrated to lead to blebbing and vesiculation on the opposing side of the membrane, very similar to apoptotic body formation (Holopainen et al. 2000a).

Hence, ceramide is a potent modulator of membrane structure. In particular, it is thought to stabilize membrane rafts by coordinating up to three SMs through hydrogen bonds (Castro et al. 2007). This in turn should facilitate activation of raft-localized proteins, such as the CD95/Fas death receptor in the case of apoptosis (van Blitterswijk et al. 2003). However, ceramide is not exclusively involved in apoptosis but has been also implicated in various other cellular processes such as necrosis, proliferation, differentiation and cytoskeletal rearrangements. Additionally, ceramides may act as second messengers and activate membrane proteins by direct binding.

While most of the debate has been focused on the effects of ceramides on membrane rafts, little attention has been paid to physiological effects within nonraft fractions. Because of the strong coordination of SM by ceramides (Castro et al. 2007), SM will be strongly enriched in ceramide-stabilized rafts. Hence, nonraft fractions are likely to get depleted from SM. How would this affect the membrane proteins that reside in nonraft fractions of the membrane? In order to address this issue, we studied the interactions of plasma membrane models composed of palmitoyl oleoyl phosphatidylcholine (POPC), egg-SM and *N*-palmitoyl-*D*-erythro-sphingosine (Cer) by a combination of osmotic stress and X-ray diffraction (Parsegian and Rand 1995). In agreement with previous studies (Castro et al. 2007; Fidorra et al. 2006; Holopainen et al. 2000b; Staneva et al. 2008), we found that Cer induces a gel–fluid phase separation. The fluid phase has essentially the same membrane thickness as a POPC/SM equimolar mixture, which does not exhibit phase coexistence. However, its bending rigidity is almost four times smaller because it lacks SM. We discuss the consequences of this membrane softening on the conformational equilibrium of a simple geometric model for an ion channel in terms of the lateral pressure concept (Cantor, 1997, 1999b).

## Materials and Methods

### Liposomes

All lipids were purchased from Avanti Polar Lipids (Alabaster, AL) and used without further purification. Dispersions of multilamellar vesicles (MLVs) were suspended from dry lipid films in 18 M $\Omega$  cm water at a lipid concentration of 50 mg/ml. The lipid films were obtained by mixing appropriate amounts of lipid stock solutions

followed by removal of the chloroform/methanol solvent using a gentle stream of N<sub>2</sub> and a vacuum chamber. Osmotically stressed samples also contained weighted amounts of polyethylene glycol (PEG, M<sub>w</sub> = 8,000), purchased from Sigma–Aldrich (St. Louis, MO). These samples were prepared by centrifuging the fully hydrated MLVs and subsequent removal of the supernatant. The supernatant was replaced by a PEG solution of given concentration, and the sample was left to equilibrate for at least 2 days. Osmotic pressures of a given PEG solution as a function of temperature were determined using a Knauer (Berlin, Germany) vapor pressure osmometer.

### X-Ray Diffraction

Synchrotron small- and wide-angle X-ray diffraction experiments were performed at the Austrian SAXS beamline at Elettra (Trieste, Italy) using 8-keV photons and a sample to detector distance of 1.126 m with typical exposure times of 2 min. SAXD patterns were recorded with a mar345 image plate detector (Marresearch, Norderstedt, Germany). A one-dimensional position sensitive gas detector was used to measure the WAXD signal. Samples were contained in 1-mm quartz-glass capillaries and equilibrated at 37°C for 10 min prior to exposure. Primary data reduction was performed using FIT2D (<http://www.esrf.eu/computing/scientific/FIT2D/>). Electron density profiles were derived from the integrated Bragg intensities of background-corrected SAXD patterns using standard techniques (Pabst et al. 2000). The membrane thickness,  $d_B$ , was defined as  $d_{HH} + 10 \text{ \AA}$  (McIntosh et al. 1987), where  $d_{HH}$  is given by the distance between the two maxima of the electron density profile. The bilayer separation for a given osmotic pressure is given by  $d - d_B$ , where the lamellar repeat distance  $d$  is calculated from the Bragg peak positions.

### Fluorescence Microscopy

Rhodamine-dipalmitoyl phosphatidylethanolamine (Invitrogen, San Diego, CA) was added to the POPC/SM/Cer mixture at a concentration of 0.5 mol%, and giant unilamellar vesicles (GUVs) were prepared by electroformation (Angelova and Dimitrov 1986). Fluorescence imaging was performed on a Leica (Solms, Germany) DMIRE2 inverted microscope using a metal halide lamp for sample illumination. Images were captured using a CoolSNAP ES<sub>2</sub> camera from Photometrics (Tucson, AZ).

### Analysis of Equation of State

In the present system, the applied osmotic pressure was calculated as follows:

$$\Pi = -\frac{H}{6\pi} \left( \frac{1}{d_W^3} - \frac{2}{(d_W + d_B)^3} + \frac{1}{(d_W + 2d_B)^3} \right) + P_h e^{\frac{d_W}{\lambda_h}} + \frac{k_B T}{32\lambda_h} \sqrt{\frac{P_h}{K_C \lambda_h} e^{\frac{d_W}{\lambda_h}}} \tag{1}$$

The first term represents the van der Waals attraction, the second term the hydration repulsion and the third term the steric repulsion due to bilayer undulations, with  $H$  being the Hamaker constant,  $P_h$  a scaling constant,  $\lambda_h$  the decay constant of the hydration forces and  $K_C$  the bilayer bending rigidity (Parsegian and Rand 1995; Podgornik and Parsegian 1992). A second form for the fluctuation contribution has been proposed, which differs essentially from the present form by using a separate decay constant,  $\lambda_n$  (Petrache et al. 1998). However, its application requires the evaluation of Bragg peak line shapes, which is impeded by the overlapping reflections of the phase separated system (Fig. 1). Nevertheless, we note that this affects the determined bending rigidities insignificantly (Pabst et al. 2007a; Pan et al. 2009).

### Geometric Model for Ion Channels

A conformational change of membrane proteins depends on the volume change of the protein and the lateral pressure density,  $p(z)$ , of the lipid bilayer along the bilayer normal,  $z$ , against which the protein either expands or contracts laterally (Cantor 1999b). Assume a change  $r \rightarrow t$  of the protein conformation from a resting to an active state. Based on thermodynamic arguments, the fraction of active states at a given  $p(z)$  relative to an initial lateral pressure density,  $p_0(z)$  can be shown as follows (Cantor 1997):

$$f = \frac{1 + K_0}{(1 + K_0 e^{\alpha})} \tag{2}$$

where

$$\alpha = (k_B T)^{-1} \int_{-d_B/2}^{d_B/2} \Delta p(z) \Delta A(z) dz \tag{3}$$

$K_0 = [r]_0/[t]_0$  is the conformational equilibrium of the initial protein state, i.e., the fraction of resting proteins  $[r]_0$  with respect to the fraction of proteins in the open state  $[t]_0$ , prior to the change of the lateral pressure profile;  $\Delta A(z)$  is the involved lateral change of the protein area. For smoothly varying cross-sectional changes, Eq. 3 can be further simplified to

$$\alpha = (k_B T)^{-1} \sum_j \Delta a_j \Delta P_j \tag{4}$$

where  $\Delta a_j$  refers to the coefficients in a power expansion of

$$\Delta A \text{ in } z \text{ and } \Delta P_j = \int_0^{d_B/2} z^j \Delta p(z) dz \text{ is the change in the } j\text{th}$$

integral moment of the lateral pressure density  $p(z)$ . For the given geometric model of an hourglass-shaped ion channel (see Fig. 4a) with a central pore opening, we thus arrive at

$$\alpha = \frac{2\pi}{k_B T} [(2r_{\max} \Delta \tan \varphi - d_B \Delta \tan^2 \varphi) \Delta P_1 + \Delta \tan^2 \varphi \Delta P_2] \tag{5}$$

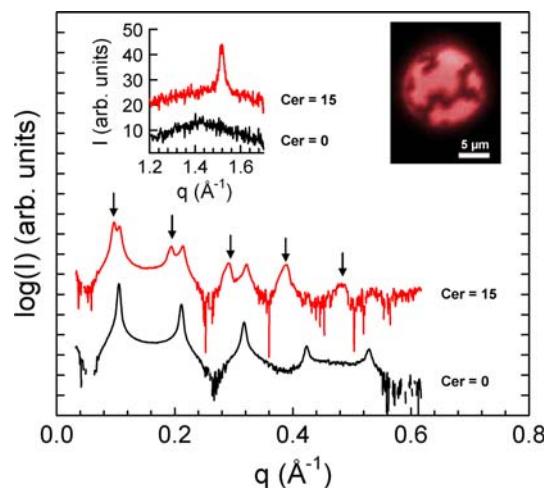
where  $r_{\max}$  is the outer radius of the pore,  $\varphi$  the angle of the bend helix with the bilayer normal (Fig. 4a) and  $\Delta P_1$  and  $\Delta P_2$  are the changes of the first and second integral moments of  $p(z)$ .

## Results and Discussion

The present study focuses on MLVs of two lipid model membrane systems composed of POPC/SM at an equimolar ratio and POPC/SM/Cer at a molar ratio of 50:35:15. A full description of the thermodynamic behavior of POPC/SM/Cer mixtures at various Cer concentrations supports the present findings and will be published elsewhere (B. Boulgaropoulos et al. unpublished).

### Structural Characterization of the Membranes

Figure 1 gives a comparison of the X-ray scattering patterns of the two samples at 37°C at medium osmotic pressure. In the small-angle regime and in the absence of Cer, a single phase with a lamellar repeat of  $d = 59.4 \text{ \AA}$  was observed. The diffuse peak at  $q \sim 1.4 \text{ \AA}^{-1}$  in the wide-angle regime demonstrates short-range order within the

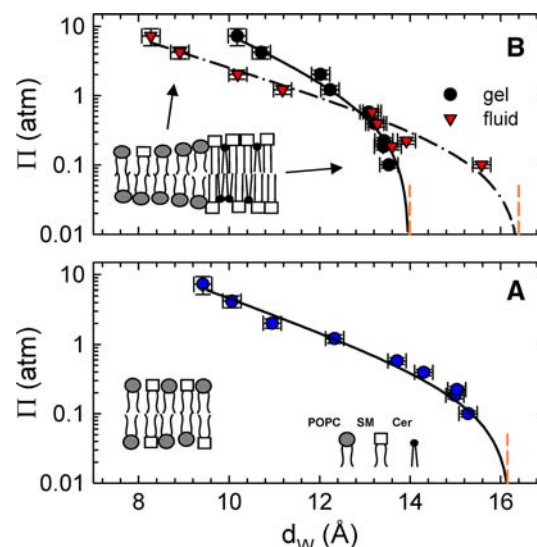


**Fig. 1** SAXD patterns of POPC/SM (Cer = 0 mol%) and POPC/SM/Cer (Cer = 15 mol%) bilayers at 37°C and osmotic pressure of 2 atm. Arrows indicate the lamellar diffraction orders of the gel phase. Insets show the corresponding wide-angle X-ray diffraction patterns and a fluorescence microscopic image of a GUV with coexisting lipid and fluid–gel domains. Bright areas correspond to the fluid phase and the dark faceted lines to the gel phase

plane of the bilayer, typical for the lamellar fluid  $L_\alpha$  phase. At Cer = 15 mol% two lamellar phases coexist with  $d = 65.3 \text{ \AA}$  and  $d = 58.8 \text{ \AA}$  and the wide-angle data show an additional sharp peak at  $q = 1.52 \text{ \AA}^{-1}$ . This indicates the presence of a gel ( $L_\beta$ ) phase, with hexagonal packing of the hydrocarbon chains and an average lateral area per chain of  $19.8 \text{ \AA}^2$ . The membrane thicknesses,  $d_B$ , were derived from electron density profiles as detailed in the previous section. For the POPC/SM mixture, we found  $d_B = 48.4 \text{ \AA}$ . In the presence of ceramide  $d_B = 53.3 \text{ \AA}$  for the large  $d$  value phase and  $d_B = 48.6 \text{ \AA}$  for the coexisting phase with the smaller repeat distance. Because  $d_B$  values strongly depend on the applied definition of the membrane thickness, we also included the head-to-headgroup distances,  $d_{HH}$ , in Table 1 in order to facilitate a comparison with values from other reports. The head-to-headgroup distance of the fluid phase of the POPC/SM/Cer mixture is about  $1.4\text{--}2 \text{ \AA}$  larger than reported for single-component membranes composed of POPC (Kucerka et al. 2005; Pabst et al. 2007b). This indicates that this phase is not a pure POPC domain. However, we presently focus on the difference in membrane thickness of the coexisting phases, which is consistent with the gel–fluid phase separation previously reported for similar lipid mixtures (Castro et al. 2007; Fidorra et al. 2006; Holopainen et al. 2000b; Staneva et al. 2008). Further, fluorescence microscopic images of POPC/SM/Cer showed gel-phase domains coexisting with a fluid phase (Fig. 1, inset). To distinguish the coexisting phases in the presence of ceramide, we denote them in the following as  $L_\alpha^c$  and  $L_\beta^c$ .

### Membrane Interactions and Mechanical Properties

Based on the membrane thickness, the two  $L_\alpha$  phases—in the presence and absence of ceramide—appear to be identical with respect to their physical properties. In order to test this notion, we exposed both lipid systems to a range of osmotic pressures,  $0 \leq \Pi \leq 7.25 \text{ atm}$ . The corresponding isotherms are presented in Fig. 2. The membrane thickness did not vary substantially for both lipid systems within the studied range of osmotic pressures. Hence, the plotted bilayer separations are obtained by subtracting a constant,  $d_B$ , from a given lamellar repeat distance. In the present case,  $\Pi$  balances membrane repulsion originating



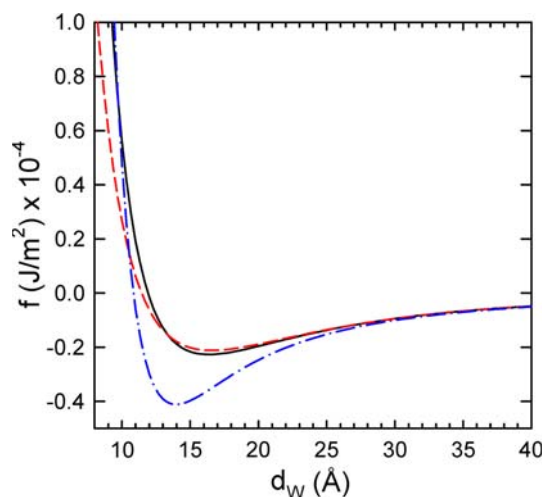
**Fig. 2**  $\Pi(d_w)$  isotherms for POPC/SM membranes (a) and POPC/SM/Cer bilayers (b) at  $37^\circ\text{C}$ . Solid/dashed-dotted lines correspond to fits and dotted lines indicate the equilibrium bilayer separation for  $\Pi = 0$ . Insets give schematics of the molecular organization

from hydration forces and bending undulations and membrane attraction due to van der Waals interactions. Hydration forces dominate at the highest osmotic pressures investigated. As  $\Pi$  decreases, steric repulsion due to thermal undulations comes increasingly into play until van der Waals attraction balances the disjoining pressures and the system finally attains its equilibrium separation at  $\Pi = 0$ . Because of the high bending rigidity of gel phases ( $\sim 100 \text{ k}_B\text{T}$ ), steric repulsion due to membrane undulations is negligible for the  $L_\beta^c$  phase. Thus, in the absence of osmotic pressure,  $d_w$  is significantly smaller than in the  $L_\alpha$  phases (Fig. 2b). Further, we found that the isotherms of the coexisting phases cross each other at  $\sim 0.6 \text{ atm}$ , upon which the gel phase is more difficult to compress than the  $L_\alpha^c$  phase. This signifies independent behavior of the coexisting phases under osmotic pressure, as expected for a macroscopically phase separated system.

To gain further insight, we analyzed the experimental pressure isotherms as described in “Materials and Methods” and by constraining the Hamaker constant to the theoretical value of  $4.3 \times 10^{-21} \text{ J}$  (Podgornik et al. 2006). This concept has been previously applied successfully in the context of peptide–lipid interactions (Pabst et al. 2007a). The remaining adjustable parameters in the present analysis are the scaling constant  $P_h$  and the decay length of  $\lambda_h$  of hydration forces, as well as the bilayer bending rigidity  $K_C$ . Fluctuation pressures were neglected for the  $L_\beta^c$  phase because of its large  $K_C$ . For the  $L_\alpha$  phases the following protocol was applied: We started with a fit of the  $\Pi > 1 \text{ atm}$  data, which are dominated by hydration interactions, using an estimate for  $K_C$  and adjusting  $P_h$  and  $\lambda_h$  only. The resulting values were then fixed

**Table 1** Experimental interaction parameters for POPC/SM multilayers at  $37^\circ\text{C}$  in the absence and presence of ceramide

Cer (mol%)	Phase	$d_B$ (Å)	$d_{HH}$ (Å)	$P_h$ (atm)	$\lambda_h$ (Å)	$K_C$ ( $\text{k}_B\text{T}$ )
0	$L_\alpha$	48.4	38.4	1,585	1.7	57.7
15	$L_\alpha^c$	48.6	38.6	616	1.7	15.7
15	$L_\beta^c$	53.3	43.3	5,000	1.6	$\geq 100$



**Fig. 3** Interaction potentials for POPC/SM bilayers (solid line) and for the  $L_\alpha$  (dashed line) and  $L_\beta$  (dash-dotted line) phases in POPC/SM/Cer membranes

in a subsequent analysis of the full data range, with  $K_C$  as the only fitting parameter. The new bending rigidity was used in a second analysis of the hydration interaction parameters for  $\Pi > 1$  atm. This cycle was repeated iteratively until satisfactory fits of the isotherms were obtained (Fig. 3). The resulting parameters (Table 1) are within the typical ranges of  $\lambda_H = 1.3\text{--}2.1$  Å and  $P_h = 500\text{--}1,000$  atm for the fluid phase (Petrache et al. 1998). Further, the  $P_h$  values are up to about one order of magnitude higher in the gel phase (Parsegian and Rand, 1995). Hydration forces decayed with similar constants for all studied systems. In agreement with previous osmotic pressure measurements on gel-phase bilayers (Parsegian and Rand 1995), the  $L_\beta$  phase exhibited the largest  $P_h$  value and consequently requires the largest work for dehydration. The  $L_\alpha$  phase exhibited the lowest  $P_h$ . Consequently, water can be removed most easily from this phase.

In the following we focus on the bending rigidities. The POPC/SM mixture yielded a bending rigidity of almost 60  $k_B T$ , which is significantly larger than the 20.5  $k_B T$  reported for pure POPC membranes at 30°C (Kucerka et al. 2005). This can be related to the melting temperature of pure SM bilayers,  $T_m = 39.2^\circ\text{C}$  (Mannock et al. 2003), which is much higher than that of POPC membranes ( $T_m = -3.5^\circ\text{C}$ ) (Pabst et al., 2007b). Thus, SM, which would be in the gel phase at 37°C, stiffens the POPC membrane. Strikingly, the  $L_\alpha$  phase turns out to be much softer than the homogeneous POPC/SM membrane, although the membrane thicknesses differ insignificantly. Its bending rigidity of  $\sim 16$   $k_B T$  closely resembles that of pure POPC (Kucerka et al. 2005), considering temperature dependence and experimental uncertainties. The softening can be rationalized by strong hydrogen bonding activity between

ceramide and SM (Castro et al. 2007). This strong coupling leads to preferred pairwise interaction of SM and Cer, whose mixture will be in the gel phase at 37°C because of the high  $T_m$  of SM (Mannock et al. 2003) and Cer (Shah et al. 1995). The consequence of SM/Cer enrichment in the gel phase is a depletion of SM from the coexisting fluid phase. The  $L_\alpha$  phase is then mainly composed of POPC and, hence, has a lower  $K_C$  than the  $L_\alpha$  phase of the POPC/SM mixture. The splitting of lipid composition into POPC-rich and SM/Cer-rich phases is further supported by calorimetric and infrared spectroscopic measurements (B. Boulgaropoulos et al., unpublished).

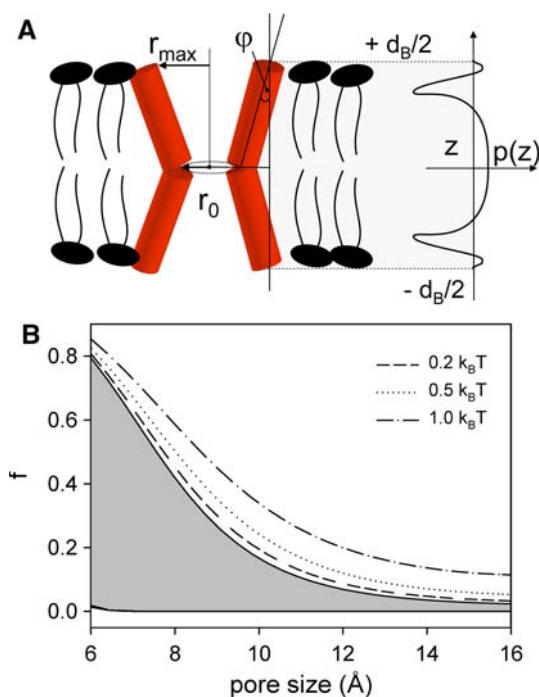
An integration of the pressure isotherms yields the interaction potentials, which are presented in Fig. 3. Clearly, the  $L_\beta$  phase has the deepest free energy minimum and the steepest increase of the potential upon further compression. Hence, the corresponding bilayers are strongly coupled and exhibit the highest stability of all studied phases. In comparison, the absolute value of the minimum for the  $L_\alpha$  phases is about two times smaller. Further, the interaction potential of the  $L_\alpha$  phase is softer than that of the homogenous POPC/SM mixture. This is a consequence of the lower  $K_C$ .

#### Changes Within the Lateral Pressure Profile

In order to address the putative effect of the membrane softening by SM depletion on membrane proteins, in the next section we consider the lateral pressure concept put forward by Cantor (1997). Further, we assume for simplicity that the  $L_\alpha$  phase is made up of pure POPC. The lateral pressure profile describes the balance of lateral pressures along the bilayer normal,  $z$ , given by the minimization of the free energy with respect to the lateral area (Ben Shaul 1995). Lateral pressures are defined as negative at the water/lipid interface and exhibit mainly positive contributions in the headgroup and the hydrocarbon tail regimes (Fig. 4a). In a balanced, tensionless membrane, the integral of all pressures along the bilayer normal is zero. However, its first and second moments, which are defined as  $P_1 = \int_0^{d_b/2} zp(z)dz$  and  $P_2 = \int_0^{d_b/2} z^2p(z)dz$ , may differ from zero. The first integral moment, which is the lateral torque tension, is related to the monolayer bending rigidity  $K_C^m$  and the spontaneous curvature  $c_0$  of the lipid monolayer by  $P_1 = K_C^m c_0$ . The second integral moment is equal to the gaussian curvature modulus,  $\kappa_G$  (Ben Shaul 1995; Seddon and Templer 1995).

Based on our measurements, we can estimate the relative change of the first integral moment due to SM depletion from the fluid phase. It is reasonable to assume that the relative change of the monolayer bending rigidity is equal





**Fig. 4** Effect of present lateral pressure changes on the activity of ion channels. **a** Applied simple geometric model, with a central pore of radius  $r_0$  and a maximum opening radius  $r_{\max}$ . Opening is achieved by decreasing the angle  $\varphi$ , while keeping  $r_{\max}$  constant. Further, a schematic of the lateral pressure profile is presented. **b** Fraction of open channels in the  $L_\alpha^c$  phase with respect to those in the  $L_\alpha$  phase of POPC/SM membranes. Calculations were performed as a function of the inner pore diameter of the open channel, using  $r_0^{\text{closed}} = 2 \text{ \AA}$ ,  $r_{\max} = 18 \text{ \AA}$  and  $d_B = 48.5 \text{ \AA}$ . Gray area gives the range of fractions between  $\Delta P_1 = 0.27 \text{ k}_B\text{T}/\text{\AA}$  (upper boundary) and  $\Delta P_1 = 1.08 \text{ k}_B\text{T}/\text{\AA}$  (lower boundary) for  $\Delta P_2 = 0 \text{ k}_B\text{T}$ . Additional lines show the effect of various  $\Delta P_2 > 0$  and  $\Delta P_1 = 0.27 \text{ k}_B\text{T}/\text{\AA}$ . Equal  $\Delta P_2$  values lead to insignificant changes of  $f$  for  $\Delta P_1 = 1.08 \text{ k}_B\text{T}/\text{\AA}$

to that of the bilayer bending rigidity. Hence,  $\Delta K_C^m/K_C^m = -0.73$  (Table 1). No  $c_0$  data have been reported for POPC and SM. Both are bilayer-forming lipids and their spontaneous curvatures will be larger than that of dioleoyl phosphatidylcholine (Zimmerberg and Kozlov 2006) but slightly smaller than zero. However, because of the kink induced by the single *cis* double bond at the ninth carbon of the *sn*-2 fatty acid chain, POPC can be expected to have a slightly more negative curvature than SM. In order to get an upper limit for the spontaneous curvature change, we assume (1)  $c_0^{\text{POPC}} = 2c_0^{\text{SM}}$  and (2) that the spontaneous curvature of the POPC/SM membrane is given by the average sum of the individual lipids. Then,  $\Delta c_0/c_0 = 0.33$ , leading to  $\Delta P_1/P_1 = -0.4$  as a lower limit of the relative change of lateral pressure. Further,  $\Delta P_1/P_1 = -0.73$  is the upper limit in case of a negligible difference of  $c_0$  between SM and POPC.

Since  $P_1 < 0$  for the present lipid systems (POPC and SM both have negative  $c_0$ ), the transfer of SM to the Cer-

rich  $L_\beta^c$  phase consequently leads to a net increase of the lateral torque tension within the  $L_\alpha^c$  phase ( $\Delta P_1 > 0$ ). In other words, there is a redistribution of repulsive lateral pressures from the bilayer interior toward the lipid/water interface. This is again due to the kink of the monounsaturated fatty acid chain of POPC, whose contribution to lateral pressure is naturally more expressed in pure POPC than in the POPC/SM mixture. In order to estimate the expected range of  $\Delta P_1$  we apply  $P_1 = -0.4 \text{ k}_B\text{T}/\text{\AA}$  from a recent molecular dynamics simulation on POPC at  $37^\circ\text{C}$  (T. Stockner, private communication). Using our above derived estimates for  $\Delta P_1/P_1$ , we then calculate  $-0.67 \text{ k}_B\text{T}/\text{\AA} < P_1 < -1.48 \text{ k}_B\text{T}/\text{\AA}$  for POPC/SM equimolar mixture. Consequently,  $\Delta P_1$  varies between  $0.27$  and  $1.08 \text{ k}_B\text{T}/\text{\AA}$  in the fluid phase, due to the transfer of SM to the  $L_\beta^c$  phase by ceramide.

### Consequences for the Activity of Ion Channels

Next, we consider a neurotransmitter-gated nicotinic acetylcholine receptor as an example of a typical ion channel. Its transmembrane domain is composed of a bundle of five bend  $\alpha$ -helices, and the channel opens by a right-handed rotation of the helices (Unwin 1995, 2005). The simplest geometric model of such an ion channel is that of an hourglass with a central pore located at the middle of the bilayer. Hence, the pore opens, simply increasing the radius in the center of the channel  $r_0$ , while the outer radius of the bundle  $r_{\max}$  remains constant. Additionally, we assumed for our calculations that the conformational changes are symmetric with respect to the center of the membrane.

Following Cantor (1999b), we derived the change in conformational equilibrium of our model of an ion channel due to the above estimated minimum and maximum changes of  $P_1$  for a range of pore sizes (see “Materials and Methods”). Figure 4b shows the corresponding fractions of open ion channels in the  $L_\alpha^c$  phase relative to those in the  $L_\alpha$  phase of the POPC/SM mixture. Because the open pore size of the ion channel is not well known, results are plotted for a range of central pore diameters. Calculations are based on the assumption that 95% of the channels are open prior to the generation of ceramide, i.e.,  $K_0 = 5/95$  (see Eq. 2). Further, according to structural data (Unwin 1995), the outer channel radius was set to  $18 \text{ \AA}$ . The inner radius of the closed pore was defined as  $2 \text{ \AA}$  and the membrane thickness was given by the average experimental value of  $48.5 \text{ \AA}$  (Table 1). Results show that opening of the ion channels is significantly inhibited under the present changes of lateral pressure. At an open pore size of  $6 \text{ \AA}$   $f \sim 0.8$  for  $\Delta P_1 = 0.27 \text{ k}_B\text{T}/\text{\AA}$  and  $f \sim 0.013$  for  $\Delta P_1 = 1.08 \text{ k}_B\text{T}/\text{\AA}$ , which means that the range of open ion channels varies between 76% and 1%, if 95% were open initially. The fraction of open states vanishes rapidly

for larger pore sizes, in particular for the larger  $\Delta P_1$ . This is due to the larger amount of mechanical work necessary to change the protein conformation against the lateral pressure change. Unwin (1995) reported a minimum pore diameter of  $\sim 10$  Å for open nicotinic acetylcholine receptors of *Torpedo* ray postsynaptic membranes. Our calculations predict that at least 85% of these channels will be inhibited under the present circumstances. We further considered the effect of changes in the second moment of the lateral pressure profile, i.e., the gaussian curvature modulus,  $\kappa_G$  (Seddon and Templer 1995). Motivated by optical  $\kappa_G$  measurements of liquid ordered and liquid disordered domains on lipid vesicles (Baumgart et al. 2005),  $\Delta P_2$  should be  $>0$  in the present case. Such changes lead to an increase of  $f$  (Fig. 4b), most significantly for the smaller  $\Delta P_1$  estimate.

Although we have deliberately excluded cholesterol from the present study, it is interesting to briefly consider its potential effect on the present scenario. Ceramide has been reported to displace cholesterol from rafts at low cholesterol concentrations, while high cholesterol concentrations are able to dissolve the Cer-enriched gel domains (Castro et al. 2009). In the absence of ceramide, cholesterol is predicted to lead to a decrease of lateral pressures near the lipid/water interface (Cantor 1999a). This is at least qualitatively the opposite effect of removing SM from fluid POPC bilayers, as in the present case. Hence, we expect that the addition of cholesterol would counteract the inhibition of the ion channel. In support of this argument, cholesterol has been reported to be an essential membrane component for the activation of nicotinic acetylcholine receptors (Rankin et al. 1997).

Finally, we did not study the effect of membrane proteins on the membrane properties. Obviously, it can be expected that this affects the lateral organization and the bulk properties of the coexisting domains. For example, it has been shown previously that the insertion of peptides into membranes leads to a decrease of membrane rigidity (Pabst et al. 2007a; Pan et al. 2009). Thus, the initial state of the membrane, i.e., prior to the generation of ceramide, will differ from our experimentally studied system, which does not contain a membrane protein. It is presently not clear if the changes in lateral pressure profile are on the same order if the membrane contains a protein. However, this is certainly an option. In this case, the relative changes discussed above would be the same. Future studies planned in our laboratory will address this point.

## Conclusions

We have demonstrated that the addition of Cer to POPC/SM model membranes leads—compared POPC/SM

mixtures—to a distinct softening of the  $L_\alpha$  phase. This fluid phase coexists with a gel phase, and its lower  $K_C$  is due to a depletion of SM, which is recruited by Cer to the gel phase. The fact that  $K_C$  is close to a recently reported value of pure POPC (Kucerka et al., 2005) further supports the notion that the  $L_\alpha$  phase is enriched in POPC. The increase of membrane flexibility induced a net shift of lateral pressures within the hydrocarbon region toward the lipid/water interface. First-order approximation calculations for nicotinic acetylcholine receptors showed that this may significantly inhibit the activation of ion channels, which are not located in the ceramide-stabilized membrane rafts. Our study, therefore, showed that Cer generation not only affects the stability of membrane rafts and signaling complexes but is also able to strongly influence the functioning of membrane proteins which are not associated to raft structures.

**Acknowledgements** We thank Robert Cantor, Hennig von Grünberg and Thomas Stockner for valuable discussions. We further thank Thomas Stockner for allowing us to use his data on the first moment of the lateral pressure profile of POPC prior to publication.

## References

- Angelova MI, Dimitrov DS (1986) Liposome electroformation. *Faraday Discuss Chem Soc* 81:303–311
- Baumgart T, Das S, Webb WW, Jenkins JT (2005) Membrane elasticity in giant vesicles with fluid phase coexistence. *Biophys J* 89:1067–1080
- Ben Shaul A (1995) Molecular theory of chain packing, elasticity and lipid–protein interaction in lipid bilayers. In: Lipowsky R, Sackmann E (eds) *Handbook of biological physics*. Elsevier, Amsterdam, pp 359–401
- Brown DA (2006) Lipid rafts, detergent-resistant membranes, and raft targeting signals. *Physiology (Bethesda)* 21:430–439
- Cantor RS (1997) Lateral pressures in cell membranes: a mechanism for modulation of protein function. *J Phys Chem B* 101:1723–1725
- Cantor RS (1999a) Lipid composition and the lateral pressure profile in bilayers. *Biophys J* 76:2625–2639
- Cantor RS (1999b) The influence of membrane lateral pressures on simple geometric models of protein conformational equilibria. *Chem Phys Lipids* 101:45–56
- Castro BM, de Almeida RF, Silva LC, Fedorov A, Prieto M (2007) Formation of ceramide/sphingomyelin gel domains in the presence of an unsaturated phospholipid: a quantitative multiprobe approach. *Biophys J* 93:1639–1650
- Castro BM, Silva LC, Fedorov A, de Almeida RF, Prieto M (2009) Cholesterol-rich fluid membranes solubilize ceramide domains: implications for the structure and dynamics of mammalian intracellular and plasma membrane. *J Biol Chem* 284:22978–22987
- Fidorra M, Duelund L, Leidy C, Simonsen AC, Bagatolli LA (2006) Absence of fluid-ordered/fluid-disordered phase coexistence in ceramide/POPC mixtures containing cholesterol. *Biophys J* 90:4437–4451
- Goni FM, Alonso A (2006) Biophysics of sphingolipids I Membrane properties of sphingosine, ceramides and other simple sphingolipids. *Biochim Biophys Acta* 1758:1902–1921

- Holopainen JM, Angelova MI, Kinnunen PK (2000a) Vectorial budding of vesicles by asymmetrical enzymatic formation of ceramide in giant liposomes. *Biophys J* 78:830–838
- Holopainen JM, Lemmich J, Richter F, Mouritsen OG, Rapp G, Kinnunen PK (2000b) Dimyristoylphosphatidylcholine/C16:0-ceramide binary liposomes studied by differential scanning calorimetry and wide- and small-angle X-ray scattering. *Biophys J* 78:2459–2469
- Kucerka N, Tristram-Nagle S, Nagle JF (2005) Structure of fully hydrated fluid phase lipid bilayers with monounsaturated chains. *J Membr Biol* 208:193–202
- Mannock DA, McIntosh TJ, Jiang X, Covey DF, McElhaney RN (2003) Effects of natural and enantiomeric cholesterol on the thermotropic phase behavior and structure of egg sphingomyelin bilayer membranes. *Biophys J* 84:1038–1046
- McIntosh TJ, Magid AD, Simon SA (1987) Steric repulsion between phosphatidylcholine bilayers. *Biochemistry* 26:7325–7332
- Pabst G, Rappolt M, Amenitsch H, Laggner P (2000) Structural information from multilamellar liposomes at full hydration: full q-range fitting with high quality X-ray data. *Phys Rev E* 62:4000–4009
- Pabst G, Danner S, Podgornik R, Katsaras J (2007a) Entropy-driven softening of fluid lipid bilayers by alamethicin. *Langmuir* 23:11705–11711
- Pabst G, Hodzic A, Strancar J, Danner S, Rappolt M, Laggner P (2007b) Rigidification of neutral lipid bilayers in the presence of salts. *Biophys J* 93:2688–2696
- Pan J, Tieleman DP, Nagle JF, Kucerka N, Tristram-Nagle S (2009) Alamethicin in lipid bilayers: combined use of X-ray scattering and MD simulations. *Biochim Biophys Acta* 1788:1387–1397
- Parsegian VA, Rand RP (1995) Interaction in membrane assemblies. In: Lipowsky R, Sackmann E (eds) *Handbook of biological physics*. Elsevier, Amsterdam, pp 643–690
- Petrache HI, Gouliaev N, Tristram-Nagle S, Zhang RT, Suter RM, Nagle JF (1998) Interbilayer interactions from high-resolution X-ray scattering. *Phys Rev E* 57:7014–7024
- Pike LJ (2006) Rafts defined: a report on the Keystone Symposium on Lipid Rafts and Cell Function. *J Lipid Res* 47:1597–1598
- Podgornik R, Parsegian VA (1992) Thermal mechanical fluctuations of fluid membranes in confined geometries—the case of soft confinement. *Langmuir* 8:557–562
- Podgornik R, French RH, Parsegian VA (2006) Nonadditivity in van der Waals interactions within multilayers. *J Chem Phys* 124:044709
- Posse de Chaves EI (2006) Sphingolipids in apoptosis, survival and regeneration in the nervous system. *Biochim Biophys Acta* 1758:1995–2015
- Rankin SE, Addona GH, Kloczewiak MA, Bugge B, Miller KW (1997) The cholesterol dependence of activation and fast desensitization of the nicotinic acetylcholine receptor. *Biophys J* 73:2446–2455
- Seddon JM, Templer RH (1995) Polymorphism of lipid water systems. In: Lipowsky R, Sackmann E (eds) *Structure and dynamics of membranes*. North-Holland, Amsterdam, pp 97–160
- Shah J, Atienza JM, Duclos RI Jr, Rawlings AV, Dong Z, Shipley GG (1995) Structural and thermotropic properties of synthetic C16:0 (palmitoyl) ceramide: effect of hydration. *J Lipid Res* 36:1936–1944
- Simons K, Ikonen E (1997) Functional rafts in cell membranes. *Nature* 387:569–572
- Staneva G, Chachaty C, Wolf C, Koumanov K, Quinn PJ (2008) The role of sphingomyelin in regulating phase coexistence in complex lipid model membranes: competition between ceramide and cholesterol. *Biochim Biophys Acta* 1778:2727–2739
- Unwin N (1995) Acetylcholine receptor channel imaged in the open state. *Nature* 373:37–43
- Unwin N (2005) Refined structure of the nicotinic acetylcholine receptor at 4 Å resolution. *J Mol Biol* 346:967–989
- van Blitterswijk WJ, van der Luit AH, Veldman RJ, Verheij M, Borst J (2003) Ceramide: second messenger or modulator of membrane structure and dynamics? *Biochem J* 369:199–211
- Zimmerberg J, Kozlov MM (2006) How proteins produce cellular membrane curvature. *Nat Rev Mol Cell Biol* 7:9–19

**8.3 Paper III** Implication of Sphingomyelin/Ceramide Molar Ratio on the Biological Activity of Sphingomyelinase (submitted to Biophysical Journal, March 2010)



# Implication of Sphingomyelin/Ceramide Molar Ratio on the Biological Activity of Sphingomyelinase

Beate Boulgaropoulos, Heinz Amenitsch, Peter Laggner and Georg Pabst

Institute of Biophysics and Nanosystems Research, Austrian Academy of Sciences,  
Schmiedlstr. 6, A-8042 Graz, Austria

**Corresponding Author:** Georg Pabst, Institute of Biophysics and Nanosystems Research,  
Austrian Academy of Sciences, Schmiedlstr. 6, A-8042 Graz, Austria, Tel.: +43 316 4120  
342, Fax: +43 316 4120 390, Email: [georg.pabst@oeaw.ac.at](mailto:georg.pabst@oeaw.ac.at)

**Running Title:** Driving Sphingomyelinase Activity

**Keywords:** Apoptosis, Lipid Bilayer, Ceramide, Enzymatic hydrolysis, Domain formation,  
X-ray scattering

submitted to Biophysical Journal, 2<sup>nd</sup> of March 2010

**Abstract**

Sphingolipid signalling plays an important, yet not fully understood role in diverse aspects of cellular life. Sphingomyelinase is a major enzyme in these signalling pathways, catalyzing hydrolysis of sphingomyelin to ceramide and phosphocholine. In order to address the related membrane dynamical structural changes and their feedback to enzyme activity, we have studied the effect of enzymatically generated ceramide *in situ* on the properties of a well-defined lipid model system. We found a gel phase formation that was about four times faster than ceramide generation, due to ceramide-sphingomyelin pairing. The gel phase formation slowed down when the ceramide molar ratios exceeded those of sphingomyelin and stopped just at the solubility limit of ceramide, due to unfavourable pair-wise interactions of ceramide with itself and with monounsaturated phosphatidylcholine. A remarkable correlation to *in vitro* experiments suggests a regulation of sphingomyelinase activity based on the sphingomyelin/ceramide molar ratio.

## INTRODUCTION

Sphingolipids are ubiquitously present in all mammalian cells and play an important role in the regulation of diverse cellular functions (5, 33, 35, 194). Sphingomyelin (SM) is a major lipid component of plasma membranes and is considered to be extensively located in membrane rafts, where it helps to assemble signalling complexes (195, 196). Of particular interest is the enzymatic degradation of SM by sphingomyelinase (SMase) to ceramide (Cer) and phosphocholine and its consequences to the lateral heterogeneity of membranes. Various cellular processes have been related to SMase activity, among which, most prominently, apoptosis (programmed cell death) (5, 33, 35). Apoptosis follows a characteristic morphological pathway and can be triggered by diverse stimuli, like death receptor clustering, hypoxia, DNA damage with chemotherapeutic agents or by  $\gamma$ -radiation (3). Apoptosis is characterized by several key phases. In the initiator phase, the cells maintain to a large extent their morphology. Rapid and transient Cer formation by SMase activity facilitates death receptor clustering at the membrane surface, possibly by Cer's property to stabilize membrane rafts (12, 13). Most recently, we were able to show that Cer generation might also indirectly affect the activity of proteins not located in rafts (197). Further, Cer may act as a second messenger during this stage (5, 33). In the effector phase of apoptosis the membrane loses its asymmetric lipid distribution, and neutral sphingomyelinase (nSMase) generates Cer in the inner leaflet at the plasma membrane. The Cer formation in this apoptotic phase occurs slowly and continuously (5). Cer levels increase significantly, and membrane blebbing and apoptotic body formation are directly visible consequences. Finally, the execution phase of apoptosis is distinguished by continuous blebbing and vesiculation, paired with cholesterol efflux from the membrane (5). Another characteristic is shrinking of the nucleus, constriction of apoptotic bodies and finally the disposal of the cell. Details of apoptosis, however, seem to depend strongly on the type of apoptotic stimulus, as well as on the cell type (4, 19).

Previous biophysical studies on model membranes of well-defined lipid composition showed that enzymatic fragmentation of SM leads to vesicle aggregation (79) and blebbing (164), very similar to the cellular events observed during apoptosis. Most recently, complex morphological membrane changes, involving stable Cer-rich and metastable SM-rich domains, respectively, have been reported in ternary lipid mixtures of dioleoyl phosphatidylcholine, SM and cholesterol (198). A direct coupling of the timeline of the chemical modifications on the molecular-level to membrane domain formation is presently missing, however. Further, it is not entirely clear, whether the various labelling techniques applied in previous studies on SMase activity influence the observed phase behaviour (199-201).

Therefore, we performed an *in-situ*, label-free, study of the SMase activity profile in mammalian model membranes composed of an equimolar mixture of palmitoyl oleoyl phosphatidylcholine (POPC) and egg-SM. Cholesterol was deliberately excluded from the present study to keep data interpretation tractable. Enzymatic hydrolysis of SM was induced by the well characterized nSMase from *Bacillus cereus* (111). The chemical and structural changes were addressed by a combination of chromatography (HPTLC) and time-resolved x-ray diffraction. We observed interdependent kinetics on different length scales, strongly correlated with the SM/Cer molar ratio. Up to molar ratios of SM/Cer = 1, we found a gel phase formation that proceeds four times faster than SM hydrolysis by SMase. At higher Cer levels no further changes of the gel phase domain size was observed and the membrane structural parameters slowly approached an equilibrium state. Hydrolysis of SM stopped just

before exceeding the solubility limit of Cer. Qualitative and quantitative agreement of our findings to cell biological experiments suggests that the biological activity of SMase depend strictly on the evolving SM/Cer molar ratio.

## METHODS

### Materials and sample preparation

POPC, Egg-SM, and C16:0-Cer (N-palmitoyl-D-*erythro*-sphingosine) were purchased from Avanti Polar Lipids (Birmingham, AL) and used without further purification. nSMase from *Bacillus cereus* was obtained from Sigma-Aldrich (St. Louis, MO) as lyophilized powder. All other chemicals (salts, solvents in pro analysis quality) and polyethylene glycol (PEG,  $M_w = 8000$ ) were from Sigma-Aldrich. 18 M $\Omega$ /cm water (UHQ PS, USF Elga, Wycombe, UK) was used for all liposomal preparations.

Dry lipid films of two different sample types were prepared as described previously (202). The first type contained a known amount of Cer in a POPC/SM mixture for reference measurements. The second sample type was a binary, equimolar mixture of POPC and SM for the enzymatic reaction. The lipid films containing Cer were hydrated in 20 mM Naphosphate buffer, (130 mM NaCl, pH = 7.4) and films for enzyme reaction experiments in 10 mM HEPES buffer (200 mM NaCl, 2 mM MgCl<sub>2</sub>, 10 mM CaCl<sub>2</sub>, pH = 6.8), using standard procedures at total lipid concentration of 50 mg/ml. Large unilamellar POPC/SM vesicles (LUVs) with a size of 1200 Å and polydispersity index < 0.1, as determined by photon correlation spectroscopy on a Zetasizer 3000 HAS (Malvern Instruments, Herrenberg, Germany), were obtained by extrusion through a 100 nm membrane filter (Nucleopore, Whatman International Ltd. Maidstone, U.K.). LUVs were subsequently concentrated to about 70 mg/ml by centrifugation through a pre-rinsed centricon centrifugal filter device with a Ultracel YM-30 membrane (Millipore, Carrigtwohill, Co. Cork, Ireland ) (30 000 NMWL, 4500g, 20 min). Finally, 10 U of nSMase were dissolved in 70  $\mu$ L of the same buffer used for the LUV preparation, but containing additionally 2 mM o-phenanthroline in order to inhibit traces of contaminant phospholipase C activity of the enzyme (82).

### High Performace Thin Layer Chromatography

HPTLC was performed on a fully automated system from CAMAG (Muttensz, Switzerland). HPTLC-plates (silica gel 60 F 254) were from Merck (Germany) and samples were sprayed automatically with 150 nL/s. During the experiment, well-defined amounts of the aqueous reaction batch were transferred into organic stop-solution (CHCl<sub>3</sub>/MeOH = 2/1) and rigorously vortex mixed for at least 3 min. Plates were developed with CHCl<sub>3</sub>: MeOH: H<sub>2</sub>O: CH<sub>3</sub>COOH (65/25/4/1 v/v/v/v) and post-chromatographic [derivatisation](#) was performed with CuSO<sub>4</sub> (10%) in H<sub>3</sub>PO<sub>4</sub> (4%) followed by 10 min incubation at 190°C. Peaks were scanned with at a wavelength of 450 nm and quantified by relating peak-height and area of the unknown lipid bands to those of POPC, SM and C16:0-Cer standards. The minimum and maximum lipid amounts detected on the plate were about 0.1  $\mu$ g and 1  $\mu$ g, respectively. To SM hydrolysis and Cer formation were fitted a hyperbolic growth  $C(t) = C_0 + Pt / (\tau_H + t)$ , where  $C_0$  is the offset,  $P$  the saturation level of the enzymatic turnover and  $\tau_H$  corresponds to the time where half of the fragmentation is achieved.

## X-ray diffraction

Time-resolved small- and wide-angle x-ray scattering (SWAXS) experiments were performed at the Austrian SAXS beamline at Elettra (Trieste, Italy). Two linear detectors were used covering the scattering vectors  $q$  from  $0.01 \text{ \AA}^{-1}$  to  $0.6 \text{ \AA}^{-1}$  and  $0.67 \text{ \AA}^{-1}$  to  $1.95 \text{ \AA}^{-1}$  for SAXS and WAXS, respectively. Alternatively, a mar345 (Marresearch Nordersted, Germany) image plate detector was used for static experiments. Procedures for angular calibration, sample holders and primary data reduction were described previously (203). Samples containing SMase were prepared by mixing of LUV and enzyme solutions. Reaction batches were rapidly transferred to the sample holder and measurements were started about 70 seconds after mixing. Diffraction patterns of 10 s exposure time were taken every minute. The exposure time with the image plate detector was set to 60 s. These samples were equilibrated at  $37^\circ\text{C}$  for ten minutes prior to measurement. No signatures of radiation damage were observed during and after all experiments.

High frequency noise was screened from the WAXS data as described previously (126). A constant background was defined by a linear fit in a narrow range of the WAXS gel peak and subsequently subtracted from the WAXS data. Peak parameters were derived from Lorentz fits. Similarly, SAXS peaks were analyzed using Lorentz functions. The full width at half maximum of the peaks  $\Delta q$  was corrected for the instrumental resolution  $\delta q = 2.2 \times 10^{-3} \text{ \AA}^{-1}$  and used to calculate the average domain size (correlation length) (121)  $L = 2\pi / \sqrt{\Delta q^2 - \delta q^2}$ . Finally, the average number of layers was estimated from the SAXS data applying  $N_{\text{layer}} = L_{\text{SAXS}} / d$ , where  $d$  is the lamellar repeat distance. The average number of positionally correlated lipids per gel phase domain was estimated from  $N_{\text{lip}} = L_{\text{WAXS}} / \sqrt{A}$ , where the lateral area per lipid was given from the WAXS peak position as  $A = 16\pi^2 / (\sqrt{3}q_{\text{WAXS}}^2)$  (127).

Static SAXS measurements were also performed on a laboratory based SWAXS camera (System 3, Hecus X-ray Systems, Graz, Austria). Samples were equilibrated for 10 min before measurement. Exposure times were 3600 s.

## RESULTS

All experiments were performed at  $37^\circ\text{C}$ . In the following, we present the experimental findings on different hierarchical levels.

### Changes on the molecular level

Enzymatic hydrolysis of SM was started by adding 30  $\mu\text{L}$  of the large unilamellar vesicle (LUV) dispersion to 70  $\mu\text{L}$  enzyme solution. This gave a reaction-batch with a lipid concentration of 27.3 mM and an enzyme activity of 100 U/mL (7.3 U/ $\mu\text{mol}$  SM). Figure 1 presents the reaction progress of SM fragmentation and C16:0-Cer production as determined by HPTLC. Within the first  $\sim 150$  min, total Cer levels increased rapidly, nearly reaching the plateau value of  $86 \pm 5\%$ , as determined by a hyperbolic fit to the SM fragmentation data. The corresponding time constant  $\tau_{\text{H}} = 12$  min, i.e.  $\sim 43\%$  of the original SM lipids were hydrolyzed after 12 min. C16:0-Cer levels increased with a similar time constant and

saturated at  $65 \pm 8\%$ . This value agrees well with the amount of SM fragmentation, as the fraction of C16:0 acyl chains of egg-SM is 84%, according to data of the supplier. It is interesting to compare these findings to SM degradation measurements of a biological system undergoing apoptosis. We found remarkable agreement with published results on human leukaemia cells (2), both in terms of kinetics and final SM levels (Fig.1). Very similar results were also reported in fibroblast cells (165, 166). This underlines the biological significance of the present study.

### Dynamic membrane structure effects

Structural changes occurring on the membrane level during the enzymatic hydrolysis of SM were followed by time-resolved SWAXS. Prior to the addition of SMase, SAXS data showed very broad first and second order Bragg reflections (Fig.2). This indicates the presence of oligolamellar vesicles (OLVs) composed of about three positionally correlated bilayers with a lamellar repeat distance  $d = 64.6 \text{ \AA}$ . This may come as a surprise, because the applied extrusion technique yielded LUVs with a narrow size distribution (see materials and methods). However, SAXS patterns are very sensitive to the presence of positionally correlated bilayers, which have a significantly stronger scattering signal than unilamellar vesicles. Thus, although LUVs are the initial major population of vesicles, OLVs are much more apparent. During the enzymatic reaction the Bragg peaks sharpened considerably and their width finally corresponded to  $\sim 7$  positionally correlated bilayers and a repeat distance of  $d = 68.7 \text{ \AA}$ . Both patterns were recorded with high counting statistics and, therefore, are suitable for a global analysis in terms of a full  $q$ -range model (144, 145). Before addition of SMase we found a cross-bilayer head-to-head distance of  $d_{\text{HH}} = 40.8 \text{ \AA}$ , indicating a fluid phase in agreement with WAXS data (see below) and previous reports (204). The final SAXS pattern corresponded to a  $d_{\text{HH}} = 45.2 \text{ \AA}$ , showing the formation of a gel phase. This is further substantiated by a comparison to membrane thickness data on POPC/SM/Cer mixtures under equilibrium conditions (205). There, too, it was found that Cer leads to macroscopic separation into fluid ( $L_{\alpha}^{\circ}$ ) and gel ( $L_{\beta}^{\circ}$ ) phases.

Fig.3 A and B show the corresponding time evolutions of the lamellar repeat distance  $d$  and the number of correlated bilayers,  $N_{\text{layer}}$ , respectively, during this transformation. We found a steep initial increase of  $d$  with a slope of  $0.1 \text{ \AA}/\text{min}$ . After about 20 minutes the slope of  $d$  decreased by about three orders of magnitude. At the same time, we observed a significantly slower increase of  $N_{\text{layer}}$ , which leveled off after  $\sim 170 \text{ min}$ .

The changes in lateral packing of the membrane lipids associated with the changes in bilayer dimensions discussed above are seen in the WAXS patterns (Fig.2, insert). Before enzyme addition we observed a diffuse chain correlation peak centred at  $q = 1.43 \text{ \AA}^{-1}$ , typical for fluid hydrocarbon chains, and as expected from the temperature of our experiments, well above the melting transition of the POPC/SM equimolar mixture,  $T_m \sim 25^{\circ}\text{C}$  (136). The final WAXS pattern exhibited a peak at  $q = 1.51 \text{ \AA}^{-1}$ , demonstrating the generation of a  $L_{\beta}^{\circ}$  gel phase with a 2D hexagonal packing of the acyl chains and with a lateral area per lipid  $A = 40.0 \text{ \AA}^2$ , similar to reports from equilibrium studies with defined Cer concentrations (see, e.g. (206)). From the peak width we further estimate an average domain size of about 13 nm, corresponding to  $\sim 200$  in-plane positionally correlated lipids.

The kinetics of gel phase domain formation is presented in Fig.3 C and D. WAXS data showed the occurrence of a gel phase already at the onset of the experiment, i.e. 70 s after addition of SMase, where the lateral area per lipid  $A$  equalled the final value. However,

the peak width indicated that  $N_{lip}$  was initially  $\sim 100$  and reached its final value of  $\sim 200$  after about 20 min. The growth rate was about four times faster than Cer generation (Fig.1), but similar to the changes of  $d$ , as observed from SAXS. This demonstrates that the SAXS results are dominated by the generation of the  $L_{\beta}^c$  phase. The lateral area per gel phase lipid decreased at a similar rate as fast as  $N_{lip}$  and  $d$  increased.  $A$  showed a minimum value of  $39.8 \text{ \AA}^2$  after about 30 - 40 min and then increased slowly back to  $40 \text{ \AA}^2$ . The increase of the WAXS peak intensities followed a double-exponential time course with a fast and a slow time constant of  $t_1 \sim 6 \text{ min}$  and  $t_2 \sim 116 \text{ min}$ , respectively .

In order to gain deeper insight into the lamellar swelling that occurs during the reaction (Fig.3 A) we studied multilamellar vesicles (MLVs) of defined POPC/SM/Cer ratios under equilibrium conditions. Fig.4 A shows the SAXS patterns of POPC/SM/Cer = 50/35/15 MLVs, fully hydrated and under osmotic stress. Osmotic pressure was applied using PEG as described in detail previously (207). Four lamellar diffraction orders were well-resolved for the fully hydrated sample. The fluid-gel phase coexistence described previously (see, e.g., (13, 208)), with two lamellar lattices of  $d = 64.2 \text{ \AA}$  and  $d = 54.0 \text{ \AA}$ , became visible upon the application of osmotic pressure ( $\Pi = 4.2 \text{ atm}$ ). The phase with the larger  $d$ -value corresponds to a  $L_{\beta}^c$  phase, rich in SM and Cer, whereas the small  $d$ -value reflects an  $L_{\alpha}^c$  phase, rich in POPC (209). A full structural characterization of the present model system, to be published separately, demonstrates that the  $L_{\beta}^c$  phase coexists with an  $L_{\alpha}^c$  phase at  $37^\circ\text{C}$  within the present Cer concentration range.

Finally, we compared the  $d$ -values of the time-resolved study to equilibrium mixtures of various Cer concentrations (Fig.4 B). In this experiment SM was gradually replaced by C16:0-Cer in order to mimic SM hydrolysis, keeping POPC/sphingolipid = 1. The  $d$ -spacings correspond to the weighted average of the lamellar repeat of fluid and the gel phases at each Cer concentration, because values for the coexisting fluid and gel lattices partially overlap at full hydration (Fig.4 A). The equilibrium  $d$ -values increased roughly linearly with Cer content, reflecting the increase of the  $L_{\beta}^c$  phase fraction. At 35 mol% C16:0 Cer, we observed an additional Bragg peak with  $d = 43.6 \text{ \AA}$ , which corresponds to a pure Cer domain (39) (Fig.4 B, insert). This shows that the solubility limit of Cer in the present system is between concentrations of 30 mol% - 35 mol%. A similar limit has been reported recently in SM/Cer monolayers (210), indicating that Cer interacts also at high concentrations primarily with SM and not POPC. For comparison with the values obtained during the enzyme reaction, the experimental time-axis was converted into a Cer concentration axis, applying the fits to the C16:0-Cer generation data from HPTLC (Fig.1). Note that the presently used SM is mainly composed of C16:0 acyl chains. Hence, C16:0-Cer generation will dominate the evolution of  $d$  during SM hydrolysis. The results showed a significant deviation of  $d$ -values during the enzyme reaction from the linear increase under equilibrium conditions up to about 20 mol% Cer, i.e. for the first  $\sim 20 \text{ min}$ . At higher Cer concentrations, the enzymatic reaction essentially follows the equilibrium  $d$ -values.

## DISCUSSION

On the basis of our results we are able link the molecular events occurring in the course of SMase action to effects on the macroscopic level. The initiation of the enzyme reaction is the attachment of the enzyme to the vesicles, where it starts to hydrolyze the SM lipids of the outer-membrane leaflet that leads to the formation of an  $L_{\beta}$  gel phase. As these domains grow in size trans-bilayer coupling might occur at some point (160) leading to the formation of a

gel phase in both monolayers, which may be further supported by Cer flip-flop (161). Asymmetric gelification of the outer membrane leaflet builds up a large mechanical strain due to differences in lateral areas per lipid in the fluid and gel phase. We found  $A = 40 \text{ \AA}^2$  for the gel phase already 70 s after the start of the enzyme reaction, which is about  $20 - 25 \text{ \AA}^2$  smaller than the area estimated for the POPC/SM mixture in the  $L_\alpha$  phase (162, 163). The spontaneous negative curvature of Cer given by its small headgroup size (71) imposes additional strain. This results in an invagination of the membrane, similar to bi-metallic strips, budding and finally shedding of vesicles in combination with transient pore formation (13, 35, 79, 164).

We found an induction of the  $L_\beta^c$  phase right at the onset of the enzyme reaction and interestingly, this domain size grows about four times faster than Cer is generated by SMase (Fig.3 C). This can be understood by the ability of SM to form hydrogen bonds with Cer, which leads to a recruitment of SM to gel phase domains, as found in equilibrium studies (152, 211). The rapid  $L_\beta^c$  phase formation stops after  $\sim 20$  min. The associated bilayer swelling, which proceeds initially at the same rate as gel-phase formation also slowed down after  $\sim 20$  min (Fig.3 A). This corresponds to a reduction of SM to 46% (Fig.1) and hence to a molar SM/Cer ratio of  $\sim 1$ . Thus, as long as Cer levels do not exceed those of SM, progression of the gel phase is faster than Cer generation. The growth of domain size stops for SM/Cer  $< 1$ . This can be rationalized by (i) the low affinity of POPC/Cer interactions (138) and (ii) by the entropic penalty of pairwise Cer interactions which lead to segregation of membrane insoluble Cer crystallites (Fig.4 B, insert). Still the amount of  $L_\beta^c$  phase, but not its packing density, continues to grow as evidenced by the continued increase of the average  $d$ -spacing (Fig.3 A) and WAXS peak intensity. This growth is slow enough to follow equilibrium  $d$ -values (Fig.4 B). However, because Cer levels are larger than those of SM (SM/Cer  $< 1$ ), POPC is increasingly incorporated into the gel domains in agreement with previous reports that show the induction of a gel phase in POPC bilayers by Cer (134, 137). This scenario is substantiated by the recovery of the lateral area per lipid after 40 min (Fig.3 C), which is related to the larger lateral size of POPC compared to SM due to its monounsaturated acyl chain.

In agreement with previous biophysical studies (79, 164) we also found an aggregation of membranes (Fig.3 B). However, growth of regularly stacked bilayers proceeded significantly slower than gel phase formation and bilayer swelling. This is expected, because the removal of interstitial water and membrane diffusion processes proceeds on a slower time scale than gel phase formation. Since the SAXS signal is dominated by the  $L_\beta^c$  phase the physical origin of vesicle aggregation during the action of SMase can be understood as follows. The gel phase macroscopically separates from the coexisting  $L_\alpha^c$  phase. Gel phase bilayers are rigid and exhibit negligible bending undulations, which are source of a long-range repulsive force in fluid (soft) membranes (see, e.g. (212)). In the absence of this force, adhesion between gel phase membranes increases. Additionally, the thicker gel membranes also experience increased van der Waals attraction. In turn, attractive interactions between macroscopically phase separated  $L_\alpha^c$  domains are much weaker. Hence, they may remain positionally uncorrelated, accounting for the absence of their signature in the SAXS data (Fig.2). Comparing the present results to previous studies on SMase activity (69, 79, 164), we generally find differences in time scales on the order of one magnitude. For example, aggregation of vesicles (79, 164) was found to proceed on the time scale of seconds, whereas we observe a growth rate of stacked bilayers of several minutes. Most likely this is related to differences in enzyme/SM ratios and/or composition of lipid



model membranes as the physical state of membranes was demonstrated to influence SM hydrolysis (45, 85).

Finally, we focus on the saturation level of Cer, which is at ~86% and indicates that SM is not fully hydrolyzed, although SMase has full access to all SM upon entry into the vesicles. One of the more obvious reasons could be that the enzyme gets entrapped during the various vesiculation processes. Another possibility is that the affinity of the SMase to the lipid surface decreases with an increase of POPC relative to SM (87). However, it is also remarkable that we did not observe any pure Cer aggregates. C16:0-Cer aggregates are readily detectable by SAXS in equilibrium systems (Fig.4 B). Hence, catalytic turnover stops just at the solubility limit of Cer in POPC/SM membranes. We therefore speculate that there is a mechanical feedback mechanism, realized for example by changes of lateral pressures at the lipid/water interface, that stops SMase activity, similar to a recent suggestion for the regulation of lipid biosynthesis in *Acholeplasma laidlawii* (213). Indeed, SMase activity has been reported to depend on the fluidity of model membranes (45, 85) and we have demonstrated previously that Cer affects the bending rigidity of both coexisting phases (214). It is interesting that in different cell biology experiments (2, 165, 166) SM hydrolysis stopped at about the same Cer concentration. This suggests that a similar feedback system may be also present in cells, which could be a natural control mechanism to reduce toxic risks of pure Cer aggregates (167).

The agreement with *in vitro* studies is even more surprising considering that our model system did not contain cholesterol, which is a major component of mammalian plasma membranes. Cholesterol has been suggested to compete with ceramide and may dissolve Cer-enriched gel domains at high concentrations, while it is displaced from raft-like domains at low concentrations (171, 177). Moreover, cholesterol was shown to increase SMase activity at high concentrations in binary mixtures with SM (175). However, it has been also shown that morphological changes induced by SMase differ significantly in lipid mixtures with an additional unsaturated lipid component (215, 216). The essential difference between POPC/SM bilayers and POPC/SM/cholesterol membranes is a macroscopic fluid-fluid phase separation occurring in the latter system prior to the addition of SMase (217). Nevertheless, if SMase activity depends strictly on the SM/Cer molar ratio, such pre-existing lateral structures might be even irrelevant to the overall enzyme kinetics. At least this would explain the agreement to cell biological data. Future studies planned in our laboratory will address this issue.

## CONCLUSION

In summary, we found that the SM/Cer molar ratio strongly affects the membrane structural rearrangements through formation of gel phase domains during the action of SMase (Fig.5). As long as each Cer has at least one SM partner,  $L_{\beta}^c$  phase formation proceeds faster than enzymatic Cer generation. Gel phase domains lead to membrane aggregation because of increased adhesive forces. If Cer levels exceed those of SM, POPC is increasingly incorporated into the gel phase until the reaction stops just below the solubility limit of Cer in membranes. Similar kinetics and SM-saturation levels in cell biology studies suggest that the evolution of apoptosis is influenced to large extend by membrane lipids and their mechanical coupling to SMase activity.

## ACKNOWLEDGEMENTS

We are grateful to Edgar Gander, Ruth Prassl and Michael Rappolt for valuable help in this study. We further thank Albin Hermetter for critical reading of the manuscript.

## FIGURE LEGENDS

Figure 1: SM hydrolysis (●) and generation of C16:0-Cer (▲) by SMase in POPC/SM bilayers as determined by HPTLC. Crosses (×) show apoptosis data on human leukaemia cells from (2). Lines show hyperbolic fits.

Figure 2: SAXS patterns of POPC/SM bilayers (i) before and (ii) 15.5 hours after enzyme addition. Control experiments in the absence of SMase did not reveal any detectable changes to membrane structure. Corresponding WAXS data are shown in the insert. The patterns are vertically shifted for better graphical presentation.

Figure 3: Evolution of lamellar repeat distance (*A*), average number of positionally correlated layers (*B*), lateral area per lipid in the gel phase (*C*) and average number of positionally correlated lipids per gel phase domain (*D*) during the enzyme reaction.

Figure 4: Comparison to equilibrium structural data. Panel *A* shows the SAXS patterns for POPC/SM/Cer = 50/35/15 (i) without and (ii) with osmotic pressure  $\Pi = 4.2$  atm. The arrow indicates the asymmetry of the second order peak due to the gel-fluid phase coexistence. Numbers (1, 2, 3, ...) refer to the lamellar diffraction orders of the gel and (1', 2', 3', ...) fluid phases. Panel *B* compares *d*-values obtained during enzyme reaction (●) to equilibrium values (□) on a common C16:0-Cer concentration scale. The insert shows the SAXS pattern at 35 mol% Cer exhibiting an additional peak (arrow) due to the presence of a pure Cer phase.

Figure 5: Schematic of SMase activity as a function of the SM/Cer molar ratio. Addition of SMase to SM/POPC vesicles induces a macroscopic phase separation into SM/Cer-rich gel and SM/POPC-rich fluid domains. As long as SM/Cer  $\geq 1$ , each Cer can pair with at least one SM and progress of gel phase formation is faster than Cer generation. For SM/Cer  $< 1$ , kinetics slow down, because POPC, which has a lower affinity to Cer, needs to be incorporated into the growing gel domains in order to avoid precipitation of Cer crystallites. The reaction stops just at the solubility limit of Cer within the membrane.

## FIGURES

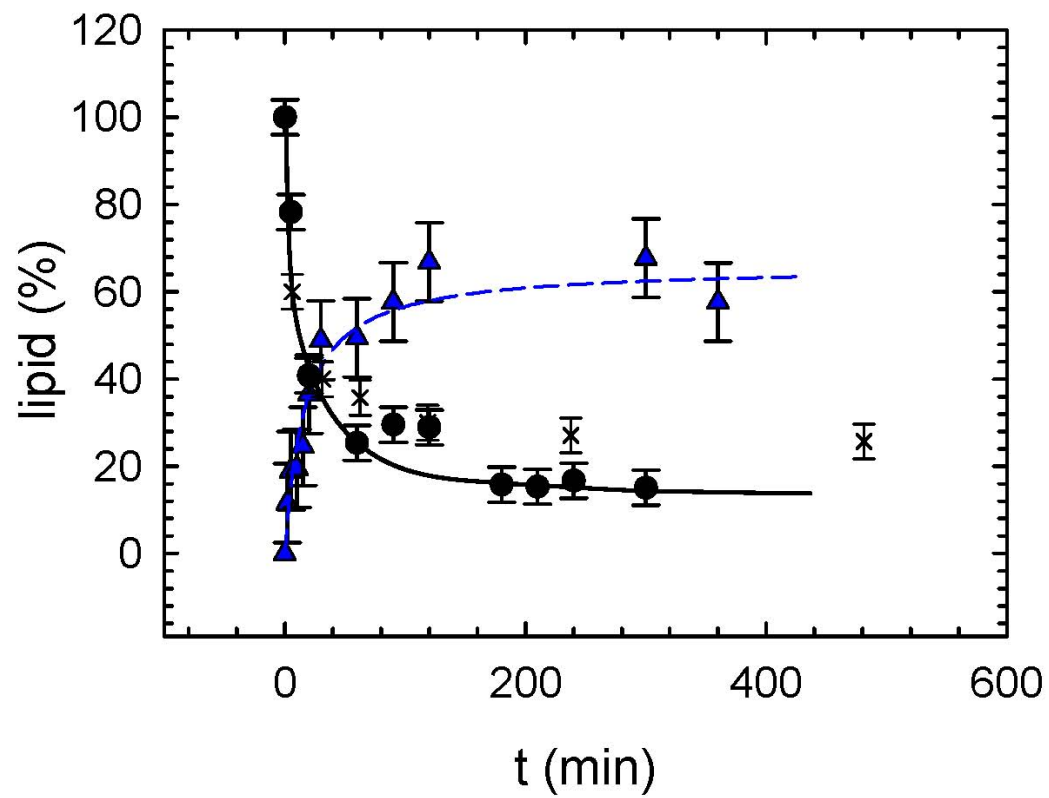


Figure 1

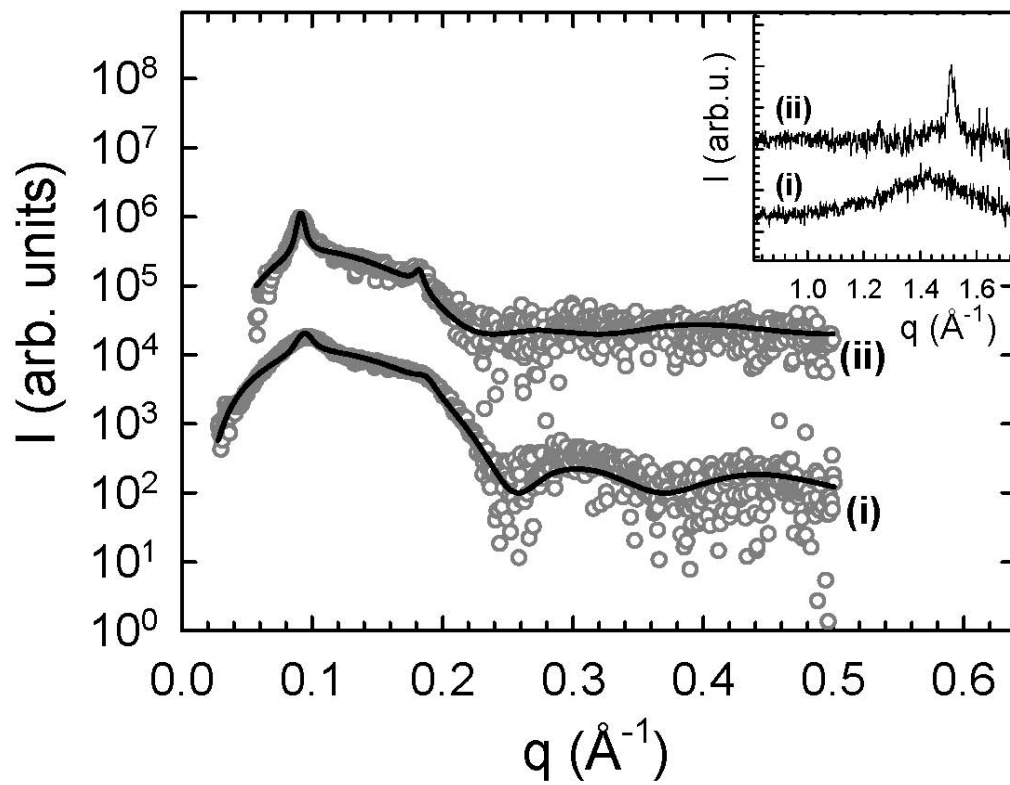


Figure 2

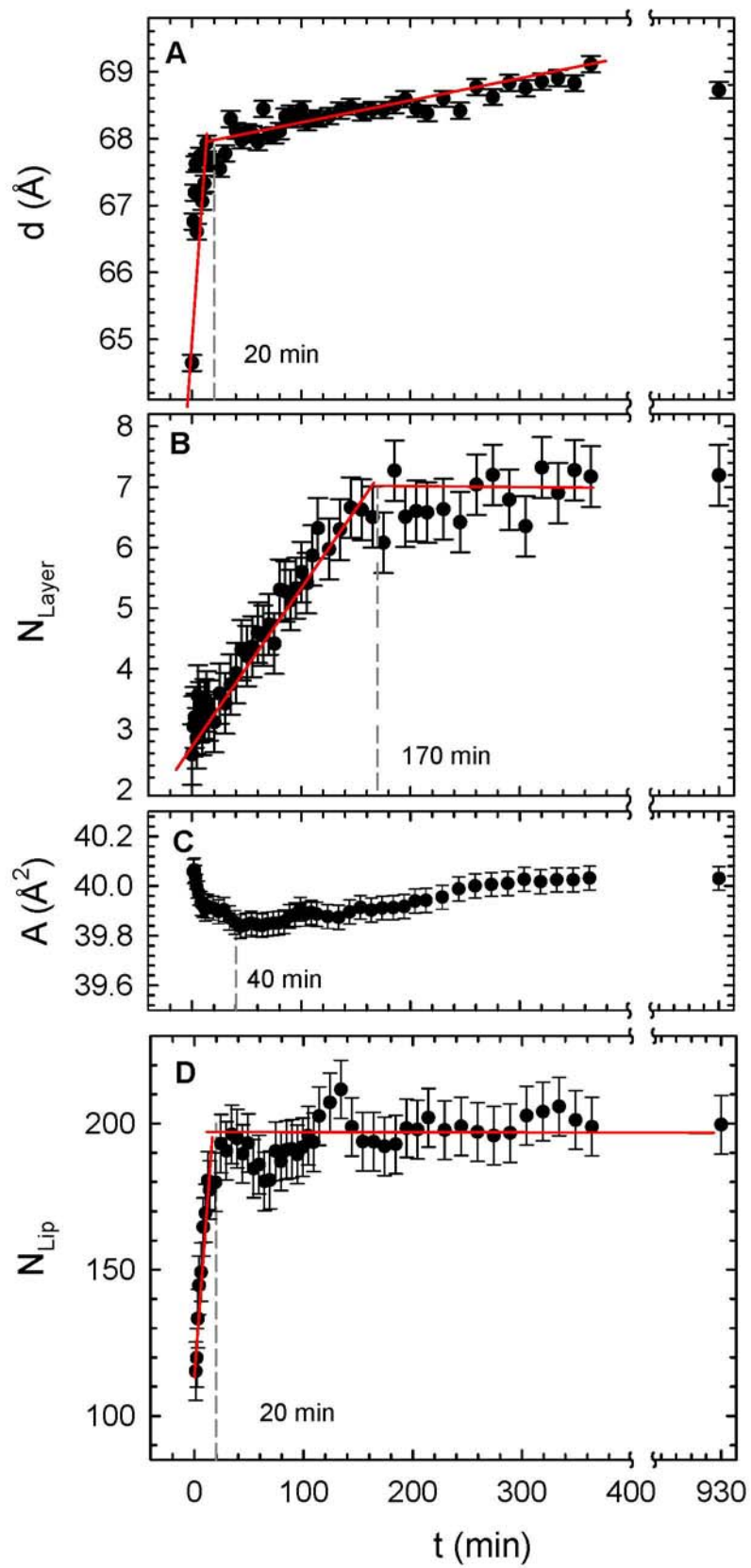


Figure 3

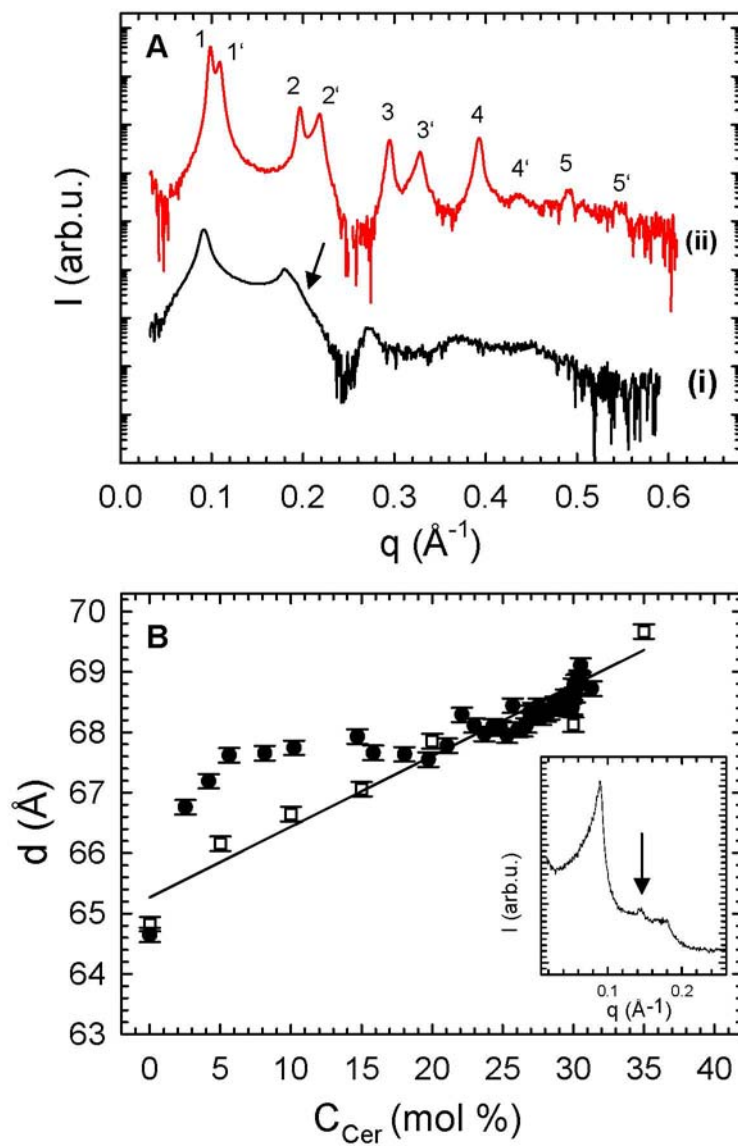


Figure 4

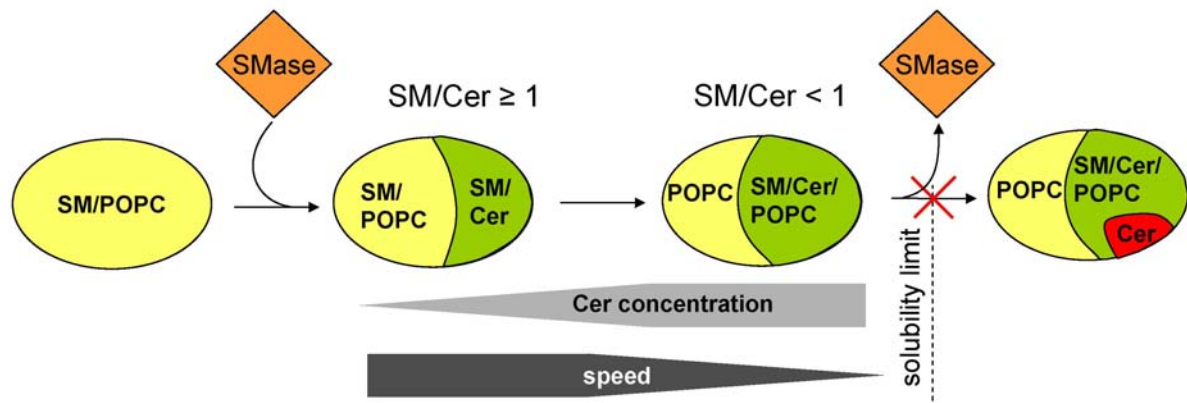


Figure 5

## Reference List

1. Kroemer, G, Zamzami, N, Susin, S A (1997) Mitochondrial control of apoptosis. *Immunol. Today* **18**: 44-51.
2. Tepper, A D, Ruurs, P, Wiedmer, T, Sims, P J, Borst, J, van Blitterswijk, W J (2000) Sphingomyelin hydrolysis to ceramide during the execution phase of apoptosis results from phospholipid scrambling and alters cell-surface morphology. *J. Cell Biol.* **150**: 155-164.
3. Elmore, S (2007) Apoptosis: a review of programmed cell death. *Toxicol. Pathol.* **35**: 495-516.
4. Andrieu-Abadie, N, Levade, T (2002) Sphingomyelin hydrolysis during apoptosis. *Biochim. Biophys. Acta* **1585**: 126-134.
5. van Blitterswijk, W J, van der Luit, A H, Veldman, R J, Verheij, M, Borst, J (2003) Ceramide: second messenger or modulator of membrane structure and dynamics? *Biochem. J.* **369**: 199-211.
6. Riboni L., T G (1997) The role of Sphingolipids in the process of signal transduction. *Prog. Lipid Res.* **35**: 153-157.
7. Yeagle, P. L. (2005) *The structure of biological membranes* (CRC Press, New York).
8. Koval M., P R (1991) Intracellular transport and metabolism of sphingomyelin. *Biochim Biophys Acta* **1082**: 113-125.
9. van Meer, G, Voelker, D R, Feigenson, G W (2008) Membrane lipids: where they are and how they behave. *Nat. Rev. Mol. Cell Biol* **9**: 112-124.
10. Ikeda, M, Kihara, A, Igarashi, Y (2006) Lipid asymmetry of the eukaryotic plasma membrane: functions and related enzymes. *Biol. Pharm. Bull.* **29**: 1542-1546.
11. Merrill, A H, Jones, D (1990) An update of the enzymology and regulation of sphingomyelin metabolism. *Biochim. Biophys. Acta* **1044**: 1-12.
12. Gulbins, E, Dreschers, S, Wilker, B, Grassme, H (2004) Ceramide, membrane rafts and infections. *J. Mol. Med.* **82**: 357-363.
13. Goni, F M, Alonso, A (2009) Effects of ceramide and other simple sphingolipids on membrane lateral structure. *Biochim. Biophys. Acta* **1788**: 169-177.
14. Ganesan, V, Perera, M N, Colombini, D, Datskovskiy, D, Chadha, K, Colombini, M (2010) Ceramide and activated Bax act synergistically to permeabilize the mitochondrial outer membrane. *Apoptosis*.
15. Colombini, M (2010) Ceramide channels and their role in mitochondria-mediated apoptosis. *Biochim Biophys Acta*.



16. Siskind, L J, Kolesnick, R N, Colombini, M (2006) Ceramide forms channels in mitochondrial outer membranes at physiologically relevant concentrations. *Mitochondrion* **6**: 118-125.
17. van Blitterswijk, W J, van der Luit, A H, Caan, W, Verheij, M, Borst, J (2001) Sphingolipids related to apoptosis from the point of view of membrane structure and topology. *Biochem. Soc. Trans.* **29**: 819-824.
18. Van Cruchten, S, Van den, B W (2002) Morphological and biochemical aspects of apoptosis, oncosis and necrosis. *Anat. Histol. Embryol.* **31**: 214-223.
19. Rudolf, E, Cervinka, M (2005) Membrane blebbing in cancer cells treated with various apoptotic inducers. *ACTA MEDICA* **48**: 29-34.
20. Coleman, M L, Sahai, E A, Yeo, M, Bosch, M, Dewar, A, Olson, M F (2001) Membrane blebbing during apoptosis results from caspase-mediated activation of ROCK I. *Nat. Cell Biol.* **3**: 339-345.
21. Shiratsuchi, A, Mori, T, Nakanishi, Y (2002) Independence of plasma membrane blebbing from other biochemical and biological characteristics of apoptotic cells. *J. Biochem.* **132**: 381-386.
22. Rudolf, E, Cervinka, M (2005) membrane blebbing in cancer cells treated with various apoptotic inducers. *ACTA MEDICA* **48**: 29-34.
23. Rudolf, E, Cervinka, M (2005) membrane blebbing in cancer cells treated with various apoptotic inducers. *ACTA MEDICA* **48**: 29-34.
24. Goldkorn, T, Balaban, N, Shannon, M, Chea, V, Matsukuma, K, Gilchrist, D, Wang, H, Chan, C (1998) H<sub>2</sub>O<sub>2</sub> acts on cellular membranes to generate ceramide signaling and initiate apoptosis in tracheobronchial epithelial cells. *J. Cell Sci.* **111**: 3209-3220.
25. Deigner, H P, Claus, R, Bonaterra, G A, Gehrke, C, Bibak, N, Blaess, M, Cantz, M, Metz, J, Kinscherf, R (2001) Ceramide induces aSMase expression: implications for oxLDL-induced apoptosis. *Faseb Journal* **15**: 807-814.
26. Goni, F M, Alonso, A (2006) Biophysics of sphingolipids I. Membrane properties of sphingosine, ceramides and other simple sphingolipids. *Biochim. Biophys. Acta* **1758**: 1902-1921.
27. Obeid, L M, Linardic, C M, Karolak, L A, Hannun, Y A (1993) Programmed cell death induced by ceramide. *Science* **259**: 1769-1771.
28. Cremesti, A, Paris, F, Grassme, H, Holler, N, Tschopp, J, Fuks, Z, Gulbins, E, Kolesnick, R (2001) Ceramide enables Fas to cap and kill. *J. Biol. Chem.* **276**: 23954-23961.
29. Hannun, Y A a L M O (1995) Ceramide: an intracellular signal for apoptosis. *Trends Biochem. Sci.* **20**: 73-77.

30. Hannun Y.A.and Lina M.Obeid (2002) The Ceramide-centric Universe of Lipid-mediated Cell Regulation: Stress Encounters of the Lipid Kind\*. *THE JOURNAL OF BIOLOGICAL CHEMISTRY* **277**: 25847-25850.
31. Hannun, Y A, Luberto, C (2000) Ceramide in the eukaryotic stress response. *Trends in Cell Biology* **10**: 73-80.
32. Hannun, Y A (1994) The Sphingomyelin Cycle and the Second Messenger Function of Ceramide . *Journal of Biological Chemistry* **269**: 3125-3128.
33. Hannun, Y A, Obeid, L M (2008) Principles of bioactive lipid signalling: lessons from sphingolipids. *Nature Rev.* **9**: 139-150.
34. Schurer, N Y, Elias, P M (1991) The biochemistry and function of stratum corneum lipids. *Adv. Lipid Res.* **24**: 27-56.
35. Kolesnick, R N, Goni, F M, Alonso, A (2000) Compartmentalization of ceramide signaling: Physical foundations and biological effects. *J. Cell. Phys.* **184**: 285-300.
36. Ballou, L R, Lauderkind, S J, Rosloniec, E F, Raghow, R (1996) Ceramide signalling and the immune response. *Biochim. Biophys. Acta* **1301**: 273-287.
37. Carrer, D C, Hartel, S, Monaco, H L, Maggio, B (2003) Ceramide modulates the lipid membrane organization at molecular and supramolecular levels. *Chem. Phys. Lipids* **122**: 147-152.
38. Sprong, H, van der Sluijs, P, van Meer, G (2001) How proteins move lipids and lipids move proteins. *Nature Rev.* **2**: 504-513.
39. Shah, J, Atienza, J M, Rawlings, A V, Shipley, G G (1995) Physical properties of ceramides: effect of fatty acid hydroxylation. *J. Lipid Res.* **36**: 1945-1955.
40. Hannun, Y A, Luberto, C (2000) Ceramide in the eukaryotic stress response. *Trends Cell Biol.* **10**: 73-80.
41. Spiegel, S, Foster, D, Kolesnick, R (1996) Signal transduction through lipid second messengers. *Curr. Opin. Cell Biol* **8**: 159-167.
42. Merrill A (2002) De Novo Sphingolipid Biosynthesis: A Necessary, but Dangerous, Pathway. *THE JOURNAL OF BIOLOGICAL CHEMISTRY* **277**: 25843-25846.
43. Weiss, B, Stoffel, W (1997) Human and murine serine-palmitoyl-CoA transferase--cloning, expression and characterization of the key enzyme in sphingolipid synthesis. *Eur J Biochem* **249**: 239-247.
44. Hannun, Y A (1994) The Sphingomyelin Cycle and the Second Messenger Function of Ceramide . *Journal of Biological Chemistry* **269**: 3125-3128.
45. Goni, F M, Alonso, A (2002) Sphingomyelinases: enzymology and membrane activity . *FEBS Lett.* **531**: 38-46.

46. Levade, T, Jaffrezou, J P (1999) Signalling sphingomyelinases: which, where, how and why? *Biochim. Biophys. Acta* **1438**: 1-17.
47. Spiegel, S, Sheldon, M (2009) Sphingosine 1-Phosphate, a Key Cell Signaling Molecule. *J. Biol. Chem.* **277**: 25851-25854.
48. Taha, T A, Mullen, T D, Obeid, L M (2006) A house divided: Ceramide, sphingosine, and sphingosine-1-phosphate in programmed cell death. *Biochim. Biophys. Acta* **1758**: 2027-2036.
49. Hannun, Y A, Obeid, L M (2002) The Ceramide-centric universe of lipid-mediated cell regulation: stress encounters of the lipid kind. *J. Biol. Chem.* **277**: 25847-25850.
50. Hannun, Y A, Obeid, L M, Wolff, R A (1993) The novel second messenger ceramide: identification, mechanism of action, and cellular activity. *Adv. Lipid Res.* **25**: 43-64.
51. Hannun, Y A (1994) The sphingomyelin cycle and the second messenger function of ceramide. *J. Biol. Chem.* **269**: 3125-3128.
52. Venkataraman, K, Futerman, A H (2000) Ceramide as a second messenger: sticky solutions to sticky problems. *Trends Cell Biol* **10**: 408-412.
53. Futerman, A H, Hannun, Y A (2004) The complex life of simple sphingolipids. *EMBO Rep.* **5**: 777-782.
54. Hannun, Y A, Obeid, L M (1995) Ceramide: an intracellular signal for apoptosis. *Trends Biochem. Sci.* **20**: 73-77.
55. Hannun, Y A, Obeid, L M (1997) Mechanisms of ceramide-mediated apoptosis. *Adv. Exp. Med. Biol* **407**: 145-149.
56. Hannun, Y A (1996) Functions of ceramide in coordinating cellular responses to stress. *Science* **274**: 1855-1859.
57. Hofmann, K, Dixit, V M (1998) Ceramide in apoptosis--does it really matter? *Trends Biochem Sci.* **23**: 374-377.
58. Zhang, Y, Yao, B, Delikat, S, Bayoumy, S, Lin, X H, Basu, S, McGinley, M, Chan-Hui, P Y, Lichenstein, H, Kolesnick, R (1997) Kinase suppressor of Ras is ceramide-activated protein kinase. *Cell* **89**: 63-72.
59. Diaz-Meco, M T, Municio, M M, Frutos, S, Sanchez, P, Lozano, J, Sanz, L, Moscat, J (1996) The product of par-4, a gene induced during apoptosis, interacts selectively with the atypical isoforms of protein kinase C. *Cell* **86**: 777-786.
60. Huwiler, A, Johansen, B, Skarstad, A, Pfeilschifter, J (2001) Ceramide binds to the CaLB domain of cytosolic phospholipase A2 and facilitates its membrane docking and arachidonic acid release. *FASEB J* **15**: 7-9.

61. van Blitterswijk, W J (1998) Hypothesis: ceramide conditionally activates atypical protein kinases C, Raf-1 and KSR through binding to their cysteine-rich domains. *Biochem J* **331**: 679-680.
62. Heinrich, M, Wickel, M, Winoto-Morbach, S, Schneider-Brachert, W, Weber, T, Brunner, J, Saftig, P, Peters, C, Kronke, M, Schutze, S (2000) Ceramide as an activator lipid of cathepsin D. *Adv. Exp. Med. Biol* **477**: 305-315.
63. Cremesti, A E, Goni, F M, Kolesnick, R (2002) Role of sphingomyelinase and ceramide in modulating rafts: do biophysical properties determine biologic outcome? *FEBS Lett.* **531**: 47-53.
64. Goni, F M, Alonso, A (2009) Effects of ceramide and other simple sphingolipids on membrane lateral structure. *Biochim Biophys Acta* **1788**: 169-177.
65. Huang, H W, Goldberg, E M, Zidovetzki, R (1998) Ceramides perturb the structure of phosphatidylcholine bilayers and modulate the activity of phospholipase A2. *Eur. Biophys. J.* **27**: 361-366.
66. Carrer, D C, Maggio, B (1999) Phase behavior and molecular interactions in mixtures of ceramide with dipalmitoylphosphatidylcholine. *J. Lipid Res.* **40**: 1978-1989.
67. Moore, D (1997) FTIR spectroscopy studies of the conformational order and phase behavior of ceramides. *J. Phys. Chem. B.* **101**: 8933-8940.
68. Huang, H W, Goldberg, E M, Zidovetzki, R (1996) Ceramide induces structural defects into phosphatidylcholine bilayers and activates phospholipase A2. *Biochem. Biophys. Res. Commun.* **220**: 834-838.
69. Holopainen, J M, Subramanian, M, Kinnunen, P K (1998) Sphingomyelinase induces lipid microdomain formation in a fluid phosphatidylcholine/sphingomyelin membrane. *Biochemistry* **37**: 17562-17570.
70. Holopainen, J M, Lemmich, J, Richter, F, Mouritsen, O G, Rapp, G, Kinnunen, P K (2000) Dimyristoylphosphatidylcholine/C16:0-ceramide binary liposomes studied by differential scanning calorimetry and wide- and small-angle x-ray scattering. *Biophys. J.* **78**: 2459-2469.
71. Veiga, M P, Arrondo, J L, Goni, F M, Alonso, A (1999) Ceramides in phospholipid membranes: effects on bilayer stability and transition to nonlamellar phases<sup>7</sup>. *Biophys. J.* **76**: 342-350.
72. Holopainen, J M, Lehtonen, J Y, Kinnunen, P K (1997) Lipid microdomains in dimyristoylphosphatidylcholine-ceramide liposomes. *Chem. Phys. Lipids* **88**: 1-13.
73. Hsueh, Y W, Giles, R, Kitson, N, Thewalt, J (2002) The effect of ceramide on phosphatidylcholine membranes: A deuterium NMR study. *Biophys. J.* **82**: 3089-3095.
74. Massey, J B (2001) Interaction of ceramides with phosphatidylcholine, sphingomyelin and sphingomyelin/cholesterol bilayers. *Biochim. Biophys. Acta* **1510**: 167-184.

75. Ruiz-Arguello, M B, Goni, F M, Alonso, A (1998) Vesicle membrane fusion induced by the concerted activities of sphingomyelinase and phospholipase C. *J. Biol. Chem.* **273**: 22977-22982.
76. Sot, J, Arada, F J, Collado, M I, Goni, F M, Alonso, A (2005) Different effects of long- and short-chain ceramides on the gel-fluid and lamellar-hexagonal transitions of phospholipids: a calorimetric, NMR, and x-ray diffraction study. *Biophys. J.* **88**: 3368-3380.
77. Siegel, D P (1999) The modified stalk mechanism of lamellar/inverted phase transitions and its implications for membrane fusion. *Biophys. J.* **76**: 291-313.
78. Siegel, D P, Burns, J L, Chestnut, M H, Talmon, Y (1989) Intermediates in membrane fusion and bilayer/nonbilayer phase transitions imaged by time-resolved cryo-transmission electron microscopy. *Biophys. J.* **56**: 161-169.
79. Ruiz-Arguello, M B, Basanez, G, Goni, F M, Alonso, A (1996) Different effects of enzyme-generated ceramides and diacylglycerols in phospholipid membrane fusion and leakage. *J. Biol. Chem.* **271**: 26616-26621.
80. Montes, L R, Ruiz-Arguello, M B, Goni, F M, Alonso, A (2002) Membrane restructuring via ceramide results in enhanced solute efflux. *J. Biol. Chem.* **277**: 11788-11794.
81. Kiessling, V, Crane, J M, Tamm, L (2006) Transbilayer Effects of Raft-Like Lipid Domains in Asymmetric Planar Bilayers Measured by Single Molecule Tracking. *Biophys. J.* **91**: 3313-3326.
82. Contreras, F X, Villar, A V, Alonso, A, Kolesnick, R N, Goni, F M (2003) Sphingomyelinase activity causes transbilayer lipid translocation in model and cell membranes. *J. Biol. Chem.* **278**: 37169-37174.
83. Goni, F M, Alonso, A (2000) Membrane fusion induced by phospholipase C and sphingomyelinases. *Biosci. Rep.* **20**: 443-463.
84. Honger, T, Jorgensen, K, Biltonen, R L, Mouritsen, O G (1996) Systematic relationship between phospholipase A2 activity and dynamic lipid bilayer microheterogeneity. *Biochemistry* **35**: 9003-9006.
85. Ruiz-Arguello, M B, Veiga, M P, Arrondo, J L R, Goni, F M, Alonso, A (2002) Sphingomyelinase cleavage of sphingomyelin in pure and mixed lipid membranes. Influence of the physical state of the sphingolipid. *Chem. Phys. Lipids* **114**: 11-20.
86. Pabst, G, Boulgaropoulos, B, Gander, E, Sarangi, B R, Amenitsch, H, Raghunathan, V A, Laggner, P (2009) Effect of Ceramide on Nonraft Proteins. *J. Membr. Biol.* **231**: 125-132.
87. Yu, B Z, Zakim, D, Jain, M K (2002) Processive interfacial catalytic turnover by *Bacillus cereus* sphingomyelinase on sphingomyelin vesicles. *Biochim. Biophys. Acta* **1583**: 122-132.

88. Berg, O G, Yu, B Z, Rogers, J, Jain, M K (1991) Interfacial Catalysis by Phospholipase A2: Determination of the Interfacial KineticRate Constants. *Biochemistry* **30**: 7283-7297.
89. Berg, O. G. & Jain, M. K. (2002) *Interfacial Enzyme Kinetics* (Wiley, London).
90. Escribá, P V, González-Rosb, J M, Goñi, F, Kinnunen, P (2008) Membranes: a meeting point for lipids, proteins and therapies. *J. Cell. Mol. Med.* **12**: 829-875.
91. S.J.Singer, G L N (1972) *Science* **175**: 720.
92. Escribá P.V., G-R J M G F K P (2008) Membranes: a meeting point for lipids, proteins and therapies. *J. Cell. Mol. Med.* **12**: 829-875.
93. Verkleij AJ, Z R R B C P K D v D LL (1973) The asymmetric distribution of phospholipids in the human red cell membrane. *Biochim BiophysActa.* 178-193.
94. Simons K, I E (1997) K. Simons und E. Ikonen. *Nature* **387**.
95. Israelachvili, J. N. (1985) *Intermolecular and Surface Force*, (Academic Press, London).
96. Luzzati V (1968) in Biological Membranes, ed. Chapmann, D. (Academic Press, London, New York,), pp. 71-123.
97. Parsegian, V A, Rand, R P (1995) in Structure and Dynamics of Membranes, eds. Lipowsky, R., Sackmann, E. pp. 643-690.
98. Helfrich, W (1973) Elastic properties of lipid bilayers: theory and possible experiments. *Z. Naturforsch. C* **28**: 693-703.
99. Chatterjee, S (1999) Neutral sphingomyelinase: past, present and future. *Chem. Phys. Lipids* **102**: 79-96.
100. Samet, D, Barenholz, Y (1999) Characterization of acidic and neutral sphingomyelinase activities in crude extracts of HL-60 cells. *Chem. Phys. Lipids* **102**: 65-77.
101. Goni, F M, Alonso, A (2002) Sphingomyelinases: enzymology and membrane activity. *FEBS Lett.* **531**: 38-46.
102. Schneider, P B, Kennedy, E P (1967) Sphingomyelinase in normal human spleens and in spleens from subjects with Niemann-Pick disease. *J Lipid Res.* **8**: 202-209.
103. Schissel, S L, Jiang, X, Tweedie-Hardman, J, Jeong, T, Camejo, E H, Najib, J, Rapp, J H, Williams, K J, Tabas, I (1998) Secretory sphingomyelinase, a product of the acid sphingomyelinase gene, can hydrolyze atherogenic lipoproteins at neutral pH. Implications for atherosclerotic lesion development. *J Biol Chem.* **273**: 2738-2746.
104. Goni, F M, Alonso, A (2002) Sphingomyelinases: enzymology and membrane activity. *FEBS Lett.* **531**: 38-46.

105. Okazaki, T, Bielawska, A, Domae, N, Bell, R M, Hannun, Y A (1994) Characteristics and partial purification of a novel cytosolic, magnesium-independent, neutral sphingomyelinase activated in the early signal transduction of 1 alpha,25-dihydroxyvitamin D3-induced HL-60 cell differentiation. *J Biol Chem.* **269**: 4070-4077.
106. Jung, S Y, Suh, J H, Park, H J, Jung, K M, Kim, M Y, Na, D S, Kim, D K (2000) Identification of multiple forms of membrane-associated neutral sphingomyelinase in bovine brain. *J Neurochem.* **75**: 1004-1014.
107. Duan, R D, Cheng, Y, Hansen, G, Hertervig, E, Liu, J J, Syk, I, Sjostrom, H, Nilsson, A (2003) Purification, localization, and expression of human intestinal alkaline sphingomyelinase. *J Lipid Res* **44**: 1241-1250.
108. Yamada, A, Tsukagoshi, N, Udaka, S, Sasaki, T, Makino, S, Nakamura, S, Little, C, Tomita, M, Ikezawa, H (1988) Nucleotide sequence and expression in *Escherichia coli* of the gene coding for sphingomyelinase of *Bacillus cereus*. *Eur. J. Biochem.* **175**: 213-220.
109. Clarke, C J, Snook, C F, Tani, M, Matmati, N, Marchesini, N, Hannun, Y A (2006) The extended family of neutral sphingomyelinases. *Biochemistry* **45**: 11247-11256.
110. Coleman, D C, Arbuthnott, J P, Pomeroy, H M, Birkbeck, T H (1986) Cloning and expression in *Escherichia coli* and *Staphylococcus aureus* of the beta-lysin determinant from *Staphylococcus aureus*: evidence that bacteriophage conversion of beta-lysin activity is caused by insertional inactivation of the beta-lysin determinant. *Microb. Pathog.* **1**: 549-564.
111. Ago, H, Oda, M, Takahashi, M, Tsuge, H, Ochi, S, Katunuma, N, Miyano, M, Sakurai, J (2006) Structural basis of the sphingomyelin phosphodiesterase activity in neutral sphingomyelinase from *Bacillus cereus*. *J. Biol. Chem.* **281**: 16157-16167.
112. Tomita, M, Ueda, Y, Tamura, H, Taguchi, R, Ikezawa, H (1993) The role of acidic amino-acid residues in catalytic and adsorptive sites of *Bacillus cereus* sphingomyelinase. *Biochim. Biophys. Acta* **1203**: 85-92.
113. Ikezawa, H, Mori, M, Ohyabu, T, Taguchi, R (1978) Studies on sphingomyelinase of *Bacillus cereus*. I. Purification and properties. *Biochim. Biophys. Acta* **528**: 247-256.
114. Milhas, D, Clarke, C J, Hannun, Y A (2009) Sphingomyelin metabolism at the plasma membrane: Implications for bioactive sphingolipids. *FEBS Lett.*
115. Montes, L R, Goñi, F M, Johnston, N C, Goldfine, H, Alonso, A (2004) Membrane Fusion Induced by the Catalytic Activity of a Phospholipase C/Sphingomyelinase from *Listeria monocytogenes*. *Biochemistry* **43**: 3688-3695.
116. Pellkofer, R, Sandhoff, K (1980) Halothane increases membrane fluidity and stimulates sphingomyelin degradation by membrane-bound neutral sphingomyelinase of synaptosomal plasma membranes from calf brain already at clinical concentrations. *J. Neurochem.* **34**: 988-992.

117. Jungner, M, Ohvo, H, Slotte, J P (1997) Interfacial regulation of bacterial sphingomyelinase activity. *Biochim. Biophys. Acta* **1344**: 230-240.
118. McElhaney, R N (1982) The use of differential scanning calorimetry and differential thermal analysis in studies of model and biological membranes. *Chem. Phys. Lipids* **30**: 229-259.
119. Ohura, K, Kashino, S, Haisa, M (1972) The crystal and molecular structure of p-bromobenzoic acid. *Bull. Chem. Soc. Japan* **45**: 2651-2652.
120. Pabst, G (2006) Global properties of biomimetic membranes. *Biophys. Rev. Lett.* **1**: 57-84.
121. Warren, B E (1941) X-ray diffraction methods. *J. Appl. Phys.* **12**: 375-383.
122. Bernstorff, S, Amenitsch, H, Laggner, P (1998) High-throughput asymmetric double-crystal monochromator of the SAXS beamline at ELETTRA. *J Synchrotron. Radiat.* **5**: 1215-1221.
123. Amenitsch, H, Rappolt, M, Kriechbaum, M, Mio, H, Laggner, P, Bernstorff, S (1998) First performance assessment of the small-angle X-ray scattering beamline at ELETTRA. *J Synchrotron. Radiat.* **5**: 506-508.
124. Hammersley, A P, Brown, K, Burmeister, W, Claustre, L, Gonzalez, A, McSweeney, S, Mitchell, E, Moy, J P, Svensson, S O, Thompson, A W (1997) Calibration and application of an X-ray image intensifier/ charge-coupled device detector for monochromatic macromolecular crystallography. *J Synchrotron. Radiat.* **4**: 67-77.
125. McIntosh, T J, Magid, A D, Simon, S A (1987) Steric repulsion between phosphatidylcholine bilayers. *Biochemistry* **26**: 7325-7332.
126. Pabst, G, Danner, S, Karmakar, S, Deutsch, G, Raghunathan, V A (2007) On the propensity of phosphatidylglycerols to form interdigitated phases. *Biophys J* **93**: 513-525.
127. McIntosh, T J, Simon, S A (1986) Area per molecule and distribution of water in fully hydrated dilauroylphosphatidylethanolamine bilayers. *Biochemistry* **25**: 4948-4952.
128. Parsegian, V A, Rand, R P (1995) in Handbook of biological physics., eds. Lipowsky, R., Sackmann, E. e. (Elsevier, Amsterdam), pp. 643-690.
129. Petrache, H I, Gouliaev, N, Tristram-Nagle, S, Zhang, R T, Suter, R M, Nagle, J F (1998) Interbilayer interactions from high-resolution X-ray scattering. *Phys. Rev. E* **57**: 7014-7024.
130. Pabst, G, Danner, S, Podgornik, R, Katsaras, J (2007) Entropy-driven softening of fluid lipid bilayers by alamethicin. *Langmuir* **23**: 11705-11711.
131. Pan, J, Tieleman, D P, Nagle, J F, Kucerka, N, Tristram-Nagle, S (2009) Alamethicin in lipid bilayers: combined use of X-ray scattering and MD simulations. *Biochim Biophys Acta* **1788**: 1387-1397.



132. Cantor, R S (1999) The influence of membrane lateral pressures on simple geometric models of protein conformational equilibria. *Chem. Phys. Lipids* **101**: 45-56.
133. Cantor, R S (1997) Lateral Pressures in Cell Membranes: A Mechanism for Modulation of Protein Function. *J. Phys. Chem.* **101**: 1723-1725.
134. Fidorra, M, Duelund, L, Leidy, C, Simonsen, A C, Bagatolli, L A (2006) Absence of fluid-ordered/fluid-disordered phase coexistence in ceramide/POPC mixtures containing cholesterol. *Biophys. J.* **90**: 4437-4451.
135. Sot, J, Bagatolli, L A, Goni, F M, Alonso, A (2006) Detergent-resistant, ceramide-enriched domains in sphingomyelin/ceramide bilayers. *Biophys. J.* **90**: 903-914.
136. Degovics, D, Latal, A, Prenner, E, Kriechbaum, M, Lohner, K (1997) Structure and Thermotropic Behaviour of Mixed Choline Phospholipid Model Membranes. *J. Appl. Cryst.* **30**: 776-780.
137. Silva, L, De Almeida, R F M, Fedorov, A, Matos, A P A, Prieto, M (2006) Ceramide-platform formation and -induced biophysical changes in a fluid phospholipid membrane. *Molecular Membrane Biology* **23**: 137-1U2.
138. Silva, L C, de Almeida, R F, Castro, B M, Fedorov, A, Prieto, M (2007) Ceramide-domain formation and collapse in lipid rafts: membrane reorganization by an apoptotic lipid. *Biophys. J.* **92**: 502-516.
139. Kucerka, N, Tristram-Nagle, S, Nagle, J F (2005) Structure of fully hydrated fluid phase lipid bilayers with monounsaturated chains. *J Membr. Biol* **208**: 193-202.
140. Podgornik, R, French, R H, Parsegian, V A (2006) Nonadditivity in van der Waals interactions within multilayers. *J Chem. Phys.* **124**: 044709.
141. Kucerka, N, Tristram-Nagle, S, Nagle, J F (2005) Structure of fully hydrated fluid phase lipid bilayers with monounsaturated chains6. *J Membr. Biol* **208**: 193-202.
142. Cantor, R S (1999) Lipid composition and the lateral pressure profile in bilayers. *Biophys. J.* **76**: 2625-2639.
143. Ben Shaul, A (1995) in Handbook of biological physics, eds. Lipowsky, R., Sackmann, E. (Elsevier, Amsterdam), pp. 359-401.
144. Pabst, G, Rappolt, M, Amenitsch, H, Laggner, P (2000) Structural information from multilamellar liposomes at full hydration: full q-rangefitting with high quality x-ray data. *Phys. Rev. E.* **62**: 4000-4009.
145. Pabst, G, Katsaras, J, Raghunathan, V A, Rappolt, M (2003) Structure and Interactions in the Anomalous SwellingRegime of Phospholipid Bilayers. *Langmuir* **19**: 1716-1722.
146. Baumgart, T, Hess, S T, Webb, W W (2003) Imaging coexisting fluid domains in biomembrane models coupling curvature and line tension. *Nature* **425**: 821-824.

147. Ipsen, J H, Karlstrom, G, Mouritsen, O G, Wennerstrom, H, Zuckermann, M J (1987) Phase equilibria in the phosphatidylcholine-cholesterol system. *Biochim Biophys Acta* **905**: 162-172.
148. Ayuyan, A G, Cohen, F S (2006) Lipid peroxides promote large rafts: effects of excitation of probes in fluorescence microscopy and electrochemical reactions during vesicle formation. *Biophys. J.* **91**: 2172-2183.
149. Zhao, J, Wu, J, Shao, H L, Kong, F, Jain, N, Hunt, G, Feigenson, G (2007) Phase studies of model biomembranes: Macroscopic coexistence of L alpha plus L beta, with light-induced coexistence of L alpha plus L<sub>o</sub> Phases. *Biochim. Biophys. Acta* **1768**: 2777-2786.
150. Veatch, S L, Leung, S S, Hancock, R E, Thewalt, J L (2007) Fluorescent probes alter miscibility phase boundaries in ternary vesicles. *J. Phys. Chem. B* **111**: 502-504.
151. Untracht, S H, Shipley, G (1977) Molecular interactions between lecithin and sphingomyelin. *J. Biol. Chem.* **252**: 4449-4457.
152. Castro, B M, de Almeida, R F, Silva, L C, Fedorov, A, Prieto, M (2007) Formation of ceramide/sphingomyelin gel domains in the presence of an unsaturated phospholipid: a quantitative multiprobe approach. *Biophys. J.* **93**: 1639-1650.
153. de Almeida, R F, Fedorov, A, Prieto, M (2003) Sphingomyelin/phosphatidylcholine/cholesterol phase diagram: boundaries and composition of lipid rafts. *Biophys. J.* **85**: 2406-2416.
154. Bunge, A, Muller, P, Stockl, M, Herrmann, A, Huster, D (2008) Characterization of the ternary mixture of sphingomyelin, POPC, and cholesterol: support for an inhomogeneous lipid distribution at high temperatures. *Biophys J* **94**: 2680-2690.
155. de Almeida, R F, Loura, L M, Fedorov, A, Prieto, M (2005) Lipid rafts have different sizes depending on membrane composition: a time-resolved fluorescence resonance energy transfer study. *J Mol. Biol* **346**: 1109-1120.
156. Niemela, P S, Hyvonen, M T, Vattulainen, I (2006) Influence of chain length and unsaturation on sphingomyelin bilayers. *Biophys. J.* **90**: 851-863.
157. Staneva, G, Chachaty, C, Wolf, C, Koumanov K., Quinn, P J (2008) The role of sphingomyelin in regulating phase coexistence in complex lipid modelmembranes: Competition between ceramide and cholesterol. *Biochim. Biophys. Acta* **1778** : 2727-2739.
158. Veiga, M P, Arrondo, J L, Goni, F M, Alonso, A (1999) Ceramides in phospholipid membranes: effects on bilayer stability and transition to nonlamellar phases. *Biophys J* **76**: 342-350.
159. Busto, J V, Fanani, M L, De Tullio, L, Sot, J, Maggio, B, Goni, F M, Alonso, A (2009) Coexistence of immiscible mixtures of palmitoylsphingomyelin and palmitoylceramide in monolayers and bilayers. *Biophys J* **97**: 2717-2726.

160. May, S (2009) Trans-monolayer coupling of fluid domains in lipid bilayers. *Soft Matter* **5**: 3148-3156.
161. Contreras, F X, Basanez, G, Alonso, A, Herrmann, A, Goni, F M (2005) Asymmetric addition of ceramides but not dihydroceramides promotes transbilayer (flip-flop) lipid motion in membranes. *Biophys. J.* **88**: 348-359.
162. Chiu, S W, Vasudevan, S, Jakobsson, E, Mashl, R J, Scott, H L (2003) Structure of sphingomyelin bilayers: a simulation study. *Biophys. J.* **85**: 3624-3635.
163. Pabst, G, Hodzic, A, Strancar, J, Danner, S, Rappolt, M, Laggner, P (2007) Rigidification of neutral lipid bilayers in the presence of salts. *Biophys. J.* **93**: 2688-2696.
164. Holopainen, J M, Angelova, M I, Kinnunen, P K (2000) Vectorial budding of vesicles by asymmetrical enzymatic formation of ceramide in giant liposomes. *Biophys. J.* **78**: 830-838.
165. Andrieu, N, Salvayre, R, Levade, T (1996) Comparative study of the metabolic pools of sphingomyelin and phosphatidylcholine sensitive to tumor necrosis factor. *Eur. J. Biochem.* **236**: 738-745.
166. Ohvo, H, Olsio, C, Slotte, J P (1997) Effects of sphingomyelin and phosphatidylcholine degradation on cyclodextrin-mediated cholesterol efflux in cultured fibroblasts. *Biochim. Biophys. Acta* **1349**: 131-141.
167. Shabbits, J A, Mayer, L D (2003) Intracellular delivery of ceramide lipids via liposomes enhances apoptosis in vitro. *Biochim Biophys Acta* **1612**: 98-106.
168. Cantor, R S (1999) Lipid composition and the lateral pressure profile in bilayers. *Biophys. J.* **76**: 2625-2639.
169. Rankin, S E, Addona, G H, Kloczewiak, M A, Bugge, B, Miller, K W (1997) The cholesterol dependence of activation and fast desensitization of the nicotinic acetylcholine receptor. *Biophys. J.* **73**: 2446-2455.
170. van Meer, G, Voelker, D R, Feigenson, G W (2008) Membrane lipids: where they are and how they behave. *Nat. Rev. Mol. Cell Biol.* **9**: 112-124.
171. Castro, B M, Silva, L C, Fedorov, A, de Almeida, R F, Prieto, M (2009) Cholesterol-rich fluid membranes solubilize ceramide domains: implications for the structure and dynamics of mammalian intracellular and plasma membranes. *J Biol Chem.* **284**: 22978-22987.
172. Megha, London, E (2004) Ceramide selectively displaces cholesterol from ordered lipid domains (rafts): implications for lipid raft structure and function. *J Biol Chem.* **279**: 9997-10004.
173. Veiga, M P, Arrondo, J L, Goni, F M, Alonso, A, Marsh, D (2001) Interaction of cholesterol with sphingomyelin in mixed membranes containing phosphatidylcholine,

- studied by spin-label ESR and IR spectroscopies. A possible stabilization of gel-phase sphingolipid domains by cholesterol. *Biochemistry* **40**: 2614-2622.
174. de Almeida, R F, Loura, L M, Fedorov, A, Prieto, M (2005) Lipid rafts have different sizes depending on membrane composition: a time-resolved fluorescence resonance energy transfer study. *J Mol. Biol* **346**: 1109-1120.
  175. Contreras, F X, Sot, J, Ruiz-Arguello, M B, Alonso, A, Goni, F M (2004) Cholesterol modulation of sphingomyelinase activity at physiological temperatures. *Chem. Phys. Lipids* **130**: 127-134.
  176. Arsov, Z, Quaroni, L (2008) Detection of lipid phase coexistence and lipid interactions in sphingomyelin/cholesterol membranes by ATR-FTIR spectroscopy. *Biochim. Biophys. Acta* **1778**: 880-889.
  177. Sot, J, Ibarguren, M, Busto, J V, Montes, L R, Goni, F M, Alonso, A (2008) Cholesterol displacement by ceramide in sphingomyelin-containing liquid-ordered domains, and generation of gel regions in giant lipidic vesicles. *FEBS Lett.* **582**: 3230-3236.
  178. Castro, B M, Silva, L C, Fedorov, A, de Almeida, R F, Prieto, M (2009) Cholesterol-Rich Fluid Membranes Solubilize Ceramide Domains. Implications for the Structure and Dynamics of Mammalian Intracellular and Plasma Membrane. *J. Biol. Chem.*
  179. Riboni L., T G (1997) The role of Sphingolipids in the process of signal transduction. *Prog. Lipid Res.* **35**: 153-157.
  180. Koval M., P R (1991) Intracellular transport and metabolism of sphingomyelin. *Biochim Biophys Acta* **1082**: 113-125.
  181. Spiegel, S, Merrill, A H, Jr. (1996) Sphingolipid metabolism and cell growth regulation. *FASEB J.* **10**: 1388-1397.
  182. Arsov, Z, Quaroni, L (2008) Detection of lipid phase coexistence and lipid interactions in sphingomyelin/cholesterol membranes by ATR-FTIR spectroscopy. *Biochim Biophys Acta* **1778**: 880-889.
  183. Leung, S, Sot, J, Alonso, A, Goni, F M, Thewalt, J (2008) Effects of Ceramide on Sphingomyelin Membranes: Increased Thermal Stability and Chain Order. *Biophys. J.* **94**: 340.
  184. Busto, J V, Fanani, M L, De Tullio, L, Sot, J, Maggio, B, Goni, F M, Alonso, A (2009) Coexistence of immiscible mixtures of palmitoylsphingomyelin and palmitoylceramide in monolayers and bilayers. *Biophys J* **97**: 2717-2726.
  185. Sun, W, Suter, R M, Knewton, M A, Worthington, C R, Tristram-Nagle, S, Zhang, R, Nagle, J F (1994) Order and disorder in fully hydrated unoriented bilayers of gel-phase dipalmitoylphosphatidylcholine. *Phys. Rev. E Stat. Phys. Plasmas. Fluids Relat Interdiscip. Topics* **49**: 4665-4676.

186. Ayuyan, A G, Cohen, F S (2006) Lipid peroxides promote large rafts: effects of excitation of probes in fluorescence microscopy and electrochemical reactions during vesicle formation. *Biophys. J.* **91**: 2172-2183.
187. Zhao, J, Wu, J, Shao, H L, Kong, F, Jain, N, Hunt, G, Feigenson, G (2007) Phase studies of model biomembranes: Macroscopic coexistence of L alpha plus L beta, with light-induced coexistence of L alpha plus L<sub>o</sub> Phases. *Biochim. Biophys. Acta* **1768**: 2777-2786.
188. Veatch, S L, Leung, S S, Hancock, R E, Thewalt, J L (2007) Fluorescent probes alter miscibility phase boundaries in ternary vesicles. *J. Phys. Chem. B* **111**: 502-504.
189. de Almeida, R F, Loura, L M, Fedorov, A, Prieto, M (2005) Lipid rafts have different sizes depending on membrane composition: a time-resolved fluorescence resonance energy transfer study. *J Mol. Biol* **346**: 1109-1120.
190. Páli, T, Bartucci, R, Horváth, L, Marsh, D (1993) Kinetics and dynamics of annealing during sub-gel phase formation in phospholipid bilayers A saturation transfer electron spin resonance study. *Biophys. J.* **64**: 1781-1788.
191. Tristram-Nagle, S, Suter, R M, Sun, W J, Nagle, J F (1994) Kinetics of subgel formation in DPPC: X-ray diffraction proves nucleation-growth hypothesis. *Biochim Biophys Acta* **1191**: 14-20.
192. Katsaras, J, Raghunathan, V A (2000) in *Lipid Bilayers Structure and Interactions* Berlin), pp. 26-30.
193. Busto, J V, Fanani, M L, De Tullio, L, Sot, J, Maggio, B, Goni, F M, Alonso, A (2009) Coexistence of immiscible mixtures of palmitoylsphingomyelin and palmitoylceramide in monolayers and bilayers. *Biophys J* **97**: 2717-2726.
194. Fruhwirth, G O, Hermetter, A (2008) Mediation of apoptosis by oxidized phospholipids. *Subcell. Biochem* **49**: 351-367.
195. Pike, L J (2006) Rafts defined: a report on the Keystone Symposium on Lipid Rafts and Cell Function. *J Lipid Res* **47**: 1597-1598.
196. Lingwood, D, Simons, K (2010) Lipid rafts as a membrane-organizing principle. *Science* **327**: 46-50.
197. Pabst, G, Boulgaropoulos, B, Gander, E, Sarangi, B R, Amenitsch, H, Raghunathan, V A, Laggner, P (2009) Effect of ceramide on nonraft proteins. *J. Membr. Biol.* **231**: 125-132.
198. Chao, L, Gast, A P, Hatton, T A, Jensen, K F (2010) Sphingomyelinase-induced phase transformations: causing morphology switches and multiple-time-domain ceramide generation in model raft membranes. *Langmuir* **26**: 344-356.
199. Ayuyan, A G, Cohen, F S (2006) Lipid peroxides promote large rafts: effects of excitation of probes in fluorescence microscopy and electrochemical reactions during vesicle formation. *Biophys. J.* **91**: 2172-2183.

200. Zhao, J, Wu, J, Shao, H L, Kong, F, Jain, N, Hunt, G, Feigenson, G (2007) Phase studies of model biomembranes: Macroscopic coexistence of L alpha plus L beta, with light-induced coexistence of L alpha plus Lo Phases. *Biochim. Biophys. Acta* **1768**: 2777-2786.
201. Veatch, S L, Leung, S S, Hancock, R E, Thewalt, J L (2007) Fluorescent probes alter miscibility phase boundaries in ternary vesicles. *J. Phys. Chem. B* **111**: 502-504.
202. Pabst, G, Boulgaropoulos, B, Gander, E, Sarangi, B R, Amenitsch, H, Raghunathan, V A, Laggner, P (2009) Effect of ceramide on nonraft proteins. *J. Membr. Biol.* **231**: 125-132.
203. Pabst, G, Boulgaropoulos, B, Gander, E, Sarangi, B R, Amenitsch, H, Raghunathan, V A, Laggner, P (2009) Effect of ceramide on nonraft proteins. *J. Membr. Biol.* **231**: 125-132.
204. Pabst, G, Boulgaropoulos, B, Gander, E, Sarangi, B R, Amenitsch, H, Raghunathan, V A, Laggner, P (2009) Effect of ceramide on nonraft proteins. *J. Membr. Biol.* **231**: 125-132.
205. Pabst, G, Boulgaropoulos, B, Gander, E, Sarangi, B R, Amenitsch, H, Raghunathan, V A, Laggner, P (2009) Effect of ceramide on nonraft proteins. *J. Membr. Biol.* **231**: 125-132.
206. Pabst, G, Boulgaropoulos, B, Gander, E, Sarangi, B R, Amenitsch, H, Raghunathan, V A, Laggner, P (2009) Effect of ceramide on nonraft proteins. *J. Membr. Biol.* **231**: 125-132.
207. Pabst, G, Boulgaropoulos, B, Gander, E, Sarangi, B R, Amenitsch, H, Raghunathan, V A, Laggner, P (2009) Effect of ceramide on nonraft proteins. *J. Membr. Biol.* **231**: 125-132.
208. Pabst, G, Boulgaropoulos, B, Gander, E, Sarangi, B R, Amenitsch, H, Raghunathan, V A, Laggner, P (2009) Effect of ceramide on nonraft proteins. *J. Membr. Biol.* **231**: 125-132.
209. Pabst, G, Boulgaropoulos, B, Gander, E, Sarangi, B R, Amenitsch, H, Raghunathan, V A, Laggner, P (2009) Effect of ceramide on nonraft proteins. *J. Membr. Biol.* **231**: 125-132.
210. Busto, J V, Fanani, M L, De Tullio, L, Sot, J, Maggio, B, Goni, F M, Alonso, A (2009) Coexistence of immiscible mixtures of palmitoylsphingomyelin and palmitoylceramide in monolayers and bilayers. *Biophys. J.* **97**: 2717-2726.
211. Pabst, G, Boulgaropoulos, B, Gander, E, Sarangi, B R, Amenitsch, H, Raghunathan, V A, Laggner, P (2009) Effect of ceramide on nonraft proteins. *J. Membr. Biol.* **231**: 125-132.
212. Pabst, G, Boulgaropoulos, B, Gander, E, Sarangi, B R, Amenitsch, H, Raghunathan, V A, Laggner, P (2009) Effect of ceramide on nonraft proteins. *J. Membr. Biol.* **231**: 125-132.

213. Alley, S H, Ces, O, Templer, R H, Barahona, M (2008) Biophysical regulation of lipid biosynthesis in the plasma membrane. *Biophys J* **94**: 2938-2954.
214. Pabst, G, Boulgaropoulos, B, Gander, E, Sarangi, B R, Amenitsch, H, Raghunathan, V A, Laggner, P (2009) Effect of ceramide on nonraft proteins. *J. Membr. Biol.* **231**: 125-132.
215. Chao, L, Gast, A P, Hatton, T A, Jensen, K F (2010) Sphingomyelinase-induced phase transformations: causing morphology switches and multiple-time-domain ceramide generation in model raft membranes. *Langmuir* **26**: 344-356.
216. Fanani, M L, De Tullio, L, Hartel, S, Jara, J, Maggio, B (2008) Sphingomyelinase-induced domain shape relaxation driven by out-of-equilibrium changes of composition. *Biophys. J.*
217. Chao, L, Gast, A P, Hatton, T A, Jensen, K F (2010) Sphingomyelinase-induced phase transformations: causing morphology switches and multiple-time-domain ceramide generation in model raft membranes. *Langmuir* **26**: 344-356.